

Continuation and Bifurcation of Frequency Combs Modeled by the Lugiato-Lefever Equation

zur Erlangung des akademischen Grades einer

Doktorin der Naturwissenschaften

von der KIT-Fakultät für Mathematik des
Karlsruher Instituts für Technologie (KIT)
genehmigte

Dissertation

von
Janina Gärtner

Referent: Prof. Dr. Wolfgang Reichel

Korreferent: Prof. Dr.-Ing. Christian Koos

Korreferent: Prof. Dr. Michael Plum

Datum der mündlichen Prüfung: 20.02.2019

Acknowledgement

Writing such a thesis without the support of many people would not be possible. First of all, I would like to thank my supervisor Prof. Dr. Wolfgang Reichel for introducing me in the topic of frequency combs and for giving me the opportunity to work within this interesting field of mathematics. Thank you for excellent supervision, constant support, patience and endless hours of discussions helping me to develop new ideas and to organize them in an understandable and structured way.

I am also very grateful to Prof. Dr.-Ing. Christian Koos for co-supervising me. The work with IPQ was very inspiring and opened new insights in applications of frequency combs. Moreover, I would like to thank Prof. Dr. Michael Plum for agreeing to review this thesis and Prof. Dr. Tobias Jahnke and Dr. Rainer Mandel for fruitful discussions.

Furthermore, I thank the Deutsche Forschungsgemeinschaft (DFG) for supporting me via CRC 1173 "Wave Phenomena".

During the last years, I enjoyed the great atmosphere in the Workgroup Nonlinear Partial Differential Equations. Special thanks goes to Jonathan Wunderlich, Peter Rupp and Simon Kohler for proof-reading parts of this thesis and giving me numerous and constructive suggestions for the improvement of my dissertation and also to Georgia Kokkala, Dominic Scheider and Carlos Hauser for providing a great working atmosphere.

Moreover, I would like to thank Philipp Trocha for explaining the physics of frequency combs over and over again and giving new suggestions from the perspective of an engineer. This really helped a lot.

Additionally, I would like to thank the Workgroup of Didactics. I always enjoyed a lot being part of this team. Thank you for giving me the opportunity to work in the young pupils lab. A special thanks goes to Verena Möhler, Judith Schilling and Peter Kaiser, we were a great team during the last years.

Last but not least, I want to thank my family, especially my parents and my husband Fabian. Thank you so much for your confidence and invaluable support, in particular during the last weeks.

Contents

I. Introduction	7
II. Continuation	15
1. Functional Analytical Framework and Outline	17
2. LLE without Forcing and without Damping	19
3. LLE with Forcing and without Damping	23
3.1. Phase plane analysis	23
3.2. Bifurcation from the sphere	26
4. LLE with Forcing and Damping	33
4.1. Nondegeneracy	33
4.2. Calculating the equilibria	36
4.3. Continuation via the Implicit Function Theorem	39
5. Numerical experiments	45
5.A. Details on the implementation	48
III. Bifurcation	49
6. Outline	51
7. pde2path and Numerical Path Continuation	53
7.1. cont	55
7.2. swibra	56
7.3. Fold continuation	57
7.4. First example of bifurcation diagrams of LLE	58
8. Soliton Quality	61
8.1. Bifurcation analysis for the LLE	61
8.2. Solitons along bifurcating branches	64
8.3. Quantitative characterization of soliton frequency combs	67
8.3.1. Characteristics of soliton frequency combs	67
8.3.2. Approximation formulas	67
8.3.3. Results	69
8.3.4. Conclusion	70
8.A. Details on the implementation	71

IV. LLE with Two-Photon-Absorption	73
9. Outline	75
10. Bifurcation	77
11. Nonexistence of Nontrivial Solutions	87
11.1. A priori bounds and nonexistence of nontrivial solutions I	87
11.2. Nonexistence of nontrivial solutions II	91
12. Continuation	95
V. Outlook and Further Results	97
13. A Priori Estimate	99
14. Spectral Properties of the Linearization	103
15. Third Order Dispersion	107
16. Summary and Outlook	111

Part I.
Introduction

Frequency combs are optical signals consisting of many equidistantly spaced modes with numerous applications. In 2015, Hänsch and Hall have been awarded the Nobel Prize in physics for the discovery made in 1998. Frequency combs serve as optical devices for example in high speed data transmission and optical metrology. Using one single fiber, a large amount of data can be transmitted which is modulated onto the frequency combs by Wavelength-Division Multiplexing (WDM).

In 1987, Lugiato and Lefever derived the Lugiato-Lefever equation

$$ia_t(x, t) = (-i + \zeta)a(x, t) - da_{xx}(x, t) - |a(x, t)|^2 a(x, t) + if$$

with $x \in \mathbb{T} := \mathbb{R}/2\pi\mathbb{Z}$, $t \in \mathbb{R}$, as a mean-field approximation to describe the dynamics of the slowly varying amplitude of the electromagnetic field $a(x, t)$ in the paraxial limit inside an optical cavity excited by a laser pump [28]. It is a nonlinear Schrödinger equation with damping and forcing. However, it can also be used as a model for the field $a(x, t) = \sum_{k \in \mathbb{Z}} \hat{a}_k(t) e^{ikx}$ inside a ring resonator pumped by a continuous wave (cw)-laser, where $\hat{a}_k(t)$ denotes the dimensionless, complex amplitude of the k -th excited mode. Therefore, the Lugiato-Lefever equation can alternatively be written as

$$i \frac{d}{dt} \hat{a}_k(t) = (\zeta - i) \hat{a}_k(t) + dk^2 \hat{a}_k(t) - \sum_{k', k'' \in \mathbb{Z}} \hat{a}_{k'}(t) \hat{a}_{k''}(t) \bar{\hat{a}}_{k'+k''-k}(t) + i \delta_{0k} f$$

with $k \in \mathbb{Z}$, which is a system of coupled ordinary differential equations. Mathematically, frequency combs can be understood as stationary solutions of this system, where d, ζ, f are real parameters and t is the normalized time. The value ζ is the detuning offset of the laser relative to the resonance frequency of the resonator. The dispersion of the material can either be anomalous ($d > 0$) or normal ($d < 0$). The expression $i \delta_{0k} f$ with Kronecker-Delta δ_{0k} describes the forcing by the cw-laser.

Figure 1 depicts the experimental setting. The cw-laser emits light at frequency ω , which is then amplified and coupled into a microresonator. As the refractive index is intensity dependent (nonlinear Kerr effect), the field inside the resonator is strongly enhanced. This leads to modulation instabilities and the cascaded degenerate and non-degenerate four-wave mixing yields the formation of a frequency comb, which is the resulting stationary pattern of equidistantly spaced excited modes.

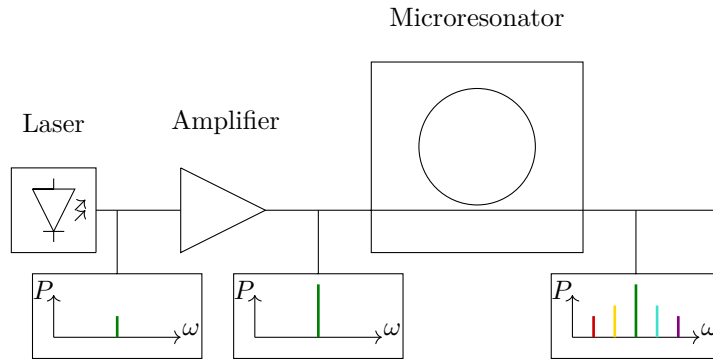


Figure 1: Scheme of the system for generation of frequency combs.

Degenerate four-wave mixing converts two photons of the same frequency ω_1 into two photons of different frequencies $\omega_2 < \omega_1 < \omega_3$ such that $2\omega_1 = \omega_2 + \omega_3 = \frac{\Delta E}{\hbar}$. For non-degenerate four-wave mixing, two photons of different frequencies ω_1, ω_2 are converted into two photons of different frequencies ω_3, ω_4 such that $\omega_1 + \omega_2 = \omega_3 + \omega_4 = \frac{\Delta E}{\hbar}$, cf. Figure 2. Four-wave mixing leads to the formation of frequency combs with equidistant mode spacing across the entire comb. For more details see [17].

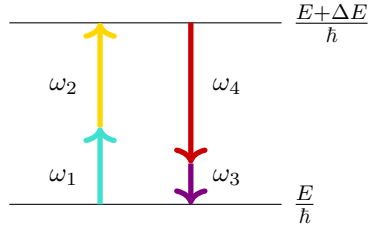


Figure 2: Energy level diagram for non-degenerate four-wave mixing.

The first experimental verification of frequency combs was done by Kondratiev, Gorodetsky and Kippenberg in [25], where they generated solitons that were stable over some time. Furthermore, they generated a large number of comblines by suitably adjusting the detuning parameter ζ , which is also consistent with their numerical simulations where they used a time-dependent detuning.

A particular challenge is the identification of parameter regimes for d, ζ, f where non-trivial and in particular soliton-like frequency combs exist. As frequency combs are stationary solutions of the Lugiato-Lefever equation, we consider the problem

$$-da'' + (\zeta - i)a - |a|^2a + if = 0, \quad a(\cdot) = a(\cdot + 2\pi). \quad (\text{LLE})$$

Therefore, throughout this thesis the *Lugiato-Lefever equation* always refers to the stationary equation.

We are especially interested in so-called soliton-frequency combs, as they are particularly useful for optical metrology and high speed data transmission. They correspond to localized solutions of (LLE) in spatial domain and are particularly broad in frequency domain, cf. Figure 3.

The time-dependent and the stationary Lugiato-Lefever equation have been studied in literature from different points of view. E.g., numerical simulations of temporal comb formation using time-integration techniques can be found in [17],[47].

Moreover, there are several publications concerning local bifurcation from the constant solutions. Snaking behavior of solution branches has been discussed in [35],[36],[37]. Furthermore, in these publications and in [16] bifurcation with respect to f, ζ from

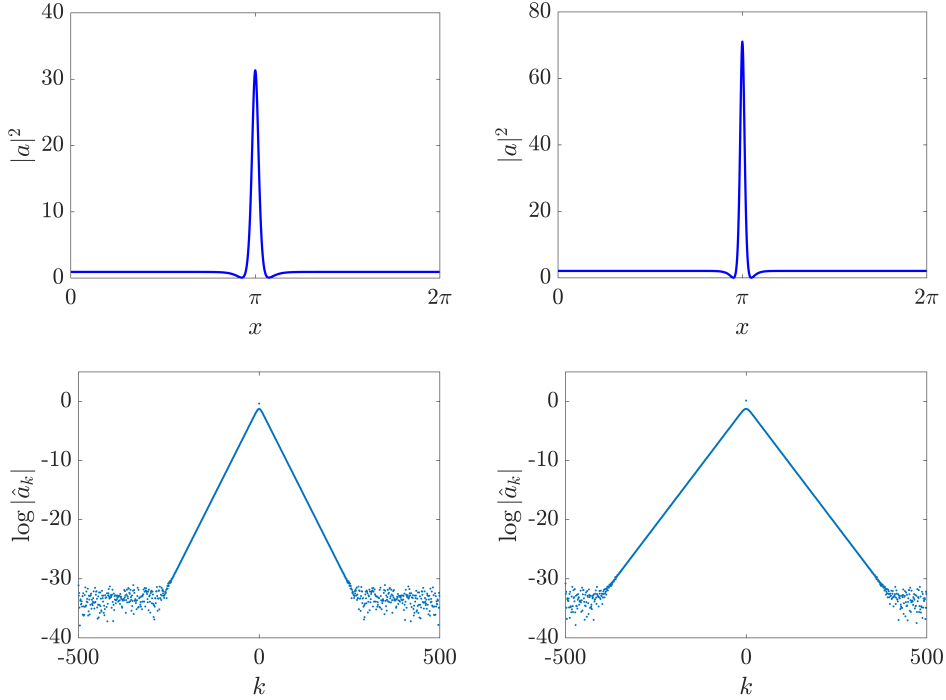


Figure 3: Left: Soliton for $d = 0.01$, $\zeta = 12$, $f = 10.5$ and corresponding frequency comb. Right: Soliton for $d = 0.01$, $\zeta = 26.5$, $f = 35$ and corresponding frequency comb.

the viewpoint of spatial dynamics is considered. However, with this approach the 2π -periodicity of the solutions is neglected. A bifurcation analysis for fixed period 2π can be found in [29].

Another analysis concerning the Lugiato-Lefever equation was done by Miyaji, Ohnishi and Tsutsumi in [31],[32]. They also considered stability and bifurcation of trivial solutions. In the case of bounded intervals, they could prove fold bifurcation of nontrivial stationary solutions around codimension two bifurcation points using center manifold reduction. Furthermore, they performed a stability analysis using Strichartz estimates.

However, up to our knowledge, a global and quantized study covering the cases of both anomalous dispersion ($d > 0$) and normal dispersion ($d < 0$) concerning soliton-frequency combs over a large range of possible parameters f, ζ has not been developed so far and is therefore the goal of this thesis. It is part of the project B3 in the CRC 1173 "Wave phenomena: analysis and numerics", which is a joint project of mathematicians from the Institute of Analysis and electrical engineers from the Institute of Photonics and Quantum Electronics at KIT. The goal of this thesis is to find an analytical and numerical framework for the existence of frequency combs and to identify suitable parameter regions.

This thesis considers two approaches, both analytically and numerically:

- continuation of solitons of the cubic NLS without damping and without forcing into the regime of positive damping and forcing,
- bifurcation from the constant solutions with respect to the detuning parameter ζ .

The first method described in Part II allows to prove the existence of soliton-frequency combs for large values of ζ and f . It consists in the continuation of the solitons of the cubic, undamped and undriven NLS into the situation of the Lugiato-Lefever equation where damping and forcing are present. However, continuation is only possible in the case of anomalous dispersion ($d > 0$). This method is applied both as an analytic and a numerical tool and the analytical results are supported by numerical experiments to identify regions in the (ζ, f) -plane, where solitons exist.

The second method in Part III starts from the knowledge of the trivial (constant) solutions parametrized by ζ for fixed d, f . It allows to detect those points on the trivial curve where nontrivial solutions bifurcate. Bifurcation is possible both for anomalous dispersion ($d > 0$) and for normal dispersion ($d < 0$). Based on [13],[29], we develop heuristics for the most localized solitons in bifurcation diagrams computed by the MATLAB-toolbox `pde2path`. Moreover, we define quality measures that allow to compare these frequency combs and identify parameters, for which highly localized solitons exist. We develop heuristics that allow us to find the most localized solutions on branches bifurcating from the trivial solutions. These can be used to perform a global study covering a large parameter range and we discover that dark solitons ($d < 0$) have a greater conversion efficiency at the expense of reduced combwidth.

Additionally, in Part IV, we consider a slightly modified equation

$$-da'' + (\zeta - i)a - (1 + i\kappa)|a|^2a + if = 0, \quad a(\cdot) = a(\cdot + 2\pi),$$

with an additional loss term due to two photon absorption (TPA). During TPA two photons are absorbed and electrons of the valence band are excited into the conducting band and hence, free carriers are generated which leads to nonlinear loss. The continuation and bifurcation methods described above are also valid in the extended equation and we prove the persistence of bifurcation points for small $\kappa < \kappa_*$, their disappearance for $\kappa > \kappa_*$ and the absence of any nontrivial solutions for $\kappa > \kappa^*$, where $0 < \kappa_* < \kappa^*$. Furthermore, we provide explicit bounds for κ_* and κ^* .

Summing up, the goal of this thesis is to analytically prove the existence of soliton solutions of (LLE). Furthermore, we support the analysis by a large number of numerical experiments, which allows us to quantify parameter regions, where soliton solutions of (LLE) exist and to evaluate their performance characteristics.

Numerical experiments. Throughout this thesis, several numerical examples are found. All of them have been computed in `MATLAB` (version R2016b) together with the toolbox `pde2path` (Versions 2.2 and 2.3) (cf. [10],[44]) on a computer with an Intel i5-6500 (4 cores with 3.2 GHz) processor and 8 GB of RAM. However, we mostly omit the details on the implementation, as the numerical experiments mainly support our analysis and serve as proof of principle.

Prepublications. Some of these results have been published in advance in a preprint with Rainer Mandel and Wolfgang Reichel: *The Lugiato-Lefever equation with nonlinear damping caused by two photon absorption*, see [14]. Moreover, some results have been published in a preprint with Philipp Trocha, Rainer Mandel, Christian Koos, Tobias Jahnke and Wolfgang Reichel: *Bandwidth and conversion efficiency analysis of dissipative Kerr soliton frequency combs based on bifurcation theory*, see [13]. The results will be pointed out at the appropriate places.

Part II.
Continuation

1. Functional Analytical Framework and Outline

In this first section, we will fix our notations and introduce the spaces used in this part of the thesis.

In Sections 2-4, we consider the stationary Lugiato-Lefever equation

$$-da'' + (\zeta - i)a - |a|^2 a + if = 0, \quad a'(0) = 0 \quad \text{on } \mathbb{R}, \quad (1.1)$$

for anomalous dispersion $d > 0$ and $\zeta > 0$, $f \in \mathbb{R}$. Especially, we are interested in homoclinic solutions, i.e., solutions of (1.1) of the form $a = \tilde{a} + a^\infty$, where \tilde{a} belongs to the space

$$\mathcal{H}_c := \{\tilde{a} \in H^2(\mathbb{R}; \mathbb{C}) : \tilde{a}'(0) = 0\}$$

and $a^\infty := \lim_{|x| \rightarrow \infty} a(x)$ solves the algebraic equation

$$(\zeta - i)a - |a|^2 a + if = 0.$$

It is sometimes convenient to split $a = v + iw$ into real and imaginary part and to consider the system

$$\begin{aligned} -dv'' + w + \zeta v - (v^2 + w^2)v &= 0, & \text{on } \mathbb{R}, \\ -dw'' - v + \zeta w - (v^2 + w^2)w + f &= 0, & \text{on } \mathbb{R}, \end{aligned}$$

where $v = \tilde{v} + v^\infty$, $w = \tilde{w} + w^\infty$, \tilde{v}, \tilde{w} belong to the space

$$\mathcal{H}_r := \{\tilde{z} \in H^2(\mathbb{R}; \mathbb{R}) : \tilde{z}'(0) = 0\}$$

and $v^\infty := \lim_{|x| \rightarrow \infty} v(x)$, $w^\infty := \lim_{|x| \rightarrow \infty} w(x)$ solve the algebraic system

$$\begin{aligned} w + \zeta v - (v^2 + w^2)v &= 0, \\ -v + \zeta w - (v^2 + w^2)w + f &= 0. \end{aligned}$$

Then obviously $\tilde{a} = \tilde{v} + i\tilde{w}$ and $a^\infty = v^\infty + iw^\infty$.

Our strategy consists of three steps. In Section 2, we calculate the solutions of (1.1) in the absence of damping and forcing

$$-da'' + \zeta a - |a|^2 a = 0, \quad a'(0) = 0, \quad \text{on } \mathbb{R},$$

with $d, \zeta > 0$. The solutions are then given by

$$a(x) = \sqrt{2\zeta} \frac{1}{\cosh(x\sqrt{\zeta/d})} e^{i\alpha},$$

where $\alpha \in [0, 2\pi)$. Hence, for fixed d, ζ , there is a one-dimensional sphere of solutions \mathcal{T} parametrized by $\alpha \in [0, 2\pi)$.

In a second step, in Section 3, we introduce the forcing term and consider

$$-da'' + \zeta a - |a|^2 a + if = 0, \quad a'(0) = 0,$$

on \mathbb{R} for $d, \zeta > 0$ and $f \in \mathbb{R}$. We show that bifurcation from the solution family \mathcal{T} with respect to the parameter f at $f = 0$ only happens if $\alpha \in \left\{\frac{\pi}{2}, \frac{3\pi}{2}\right\}$, which means that only purely imaginary solutions bifurcate. Subsequently, a phase-plane analysis of these purely imaginary solutions is performed for $|f| < \frac{2\sqrt{3}}{9}$. The bound for f is crucial, since only for these values of f homoclinic orbits exist, which represent the soliton solutions.

In Section 4, we will prove existence of homoclinic solutions of the full problem (1.1). We can prove that for $d, \zeta > 0$ and $f < \frac{2\sqrt{3}}{9}\tilde{\zeta}^{3/2}$ homoclinic solutions of (1.1) with $\zeta = \tilde{\zeta}\varepsilon^{-1}$, $f = \tilde{f}\varepsilon^{-3/2}$ exist for small $\varepsilon > 0$. For the proof, we use a suitable singular rescaling of the problem as well as the Implicit Function Theorem. The theorem proves in particular the existence of solutions of (1.1) for large parameters ζ and f .

The approach of considering (1.1) on the real line is a valid approach, since highly localized solutions of (1.1) serve as good approximations for solutions of (LLE), cf. [19].

Finally, in Section 5, we will use the results of Sections 2-4 as a basis for a numerical method that allows to compute 2π -periodic and localized solutions of (LLE). It is a numerical continuation algorithm that allows to continue solutions for $\tilde{f} = \varepsilon = 0$ into the situation where $\tilde{f} > 0$ and $\varepsilon > 0$. This approach, together with the rescaling, allows us to perform a large parameter study in the (ζ, f) -plane and to identify regions where solitons exist. As a result, we get a lower envelope, such that above this envelope soliton solutions exist. Furthermore, we investigate spectral stability and discuss the connection to nonlinear stability. Finally, we compare our results with the approximation of [19], stating that for

$$f > \frac{\sqrt{8\zeta}}{\pi}$$

soliton solutions exist and we present a method how to numerically calculate these solutions in a systematic way.

2. LLE without Forcing and without Damping

As a first step, we consider solutions of (1.1) without forcing and without damping, i.e., the stationary cubic nonlinear Schrödinger equation (NLS)

$$-da'' + \zeta a = |a|^2 a, \quad a'(0) = 0, \quad (2.1)$$

on \mathbb{R} with fixed $\zeta, d > 0$. Of course, this equation is well-studied and understood, cf. [4]. However, for completeness, we will rigorously calculate the solitons of (2.1) in the following theorem.

Theorem 2.1. *The solutions $a \in \mathcal{H}_c$ of (2.1) are given by $a(x) = e^{i\alpha}\varphi(x)$, where $\alpha \in [0, 2\pi)$ and*

$$\varphi(x) := \sqrt{2\zeta} \frac{1}{\cosh(x\sqrt{\zeta/d})}.$$

Proof. Let $\varphi \in \mathcal{H}_r$ be a real-valued solution of (2.1). Due to $\varphi'(0) = 0$, we have the symmetry $\varphi(x) = \varphi(-x)$. Multiplying

$$-d\varphi'' + \zeta\varphi = |\varphi|^2\varphi \quad (2.2)$$

by φ' leads to

$$\frac{d}{dx} \left(-\frac{1}{2}d\varphi'^2 + \frac{1}{2}\zeta\varphi^2 - \frac{1}{4}\varphi^4 \right) = 0$$

and therefore

$$-d\varphi'^2 + \zeta\varphi^2 - \frac{1}{2}\varphi^4 = c$$

for a constant $c \in \mathbb{R}$. As $\varphi \in \mathcal{H}_r$, we know $\lim_{x \rightarrow \pm\infty} \varphi(x) = 0$ and by (2.2), we get $\lim_{x \rightarrow \pm\infty} \varphi''(x) = 0$. Thus, $\lim_{x \rightarrow \pm\infty} \varphi'(x) = 0$ and consequently $c = 0$, which leads to

$$-d\varphi'^2 + \zeta\varphi^2 - \frac{1}{2}\varphi^4 = 0. \quad (2.3)$$

Together with $\varphi'(0) = 0$, it is clear that $\varphi(0) = \pm\sqrt{2\zeta}$. As with φ also $-\varphi$ is a solution of (2.2), we will concentrate on $\varphi(0) = \sqrt{2\zeta}$.

By inserting $\varphi(0) = \sqrt{2\zeta}$ into the equation, we get $\varphi''(0) = -\frac{\zeta}{d}\sqrt{2\zeta} < 0$. Therefore, there is a $b_1 > 0$ with $\varphi' < 0$ on $(0, b_1)$. We will now show, that $\varphi' < 0$ on $(0, \infty)$. Assuming $\varphi' < 0$ on $(0, b_2)$ and $\varphi'(b_2) = 0$, we get by (2.3) that $\varphi(b_2) = -\sqrt{2\zeta}$. Hence, there exists a value $b_3 \in (0, b_2)$ with $\varphi(b_3) = 0$. Using (2.3) again, we get $\varphi'(b_3) = 0$ and

consequently, $\varphi \equiv 0$ which leads to a contradiction and means that $\varphi' < 0$ in $(0, \infty)$. Furthermore, $\varphi > 0$ on $[0, \infty)$ and by symmetry $\varphi > 0$ on \mathbb{R} .

Now the solutions of $-d\varphi'^2 + \zeta\varphi^2 - \frac{1}{2}\varphi^4 = 0$ can be calculated using separation of variables. As

$$\left(\frac{d\varphi}{dx}\right)^2 = \frac{\zeta}{d}\varphi^2 - \frac{1}{2d}\varphi^4,$$

and $\varphi' < 0$ in $(0, \infty)$, we get

$$x = - \int_{\sqrt{2\zeta}}^{\varphi(x)} \frac{1}{\sqrt{\frac{\zeta}{d}\varphi^2 - \frac{1}{2d}\varphi^4}} d\varphi = \sqrt{\frac{d}{\zeta}} \operatorname{arcosh} \sqrt{2\zeta} \frac{1}{\varphi(x)}$$

and therefore,

$$\varphi(x) = \sqrt{2\zeta} \frac{1}{\cosh(x\sqrt{\zeta/d})}.$$

Now let

$$A = \{a \in \mathcal{H}_c : -da'' + \zeta a = |a|^2 a\}.$$

As in [4], we show that $A = \cup\{e^{i\alpha}\varphi : \alpha \in \mathbb{R}\}$. Take $a \in A$ and multiply (2.1) by \bar{a}' . As above, we have

$$-d|a'|^2 + \zeta|a|^2 - \frac{1}{2}|a|^4 = 0. \quad (2.4)$$

Additionally, we know $|a| > 0$, because if $a(x) = 0$ for any x , by (2.4) we would also have $a'(x) = 0$ and thus, $a \equiv 0$. Consequently, we can write $a = \varrho e^{i\alpha}$ with $\alpha > 0$ and $\varrho, \alpha \in C^2(\mathbb{R})$. Inserting this into (2.1), we get

$$(-d\varrho'' + d\varrho\alpha'^2 + \zeta\varrho - \varrho^2\varrho)e^{i\alpha} - id(2\varrho'\alpha' + \varrho\alpha'')e^{i\alpha} = 0,$$

i.e., $2\varrho'\alpha' + \varrho\alpha'' = 0$. Then, there exists $c \in \mathbb{R}$ with $\varrho^2\alpha' \equiv c$. We have $\lim_{x \rightarrow \pm\infty} |a(x)| = 0$ and $\lim_{x \rightarrow \pm\infty} |a'(x)| = 0$ and $|a'| = \sqrt{\varrho^2\alpha'^2 + \rho'^2}$ is bounded. Thus, $\varrho^2\alpha'^2 = \frac{c^2}{\varrho^2}$ is also bounded. From $\lim_{x \rightarrow \pm\infty} |a(x)| = 0$, we get $\varrho(x) \rightarrow 0$ as $x \rightarrow \pm\infty$ and consequently, $c = 0$. Now we have $\alpha \equiv \alpha_0$ for $\alpha_0 \in \mathbb{R}$ and $a = \varrho e^{i\alpha_0}$. As $\varrho \in H^1(\mathbb{R})$, there is a $x_0 \in \mathbb{R}$ with $\varrho'(x_0) = 0$ and $a \in \mathcal{H}_c$ yields $x_0 = 0$. Inserting $a = \varrho e^{i\alpha_0}$ in (2.4) leads to $\varrho(0) = \sqrt{2\zeta}$. Hence, ϱ solves (2.2), $\varrho(0) = \sqrt{2\zeta}$ and $\varrho'(0) = 0$. The corresponding initial value problem has a unique solution and therefore $\varrho \equiv \varphi$ and finally

$$a(x) = \varphi(x)e^{i\alpha_0} = \sqrt{2\zeta} \frac{1}{\cosh(x\sqrt{\zeta/d})} e^{i\alpha_0}.$$

□

Remark 2.2. *Decomposing $a := v + iw$ into real and imaginary part, we have seen that the solutions (v, w) of the system*

$$\begin{aligned} -dv'' + \zeta v - (v^2 + w^2)v &= 0, & \text{on } \mathbb{R} \\ -dw'' + \zeta w - (v^2 + w^2)w &= 0, & \text{on } \mathbb{R}, \end{aligned}$$

are given by the family

$$\mathcal{T} := \{(\cos(\alpha)\varphi, \sin(\alpha)\varphi) : 0 \leq \alpha < 2\pi\}.$$

3. LLE with Forcing and without Damping

3.1. Phase plane analysis

In this section, we will consider purely imaginary solutions $a = iw$ of

$$-da'' + \zeta a - |a|^2 a + if = 0, \quad (3.1)$$

i.e., purely imaginary solutions of (1.1) with forcing and without damping. They satisfy

$$-dw'' + \zeta w - w^3 + f = 0. \quad (3.2)$$

This second-order differential equation can be written as a first-order system

$$\begin{pmatrix} w' \\ dy' \end{pmatrix} = h(w, y) \quad \text{with } h(w, y) := \begin{pmatrix} y \\ \zeta w - w^3 + f \end{pmatrix} \quad (3.3)$$

and the solutions can be studied in the phase plane (w, w') , i.e., the trajectories of the phase plane correspond to the level sets of the first integral

$$I = -dy^2 + \zeta w^2 - \frac{1}{2}w^4 + 2fw = c \quad (3.4)$$

for $c \in \mathbb{R}$. As we are interested in soliton solutions, we need to find all homoclinic orbits of this system, i.e., all solutions $iw = i\tilde{w} + iw^\infty$ with $\tilde{w} \in \mathcal{H}_r$ and $w^\infty := \lim_{|x| \rightarrow \infty} w(x)$. In Lemma 3.1, we will prove that they exist for all $|f| < \frac{2\sqrt{3}}{9}\zeta^{3/2}$.

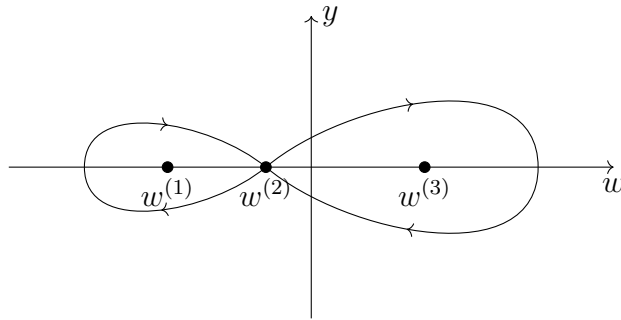


Figure 4: Homoclinic orbits

Lemma 3.1. *Let $d, \zeta > 0$ and $|f| < \frac{2\sqrt{3}}{9}\zeta^{3/2}$. There exist two even homoclinic solutions iw_i for $i = 1, 2$ of (3.1) with w_1 symmetrically increasing and w_2 symmetrically decreasing.*

Proof. We observe that all trajectories are bounded in the (w, y) -plane. Indeed, consider an arbitrary trajectory

$$-dy^2 + \zeta w^2 - \frac{1}{2}w^4 + 2fw = c^*,$$

for $c^* \in \mathbb{R}$ and let $N := \max_{w \in \mathbb{R}} \{\zeta w^2 - \frac{1}{2}w^4 + 2fw\}$. Then, there exist $\xi, \eta > 0$ such that

$$-dy^2 < c^* - N \quad \text{for all } |y| > \xi$$

and

$$\zeta w^2 - \frac{1}{2}w^4 + 2fw < c^* \quad \text{for all } |w| > \eta.$$

Hence, for all (y, w) with $|y| > \xi$, we have

$$-dy^2 + \zeta w^2 - \frac{1}{2}w^4 + 2fw < c^* - N + N = c^*$$

and for all (y, w) with $|w| > \eta$

$$-dy^2 + \zeta w^2 - \frac{1}{2}w^4 + 2fw < c^*.$$

Finally, the set

$$\{(y, w) : -dy^2 + \zeta w^2 - \frac{1}{2}w^4 + 2fw = c^*\} \subseteq [-\zeta, \zeta] \times [-\eta, \eta]$$

is bounded. Furthermore, every trajectory crosses the w -axis, as for all $c \in (-\infty, N]$ there exists a \hat{w} with $\zeta \hat{w}^2 - \frac{1}{2}\hat{w}^4 + 2f\hat{w} = c$ and hence $(\hat{w}, 0) \in \{(y, w) : -dy^2 + \zeta w^2 - \frac{1}{2}w^4 + 2fw = c\}$. Additionally, by symmetry $y \rightarrow -y$ of (3.4), all trajectories of (3.2) are symmetric with respect to the w -axis.

The equilibria of the system are characterized by $w' = y = 0$ and they solve the algebraic equation

$$\zeta w - w^3 + f = 0. \tag{3.5}$$

This equation has three distinct real-valued solutions $w^{(j)}$, $j = 1, 2, 3$ for $|f| < \frac{2\sqrt{3}}{9}\zeta^{3/2}$, two real-valued solutions $w^{(j)}$, $j = 1, 2$ for $|f| = \frac{2\sqrt{3}}{9}\zeta^{3/2}$ and only one real valued solution for $|f| > \frac{2\sqrt{3}}{9}\zeta^{3/2}$. Due to the Theorem of Poncaré-Bendixson, homoclinic orbits are only possible in the case $|f| < \frac{2\sqrt{3}}{9}\zeta^{3/2}$. To study the behavior of the system (3.3), we need to linearize and get

$$Dh(w, y) = \begin{pmatrix} 0 & 1 \\ \zeta - 3w^2 & 0 \end{pmatrix}.$$

Evaluating the Jacobian at some equilibrium $(0, w^{(j)})$, we find

$$A := Dh(w^{(j)}, 0) = \begin{pmatrix} 0 & 1 \\ \zeta - 3(w^{(j)})^2 & 0 \end{pmatrix}.$$

The characteristic equation reads

$$0 = \det(A - \lambda Id) = \lambda^2 + \Delta,$$

where

$$\Delta := \det(A) = -\zeta + 3(w^{(j)})^2.$$

Then,

$$\lambda_1 = \sqrt{-\Delta} \quad \text{and} \quad \lambda_2 = -\sqrt{-\Delta}$$

are solutions to the characteristic equation. Hence, the linear stability analysis, which allows us to characterize the equilibria of the nonlinear system, reduces to the analysis of Δ .

For $|f| < \frac{2\sqrt{3}}{9}\zeta^{3/2}$ and $w^{(1)} < w^{(2)} < w^{(3)}$, we see immediately that

$$\begin{aligned} \Delta &> 0 & \text{for } j = 1, 3 \\ \Delta &< 0 & \text{for } j = 2 \end{aligned}$$

as $w^{(j)}$ solve the algebraic equation (3.5).

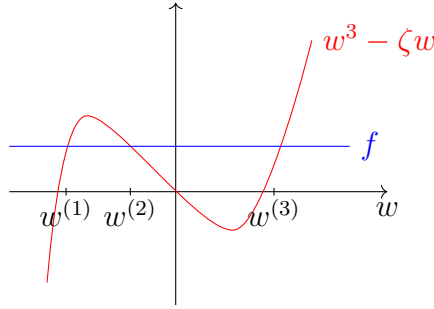


Figure 5: Sketch of (3.5).

This means in particular, that for $j = 2$ we have two real valued eigenvalues of opposite sign and the equilibrium is an unstable saddle. However, for $j = 1, 3$, we have two purely imaginary eigenvalues of opposite sign and these equilibria are stable centers, surrounded by periodic orbits.

Since the stable and the unstable manifold of the saddle are symmetric around the y -axis, they are identical and thus, provide the two homoclinic orbits.

□

The homoclinic orbits represent the soliton solutions $iw_i = i\tilde{w}_i + iw_i^\infty$ of this problem. In the following, we will work in the regime where $0 \leq |f| < \frac{2\sqrt{3}}{9}\zeta^{3/2}$ and define $w_i^\infty := w^{(2)}$, where $w^{(2)}$ is as in the proof above.

3.2. Bifurcation from the sphere

Here, we will consider

$$-da'' + \zeta a - |a|^2 a + if = 0, \quad (3.6)$$

on \mathbb{R} , i.e., (1.1) with forcing and without damping. Writing $a = v + iw$, we get the system

$$-dv'' = -\zeta v + (v^2 + w^2)v, \quad (3.7)$$

$$-dw'' = -\zeta w + (v^2 + w^2)w - f, \quad (3.8)$$

on \mathbb{R} . In the previous section, we have seen that in the situation without damping and without forcing the solutions of (1.1) are given by the one-dimensional sphere \mathcal{T} consisting of $(v_\alpha, w_\alpha) = (\cos(\alpha)\varphi, \sin(\alpha)\varphi)$ where $\alpha \in [0, 2\pi)$ and

$$\varphi(x) = \sqrt{2\zeta} \frac{1}{\cosh(x\sqrt{\zeta/d})}. \quad (3.9)$$

We will show that bifurcation from \mathcal{T} with respect to the parameter f is only possible for $\alpha \in \left\{\frac{\pi}{2}, \frac{3\pi}{2}\right\}$.

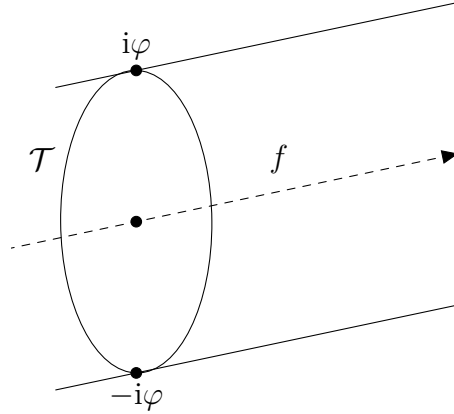


Figure 6: Symbolic picture: Bifurcation from the sphere of solutions for $f = 0$

The theorem reads as follows.

Theorem 3.2. *Let $d, \zeta > 0$ and $|f| < \frac{2\sqrt{3}}{9}\zeta^{3/2}$. Then*

- (i) *bifurcation with respect to f from \mathcal{T} happens exactly at $\alpha \in \left\{\frac{\pi}{2}, \frac{3\pi}{2}\right\}$;*
- (ii) *the bifurcating solutions consist of the purely imaginary homoclinic solutions found in Section 3.1.*

Proof. The proof of (i) is a consequence of Theorems 3.6 and 3.8 below. Theorem 3.6 shows that there is no bifurcation for $\alpha \notin \left\{\frac{\pi}{2}, \frac{3\pi}{2}\right\}$ and Theorem 3.8 shows that the curve of purely imaginary solutions from Section 3.1 connect to \mathcal{T} at $f = 0$ and $\alpha \in \left\{\frac{\pi}{2}, \frac{3\pi}{2}\right\}$.

(ii) holds due to Theorem 3.7. We prove that the purely imaginary solutions of Section 3.1 are locally unique and are given by two curves (f, iw_1) and (f, iw_2) ¹. \square

For the proofs, we need the following two theorems of Crandall-Rabinowitz. The first one gives conditions under which no bifurcation occurs (cf. Theorem 3.2 in [7] or Theorem I.4.1 in [24]).

Theorem 3.3. *Let X, Z be Banach spaces and $U \subset X$ an open neighborhood of x_0 , and $I \subset \mathbb{R}$ an open neighborhood of λ_0 . Furthermore, assume that $F \in C^1(U \times I, Z)$ and*

$$\dim(\ker(D_x F(x_0, \lambda_0))) = \text{codim}(\text{ran}(D_x F(x_0, \lambda_0))) = 1$$

with

$$D_\lambda F(x_0, \lambda_0) \notin \text{ran}(D_x F(x_0, \lambda_0)).$$

Then there is a continuously differentiable curve through (x_0, λ_0) , that is, there exists

$$\{(x(s), \lambda(s)) \mid s \in (-\delta, \delta), (x(0), \lambda(0)) = (x_0, \lambda_0)\}$$

such that $F(x(s), \lambda(s)) = 0$ for $s \in (-\delta, \delta)$ and all solutions of $F(x, \lambda) = 0$ in a neighborhood of (x_0, λ_0) belong to this curve.

For the proof of bifurcation for $\alpha \in \left\{\frac{\pi}{2}, \frac{3\pi}{2}\right\}$, we need a second Theorem of Crandall Rabinowitz (cf. [6] or Theorem I.5.1 in [24]).

Theorem 3.4. *Let X, Z be Banach spaces and $U \subset X$ an open neighborhood of 0, and $I \subset \mathbb{R}$ an open neighborhood of λ_0 . Furthermore, assume that $F \in C^2(U \times I, Z)$, $F(0, \lambda) = 0$ for all $\lambda \in I$ and*

$$\dim(\ker(D_x F(0, \lambda_0))) = \text{codim}(\text{ran}(D_x F(0, \lambda_0))) = 1$$

with

$$\ker(D_x F(0, \lambda_0)) = \text{span}\{\phi\}, \quad D_{x\lambda} F(0, \lambda_0)[\phi] \notin \text{ran}(D_x F(0, \lambda_0)).$$

Then there is a continuously differentiable curve through $(0, \lambda_0)$, that is, there exists

$$\{(x(s), \lambda(s)) \mid s \in (-\delta, \delta), (x(0), \lambda(0)) = (0, \lambda_0)\} \tag{3.10}$$

such that $F(x(s), \lambda(s)) = 0$ for $s \in (-\delta, \delta)$ and all solutions of $F(x, \lambda) = 0$ are on the trivial solution curve or on the nontrivial curve (3.10).

¹Note that in this notation iw_1 and iw_2 depend on f .

Let (v^∞, w^∞) satisfy

$$\begin{aligned} 0 &= -\zeta v^\infty + (v^\infty)^3 + (w^\infty)^2 v^\infty = v^\infty(-\zeta + (v^\infty)^2 + (w^\infty)^2), \\ 0 &= \zeta w^\infty - (v^\infty)^2 w^\infty - (w^\infty)^3 + f = -w^\infty(-\zeta + (v^\infty)^2 + (w^\infty)^2) + f. \end{aligned}$$

Then, for $f \neq 0$, the only possibility is $v^\infty = 0$ and w^∞ solves

$$\zeta w^\infty - (w^\infty)^3 + f = 0,$$

and for $f = 0$ the requirement of homoclinic solutions also leads to $v^\infty = w^\infty = 0$, cf. Section 2. Hence, $v^\infty = 0$ for all $f \in \mathbb{R}$.

Differentiating by f yields

$$(3(w^\infty)^2 - \zeta) \frac{\partial w^\infty}{\partial f} = 1$$

and consequently $\frac{\partial w^\infty}{\partial f} = \frac{1}{3(w^\infty)^2 - \zeta}$. As a first step, we define for $d, \zeta > 0$ and the map $F : \mathcal{H}_r \times \mathcal{H}_r \times \mathbb{R} \rightarrow L^2(\mathbb{R}) \times L^2(\mathbb{R})$ by

$$F(\tilde{v}, \tilde{w}, f) := \begin{pmatrix} \tilde{v} - \frac{1}{d} \left(-\frac{d^2}{dx^2} + \frac{\zeta}{d} \right)^{-1} \left((\tilde{v}^2 + (\tilde{w} + w^\infty)^2) \tilde{v} \right) \\ \tilde{w} - \frac{1}{d} \left(-\frac{d^2}{dx^2} + \frac{\zeta}{d} \right)^{-1} \left((\tilde{v}^2 + (\tilde{w} + w^\infty)^2) (\tilde{w} + w^\infty) - f - \zeta w^\infty \right) \end{pmatrix}.$$

For $\phi = (\phi_1, \phi_2) \in \mathcal{H}_r \times \mathcal{H}_r$, the following formulas for the derivatives of F hold

$$(D_{\tilde{a}} F)_1(\tilde{v}, \tilde{w}, f)[\phi] = \phi_1 - \frac{1}{d} \left(-\frac{d^2}{dx^2} + \frac{\zeta}{d} \right)^{-1} \left((3\tilde{v}^2 + (\tilde{w} + w^\infty)^2) \phi_1 + 2\tilde{v}(\tilde{w} + w^\infty) \phi_2 \right), \quad (3.11)$$

$$(D_{\tilde{a}} F)_2(\tilde{v}, \tilde{w}, f)[\phi] = \phi_2 - \frac{1}{d} \left(-\frac{d^2}{dx^2} + \frac{\zeta}{d} \right)^{-1} \left((\tilde{v}^2 + 3(\tilde{w} + w^\infty)^2) \phi_2 + 2\tilde{v}(\tilde{w} + w^\infty) \phi_1 \right), \quad (3.12)$$

$$(D_f F)_1(\tilde{v}, \tilde{w}, f) = -\frac{1}{d} \left(-\frac{d^2}{dx^2} + \frac{\zeta}{d} \right)^{-1} \left(2\tilde{v}(\tilde{w} + w^\infty) \frac{1}{3(w^\infty)^2 - \zeta} \right) \quad (3.13)$$

$$(D_f F)_2(\tilde{v}, \tilde{w}, f) = -\frac{1}{d} \left(-\frac{d^2}{dx^2} + \frac{\zeta}{d} \right)^{-1} \left((\tilde{v}^2 + 3\tilde{w}^2 + 6\tilde{w}w^\infty) \frac{1}{3(w^\infty)^2 - \zeta} \right) \quad (3.14)$$

and (3.6) is equivalent to finding nontrivial solutions of

$$F(\tilde{v}, \tilde{w}, f) = 0.$$

By Section 2, it is clear that $F(v_\alpha, w_\alpha, 0) = 0$. Theorem 3.3 applies if $D_f F(v_\alpha, w_\alpha, 0) \notin \text{ran}(D_{\tilde{a}} F(v_\alpha, w_\alpha, 0))$. Therefore, we have a closer look at $D_{\tilde{a}} F(v_\alpha, w_\alpha, 0)$.

Lemma 3.5. For all $\alpha \in [0, 2\pi)$ we have

$$\begin{aligned}\ker(D_{\bar{a}}F(v_\alpha, w_\alpha, 0)) &= \text{span} \{(\sin(\alpha)\varphi, -\cos(\alpha)\varphi)\}, \\ \text{ran}(D_{\bar{a}}F(v_\alpha, w_\alpha, 0)) &= \text{span} \{(\sin(\alpha)\varphi, -\cos(\alpha)\varphi)\}^{\perp L^2},\end{aligned}$$

with φ from (3.9).

Proof. We first prove that $D_{\bar{a}}F(v_\alpha, w_\alpha, 0)$ is Fredholm of index 0. For that, we use the splitting $D_{\bar{a}}F(v_\alpha, w_\alpha, 0) = A - K$ where the two operators $K : L^2(\mathbb{R}) \times L^2(\mathbb{R}) \rightarrow L^2(\mathbb{R}) \times L^2(\mathbb{R})$ and $A : L^2(\mathbb{R}) \times L^2(\mathbb{R}) \rightarrow L^2(\mathbb{R}) \times L^2(\mathbb{R})$ are given by

$$K \begin{pmatrix} \phi_1 \\ \phi_2 \end{pmatrix} := \begin{pmatrix} \frac{1}{d} \left(-\frac{d^2}{dx^2} + \frac{\zeta}{d}\right)^{-1} \left((3\tilde{v}^2 + \tilde{w}^2) \phi_1 + 2\tilde{v}(\tilde{w} + w^\infty)\phi_2 \right) \\ \frac{1}{d} \left(-\frac{d^2}{dx^2} + \frac{\zeta}{d}\right)^{-1} \left((\tilde{v}^2 + 3\tilde{w}^2) \phi_2 + 2\tilde{v}(\tilde{w} + w^\infty)\phi_1 \right) \end{pmatrix}$$

and

$$A \begin{pmatrix} \phi_1 \\ \phi_2 \end{pmatrix} := \begin{pmatrix} \phi_1 - \frac{1}{d} \left(-\frac{d^2}{dx^2} + \frac{\zeta}{d}\right)^{-1} \left((w^\infty)^2 \phi_1 \right) \\ \phi_2 - \frac{1}{d} \left(-\frac{d^2}{dx^2} + \frac{\zeta}{d}\right)^{-1} \left(3(w^\infty)^2 \phi_2 \right) \end{pmatrix}.$$

From the Fourier transform

$$\mathcal{F}\phi(k) = \int_{\mathbb{R}} \phi(x) e^{-ikx} dx,$$

we obtain that A is an isomorphism, if

$$\begin{pmatrix} 1 - \frac{(w^\infty)^2}{dk^2 + \zeta} & 0 \\ 0 & 1 - \frac{3(w^\infty)^2}{dk^2 + \zeta} \end{pmatrix}$$

is invertible for all $k \in \mathbb{R}$. This holds if $1 - \frac{3}{d}(w^\infty)^2 > 0$ or equivalently $\zeta - 3(w^\infty)^2 > 0$, which is true by Section 3.1. The equation $-u'' + \frac{\zeta}{d}u = h$ with $h \in L^2(\mathbb{R})$ is solved by $u(x) = c \int_{\mathbb{R}} e^{-|x-y|} h(y) dy$ with $c \in \mathbb{R}$. Hence, we observe that K is compact as the operator $L^2 \rightarrow L^2$, $f \mapsto \int_{\mathbb{R}} e^{-|x-y|} h(y) f(y) dy$ is compact for $h \in L^2(\mathbb{R})$ since it is a Hilbert-Schmidt operator due to

$$\int_{\mathbb{R}} \int_{\mathbb{R}} e^{-2|x-y|} (h(y))^2 dx dy = \tilde{c} \int_{\mathbb{R}} (h(y))^2 dy$$

for some $\tilde{c} \in \mathbb{R}$. Finally, $D_{\bar{a}}F(v_\alpha, w_\alpha, 0) = A - K$ is Fredholm of index 0 as a compact perturbation of an isomorphism. Furthermore, $D_{\bar{a}}F(v_\alpha, w_\alpha, 0)$ is self-adjoint and hence it is enough to prove the assertion for $\ker(D_{\bar{a}}F(v_\alpha, w_\alpha, 0))$. Let $\phi = (\phi_1, \phi_2) \in \ker(D_{\bar{a}}F(v_\alpha, w_\alpha, 0))$. Then, the formulas on the derivatives (3.11) and (3.12) yield

$$-\phi_1'' + \frac{\zeta}{d}\phi_1 = \frac{1}{d} \left(2\cos^2(\alpha) + 1 \right) \varphi^2 \phi_1 + \frac{2}{d} \sin(\alpha) \cos(\alpha) \varphi^2 \phi_2, \quad (3.15)$$

$$-\phi_2'' + \frac{\zeta}{d}\phi_2 = \frac{1}{d} \left(2\sin^2(\alpha) + 1 \right) \varphi^2 \phi_2 + \frac{2}{d} \sin(\alpha) \cos(\alpha) \varphi^2 \phi_1. \quad (3.16)$$

Multiplying (3.15) by $\cos(\alpha)$, (3.16) by $\sin(\alpha)$ and adding up the resulting equations, we observe

$$\begin{aligned} & \left(-\frac{d^2}{dx^2} + \frac{\zeta}{d}\right) (\cos(\alpha)\phi_1 + \sin(\alpha)\phi_2) \\ &= \cos(\alpha) \left(\frac{1}{d} (2\cos^2(\alpha) + 1) \varphi^2 \phi_1 + \frac{2}{d} \sin(\alpha) \cos(\alpha) \varphi^2 \phi_2\right) \\ & \quad + \sin(\alpha) \left(\frac{1}{d} (2\sin^2(\alpha) + 1) \varphi^2 \phi_2 + \frac{2}{d} \sin(\alpha) \cos(\alpha) \varphi^2 \phi_1\right) \\ &= \frac{3}{d} \varphi^2 (\cos(\alpha)\phi_1 + \sin(\alpha)\phi_2). \end{aligned}$$

We show in Section 4.1 that

$$\ker_{\mathcal{H}_r} \left(-\frac{d^2}{dx^2} + \frac{\zeta}{d} - \frac{3}{d} \varphi^2\right) = \{0\},$$

where $\ker_{\mathcal{H}_r}(-\frac{d^2}{dx^2} + \frac{\zeta}{d} - \frac{3}{d} \varphi^2)$ refers to the kernel of the differential operator on \mathcal{H}_r . Consequently, $\cos(\alpha)\phi_1 + \sin(\alpha)\phi_2 = 0$. Therefore, there exists a function $\phi_0 \in H^1(\mathbb{R})$ such that $\phi = (\sin(\alpha)\phi_0, -\cos(\alpha)\phi_0)$ and we get from (3.15)

$$\begin{aligned} \left(-\frac{d^2}{dx^2} + \frac{\zeta}{d}\right) (\sin(\alpha)\phi_0) &= \frac{1}{d} (2\cos^2(\alpha) + 1) \varphi^2 \sin(\alpha)\phi_0 - \frac{2}{d} \sin(\alpha) \cos(\alpha) \varphi^2 \cos(\alpha)\phi_0 \\ &= \frac{1}{d} \varphi^2 \sin(\alpha)\phi_0, \end{aligned}$$

as well as from (3.16)

$$\begin{aligned} \left(-\frac{d^2}{dx^2} + \frac{\zeta}{d}\right) (-\cos(\alpha)\phi_0) &= -\frac{1}{d} (2\sin^2(\alpha) + 1) \varphi^2 \cos(\alpha)\phi_0 + \frac{2}{d} \sin(\alpha) \cos(\alpha) \varphi^2 \sin(\alpha)\phi_0 \\ &= -\frac{1}{d} \varphi^2 \cos(\alpha)\phi_0. \end{aligned}$$

Due to positivity [15] (Theorem 8.38), $\varphi \in \mathcal{H}_r$ is the unique eigenfunction of $-\frac{d^2}{dx^2} + \frac{\zeta}{d} - \frac{1}{d} \varphi^2$ corresponding to the eigenvalue 0 (up to a constant factor) and therefore, $\phi_0 \in \text{span}\{\varphi\}$ implying $\phi \in \text{span}\{(\sin(\alpha)\varphi, -\cos(\alpha)\varphi)\}$. \square

This lemma allows us to prove the following result.

Theorem 3.6. *Let $\alpha \in [0, 2\pi)$ with $\alpha \notin \left\{\frac{\pi}{2}, \frac{3\pi}{2}\right\}$. Then there exists a neighborhood U of $(v_\alpha, w_\alpha, 0)$ in $\mathcal{H}_r \times \mathcal{H}_r \times \mathbb{R}$, such that all solutions (v, w, f) of (3.6) in U belong to \mathcal{T} . In particular, there is no bifurcation for $\alpha \notin \left\{\frac{\pi}{2}, \frac{3\pi}{2}\right\}$.*

Proof. From (3.13) and (3.14), we have for all $\alpha \in [0, 2\pi)$

$$D_f F(v_\alpha, w_\alpha, 0) = \left(\frac{2}{d\zeta} \sin(\alpha) \cos(\alpha), \frac{1}{d\zeta} (1 + 2\sin^2(\alpha))\right) \left(-\frac{d^2}{dx^2} + \frac{\zeta}{d}\right)^{-1} \varphi^2.$$

Hence,

$$\begin{aligned}
& \langle D_f F(v_\alpha, w_\alpha, 0), (\sin(\alpha)\varphi, -\cos(\alpha)\varphi) \rangle \\
&= \frac{1}{d\zeta} \langle (2\sin(\alpha)\cos(\alpha), 1 + 2\sin^2(\alpha)) \left(-\frac{d^2}{dx^2} + \frac{\zeta}{d} \right)^{-1} \varphi^2, (\sin(\alpha)\varphi, -\cos(\alpha)\varphi) \rangle \\
&= -\frac{1}{d\zeta} \cos(\alpha) \int_{\mathbb{R}} \varphi \left(-\frac{d^2}{dx^2} + \frac{\zeta}{d} \right)^{-1} \varphi^2 dx \neq 0
\end{aligned}$$

for $\alpha \notin \left\{ \frac{\pi}{2}, \frac{3\pi}{2} \right\}$, as $\varphi > 0$ and $\left(-\frac{d^2}{dx^2} + \frac{\zeta}{d} \right)^{-1} \varphi^2 > 0$. Then, by the previous lemma, $D_f F(v_\alpha, w_\alpha, 0) \notin \text{ran}(D_{\bar{a}} F(v_\alpha, w_\alpha, 0))$ and hence Theorem 3.3 proves there is no bifurcation for $\alpha \notin \left\{ \frac{\pi}{2}, \frac{3\pi}{2} \right\}$. \square

In the next theorems, we will prove that bifurcation from \mathcal{T} occurs for $\alpha \in \left\{ \frac{\pi}{2}, \frac{3\pi}{2} \right\}$. Moreover, we prove that the bifurcating branches only contain purely imaginary solutions for $0 < |f| < \frac{2\sqrt{3}}{9}\zeta^{3/2}$.

Theorem 3.7. *Let $d, \zeta > 0$, $0 < |f| < \frac{2\sqrt{3}}{9}\zeta^{3/2}$ and iw_i the purely imaginary and homoclinic solutions of (3.6) for $i = 1, 2$. Then, there exist open neighborhoods U of iw_i in \mathcal{H}_c and J of f in \mathbb{R} such that (3.6) is uniquely solvable in $U \times J$.*

Proof. Consider $G : \mathcal{H}_r \times \mathcal{H}_r \times \mathbb{R} \rightarrow L^2(\mathbb{R}) \times L^2(\mathbb{R})$ by

$$G(\tilde{v}, \tilde{w}, f) := \begin{pmatrix} -d\tilde{v}'' + \zeta\tilde{v} - \tilde{v}^3 - (\tilde{w} + w^\infty)^2\tilde{v} \\ -d\tilde{w}'' + \zeta\tilde{w} - \tilde{v}^2(\tilde{w} + w^\infty) - \tilde{w}^3 - 3\tilde{w}^2w^\infty - 3\tilde{w}(w^\infty)^2 \end{pmatrix}.$$

Then, by definition of \tilde{w}_i , we have

$$G(0, \tilde{w}_i, f) = 0$$

and

$$D_{\bar{a}}G(\tilde{v}, \tilde{w}, f)[\phi] = \begin{pmatrix} -d\phi_1'' + \zeta\phi_1 - 3\tilde{v}^2\phi_1 - (\tilde{w} + w^\infty)^2\phi_1 - 2(\tilde{w} + w^\infty)\tilde{v}\phi_2 \\ -d\phi_2'' + \zeta\phi_2 - 2\tilde{v}(\tilde{w} + w^\infty)\phi_1 - \tilde{v}^2\phi_2 - 3(\tilde{w}_i + w_i^\infty)^2\phi_2 \end{pmatrix}.$$

Hence

$$D_{\bar{a}}G(0, \tilde{w}_i, f)[\phi] = \begin{pmatrix} -d\phi_1'' + \zeta\phi_1 - (\tilde{w}_i + w_i^\infty)^2\phi_1 \\ -d\phi_2'' + \zeta\phi_2 - 3(\tilde{w}_i + w_i^\infty)^2\phi_2 \end{pmatrix}.$$

In Section 4.1, we prove that $\ker(D_{\bar{a}}G(0, \tilde{w}_i, f)) = \{0\}$ for $i = 1, 2$. Since $D_{\bar{a}}G(0, \tilde{w}_i, f)$ is Fredholm of index 0 (cf. proof of Theorem 4.11), it has a bounded inverse and thus the statement of the theorem follows from the Implicit Function Theorem. \square

The above theorem proves in particular that for $0 < |f| < \frac{2\sqrt{3}}{9}\zeta^{3/2}$, the purely imaginary solutions calculated in Section 3.1 are locally unique and given by two curves (f, iw_1) and (f, iw_2) .

Theorem 3.8. *Let $d, \zeta > 0$, $|f| < \frac{2\sqrt{3}}{9}\zeta^{3/2}$ and iw_i the purely imaginary and homoclinic solutions of (3.6) for $i = 1, 2$. Bifurcation from the curve of purely imaginary and homoclinic solutions occurs only for $f = 0$.*

Proof. Let $G : \mathcal{H}_r \times \mathcal{H}_r \times \mathbb{R} \rightarrow L^2(\mathbb{R}) \times L^2(\mathbb{R})$ such that $G(\tilde{v}, \tilde{z}, f) := F(\tilde{v}, \tilde{w}_i + \tilde{z}, f)$ with $F : \mathcal{H}_r \times \mathcal{H}_r \times \mathbb{R} \rightarrow L^2(\mathbb{R}) \times L^2(\mathbb{R})$ as above. Then, we have by Theorem 3.6 that there is no bifurcation for $f \neq 0$. Furthermore, $G(0, 0, f) = F(0, \tilde{w}_i, f) = 0$ for all $|f| < \frac{2\sqrt{3}}{9}\zeta^{3/2}$ and by Theorem 2.1, $\tilde{w}_i = \varphi$ for $f = 0$ with φ as in (3.9). As in Lemma 3.5, we obtain

$$\begin{aligned} \ker(D_{\bar{a}}G(0, 0, 0)) &= \ker(D_{\bar{a}}F(0, \varphi, 0)) = \text{span}\{(\varphi, 0)\}, \\ \text{ran}(D_{\bar{a}}G(0, 0, 0)) &= \text{ran}(D_{\bar{a}}F(0, \varphi, 0)) = \text{span}\{(\varphi, 0)\}^{\perp L^2}. \end{aligned}$$

Moreover,

$$D_{\bar{a}f}F(\tilde{v}, \tilde{w}, f)[\phi] = \begin{pmatrix} -\frac{1}{d} \left(-\frac{d^2}{dx^2} + \frac{\zeta}{d}\right)^{-1} \left(\frac{2(\tilde{w}+w^\infty)}{3(w^\infty)^2-\zeta}\phi_1 + \frac{2\tilde{v}}{3(w^\infty)^2-\zeta}\phi_2\right) \\ -\frac{1}{d} \left(-\frac{d^2}{dx^2} + \frac{\zeta}{d}\right)^{-1} \left(\frac{6(\tilde{w}+w^\infty)}{3(w^\infty)^2-\zeta}\phi_2 + \frac{2\tilde{v}}{3(w^\infty)^2-\zeta}\phi_1\right) \end{pmatrix}$$

and hence

$$D_{\bar{a}f}G(0, 0, 0)[(\varphi, 0)] = D_{\bar{a}f}F(0, \varphi, 0)[(\varphi, 0)] = \begin{pmatrix} -\frac{2}{3d\zeta} \left(-\frac{d^2}{dx^2} + \frac{\zeta}{d}\right)^{-1} \varphi^2 \\ 0 \end{pmatrix}.$$

Thus, $D_{\bar{a}f}G(0, 0, 0)[(\varphi, 0)] \notin \text{ran}(D_{\bar{a}}G(0, 0, 0))$, as

$$\langle D_{\bar{a}f}G(0, 0, 0), (\varphi, 0) \rangle = -\frac{2}{3d\zeta} \int_{\mathbb{R}} \varphi \left(-\frac{d^2}{dx^2} + \frac{\zeta}{d}\right)^{-1} \varphi^2 dx \neq 0$$

and Theorem 3.4 proves the assertion. \square

Remark 3.9. *As for $f = 0$ the bifurcating branch from the curve of purely imaginary and homoclinic solutions are exactly the solutions on \mathcal{T} , the theorems above prove in particular, that bifurcation from \mathcal{T} for $f = 0$ is only possible for $\alpha \in \left\{\frac{\pi}{2}, \frac{3\pi}{2}\right\}$ and that the bifurcating solutions are purely imaginary.*

4. LLE with Forcing and Damping

4.1. Nondegeneracy

In this section, we will show nondegeneracy of the purely imaginary homoclinic solutions iw_i for $i = 1, 2$, from Lemma 3.1, i.e., we will show that

$$\ker_{H^2} \left(-d \frac{d^2}{dx^2} + \zeta - Dg(iw_i) \right) = \text{span} \{i\tilde{w}'_i\}.$$

Here, $\ker_{H^2} \left(-d \frac{d^2}{dx^2} + \zeta - Dg(iw_i) \right)$ refers to the kernel of the differential operator on the domain $H^2(\mathbb{R})$ and $g(a) = |a|^2 a - if$, $Dg(a)z := \left. \frac{d}{dt} g(a + tz) \right|_{t=0} = 2|a|^2 z + a^2 \bar{z}$. Splitting the linearized operator $L := -d \frac{d^2}{dx^2} + \zeta - Dg(iw_i)$ into real and imaginary part and using $w_i = \tilde{w}_i + w_i^\infty$ with $\tilde{w}_i \in H^2(\mathbb{R})$ and $w_i^\infty := \lim_{|x| \rightarrow \infty} w_i(x)$, we get

$$L_1 := -d \frac{d^2}{dx^2} + \underbrace{\zeta - (w_i^\infty)^2 - 2w_i^\infty \tilde{w}_i - \tilde{w}_i^2}_{=:p(x)}$$

and

$$L_2 := -d \frac{d^2}{dx^2} + \underbrace{\zeta - 3(w_i^\infty)^2 - 6\tilde{w}_i w_i^\infty - 3\tilde{w}_i^2}_{=:q(x)}.$$

Observe that nondegeneracy is equivalent to the fact that $\ker_{H^2}(L_2) = \text{span} \{\tilde{w}'_i\}$ and $\ker_{H^2}(L_1) = \{0\}$.

As a first step, we need the following lemma (cf. Theorem 3.3 in [2]).

Lemma 4.1. *Let $r \in C(\mathbb{R})$ with $r(x) \geq a > 0$ for $x > R$. Then for any solution u of*

$$-u'' + ru = 0 \quad \text{on } \mathbb{R},$$

one of the following two limits holds

$$(a) \quad \lim_{x \rightarrow \infty} u(x) = 0,$$

$$(b) \quad \lim_{x \rightarrow \infty} |u(x)| = \infty.$$

A nontrivial solution satisfying the first condition is unique (up to a multiplicative factor).

Lemma 4.2. *Let $d, \zeta > 0$, $|f| < \frac{2\sqrt{3}}{9}\zeta^{3/2}$, $\phi_1 \in \ker_{H^2}(L_1)$ and $\phi_2 \in \ker_{H^2}(L_2)$. Then ϕ_1 and ϕ_2 are unique (up to a multiplicative factor).*

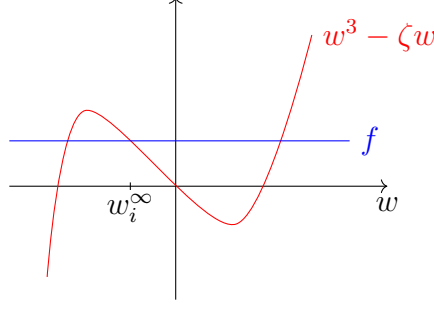


Figure 7: Property of w_i^∞ for $f > 0$.

Proof. $w_i^\infty = w^{(2)}$ solves the equation $w^3 - \zeta w = f$ and thus, $3(w_i^\infty)^2 - \zeta < 0$. Hence,

$$\lim_{x \rightarrow \infty} p(x) = \zeta - (w_i^\infty)^2 > \zeta - 3(w_i^\infty)^2 > 0$$

and

$$\lim_{x \rightarrow \infty} q(x) = \zeta - 3(w_i^\infty)^2 > 0.$$

Therefore, Lemma 4.1 proves the claim since

$$\lim_{x \rightarrow \infty} \phi_1(x) = \lim_{x \rightarrow \infty} \phi_2(x) = 0.$$

□

Lemma 4.3. *Let $d, \zeta > 0$ and $|f| < \frac{2\sqrt{3}}{9}\zeta^{3/2}$. Then*

$$\ker_{H^2}(L_2) = \text{span}\{\tilde{w}'_i\}.$$

Proof. To show that $\tilde{w}'_i \in \ker_{H^2}(L_2)$, we note that

$$\begin{aligned} & \left[-d \frac{d^2}{dx^2} + \zeta - 3(w_i^\infty)^2 - 6\tilde{w}_i w_i^\infty - 3\tilde{w}_i^2 \right] \tilde{w}'_i \\ &= -d \frac{d^2}{dx^2} \tilde{w}'_i + \zeta \tilde{w}'_i - 3(w_i^\infty)^2 \tilde{w}'_i - 6\tilde{w}_i w_i^\infty \tilde{w}'_i - 3\tilde{w}_i^2 \tilde{w}'_i \\ &= \frac{d}{dx} \left(-d \frac{d^2}{dx^2} \tilde{w}_i + \zeta \tilde{w}_i - 3(w_i^\infty)^2 \tilde{w}_i - 3\tilde{w}_i^2 w_i^\infty - \tilde{w}_i^3 \right) \\ &= \frac{d}{dx} \left(-d \frac{d^2}{dx^2} (\tilde{w}_i + w_i^\infty) + \zeta (\tilde{w}_i + w_i^\infty) - (\tilde{w}_i + w_i^\infty)^3 + f \right) \stackrel{(3.8)}{=} 0. \end{aligned}$$

As $\lim_{x \rightarrow \infty} \tilde{w}'_i = 0$, the solution is unique by the previous lemma (up to a multiplicative factor). □

For the following results, let $\phi_1 \in \ker_{H^2}(L_1)$ and split $\phi_1 := \phi_{1,even} + \phi_{1,odd}$ into even and odd part. Then we observe $\phi_{1,even}, \phi_{1,odd} \in \ker_{H^2}(L_1)$ with $\phi'_{1,even}(0) = 0$ and $\phi_{1,odd}(0) = 0$.

Lemma 4.4. *Let $d, \zeta > 0$, $|f| < \frac{2\sqrt{3}}{9}\zeta^{3/2}$ and $\phi_{1,even}, \phi_{1,odd}$ defined as above. Then either $\phi_{1,even} \equiv 0$ or $\phi_{1,even}$ has no zero on \mathbb{R} . Likewise, either $\phi_{1,odd} \equiv 0$ or $\phi_{1,odd}$ has exactly zero on \mathbb{R} at $x = 0$.*

Proof. We prove this lemma only for $i = 1$ and $\phi_{1,even}$. By Lemma 4.3, we know that

$$L_2\tilde{w}'_1 = 0. \quad (4.1)$$

Now, assume that $\phi_{1,even}$ had a first positive zero $x_0 > 0$, i.e., $\phi_{1,even}(x_0) = 0$. Then we can assume $\phi_{1,even} > 0$ on $(0, x_0)$. Since $\phi_{1,even}(x) \rightarrow 0$ as $x \rightarrow \infty$, there is $x_1 \in (x_0, \infty]$ such that $\phi_{1,even} < 0$ on (x_0, x_1) and $\lim_{x \rightarrow x_1} \phi_{1,even}(x) = 0$. Additionally, we observe

$$p(x) = \zeta - (w_1^\infty + \tilde{w}_1)^2 > \zeta - 3(w_1^\infty + \tilde{w}_1)^2 = q(x).$$

Multiplying (4.1) by $\phi_{1,even}$, $L_1\phi_{1,even} = 0$ by \tilde{w}'_1 and integrating the difference yields

$$\begin{aligned} 0 &= \int_{x_0}^{x_1} -d(\tilde{w}_1''' \phi_{1,even} - \phi_{1,even}'' \tilde{w}'_1) dx + \int_{x_0}^{x_1} \underbrace{(q-p)\tilde{w}'_1 \phi_{1,even}}_{\geq 0} dx \\ &\geq - \int_{x_0}^{x_1} d(\tilde{w}_1''' \phi_{1,even} - \phi_{1,even}'' \tilde{w}'_1) dx \\ &= - \int_{x_0}^{x_1} d \frac{d}{dx} (\tilde{w}_1'' \phi_{1,even} - \phi_{1,even}' \tilde{w}'_1) dx \\ &= -d \left[\tilde{w}_1'' \phi_{1,even} - \phi_{1,even}' \tilde{w}'_1 \right]_{x_0}^{x_1} \\ &= -d \left(\underbrace{\phi_{1,even}'(x_0)}_{<0} \underbrace{\tilde{w}'_1(x_0)}_{>0} - \underbrace{\phi_{1,even}'(x_1)}_{\geq 0} \underbrace{\tilde{w}'_1(x_1)}_{\geq 0} \right) > 0, \end{aligned}$$

which is a contradiction. Hence $\phi_{1,even}$ has no zero on \mathbb{R} . An almost identical argument applied to $\phi_{1,odd}$ proves that either $\phi_{1,odd} \equiv 0$ or $\phi_{1,odd}$ has no zero on $(0, \infty)$. \square

Lemma 4.5. *Let $d, \zeta > 0$ and $0 < |f| < \frac{2\sqrt{3}}{9}\zeta^{3/2}$. Then $\ker_{H^2}(L_1) = \{0\}$.*

Proof. We again prove this lemma only for $i = 1$ and assume for contradiction that there is a non-trivial solution $\phi_1 = \phi_{1,even} + \phi_{1,odd}$ of $L_1\phi_1 = 0$.

For the odd part, suppose $\phi_{1,odd}$ is not identically zero. Then $\phi_{1,odd} \in H_0^1((0, \infty); \mathbb{R})$ is w.l.o.g. a positive Dirichlet eigenfunction to the eigenvalue 0 of L_1 on $(0, \infty)$. Observe that $\tilde{w}'_1 \in H_0^1((0, \infty); \mathbb{R})$ is a positive Dirichlet eigenfunction of L_2 on $(0, \infty)$ corresponding to the smallest eigenvalue 0. We also have the following inequality between the quadratic forms of L_2 and L_1

$$b_{L_1}(\phi) = \int_0^\infty d(\phi')^2 + p\phi^2 dx > \int_0^\infty d(\phi')^2 + q\phi^2 dx = b_{L_2}(\phi)$$

for all $\phi \in H_0^1((0, \infty); \mathbb{R}) \setminus \{0\}$. Therefore, by the Poincaré min-max principle, we obtain a strict ordering between the Dirichlet eigenvalues of L_1 and L_2 , and hence, the smallest

Dirichlet eigenvalue of L_1 is strictly larger than the first Dirichlet eigenvalue of L_2 which is impossible. This implies $\phi_{1,odd} \equiv 0$.

Let us now consider the even part $\phi_{1,even}$. We know that $\phi_{1,even}$ has no zero on \mathbb{R} . Testing (3.2) with $\phi_{1,even}$ and integrating twice by parts, we obtain

$$\begin{aligned} 0 &\neq - \int_{\mathbb{R}} f \phi_{1,even} dx = \int_{\mathbb{R}} -d(\tilde{w}_1 + w_1^\infty)'' \phi_{1,even} + (\zeta - (\tilde{w}_1 + w_1^\infty)^2)(\tilde{w}_1 + w_1^\infty) \phi_{1,even} dx \\ &= \int_{\mathbb{R}} -d(\tilde{w}_1 + w_1^\infty) \phi_{1,even}' + (\zeta - (\tilde{w}_1 + w_1^\infty)^2)(\tilde{w}_1 + w_1^\infty) \phi_{1,even} dx = 0. \end{aligned}$$

This is a contraction, and hence, $\phi_{1,even} \equiv 0$. Together with $\phi_{1,odd} \equiv 0$, we finally see $\phi \equiv 0$. \square

Now the previous lemmas immediately prove the following theorem.

Theorem 4.6. *Let $d, \zeta > 0$, $|f| < \frac{2\sqrt{3}}{9}\zeta^{3/2}$ and $w_i = \tilde{w}_i + w_i^\infty$ the homoclinic solutions of Lemma 3.1. Then*

$$\ker_{H^2} \left(-d \frac{d^2}{dx^2} + \zeta - Dg(iw_i) \right) = \text{span} \{i\tilde{w}_i'\}.$$

Remark 4.7. *If we set the domain of the differential operator as \mathcal{H}_c we get $\ker_{\mathcal{H}_c}(-d \frac{d^2}{dx^2} + \tilde{\zeta} - Dg(iw_i)) = \{0\}$. This is true because \mathcal{H}_c only contains functions a with $a'(0) = 0$ so that $i\tilde{w}_i' \notin \mathcal{H}_c$ because (3.2) yields*

$$dw_i''(0) = \zeta w_i(0) - w_i(0)^3 + f.$$

The latter expression is non-zero since $w_i(0) \neq w^{(j)}$ for $j = 1, 2, 3$ where $w^{(1)}, w^{(2)}, w^{(3)}$ are the solutions of the algebraic equation (3.5) and hence the constant solutions of (3.2).

4.2. Calculating the equilibria

In the following, we calculate the equilibria, i.e., we want to determine $a^\infty = v^\infty + iw^\infty$ which satisfy the equation

$$(\zeta - i)a - |a|^2 a + if = 0, \tag{4.2}$$

or equivalently (v^∞, w^∞) which satisfy the system

$$0 = -\zeta v - w + v^3 + w^2 v, \tag{4.3}$$

$$0 = \zeta w - v - v^2 w - w^3 + f. \tag{4.4}$$

Lemma 4.8. Consider the equation

$$f^2x^3 - 2\zeta fx^2 + (1 + \zeta^2)x - f = 0. \quad (4.5)$$

Then $x \in \mathbb{R}$ is a solution of (4.5) if and only if $a^\infty = v^\infty + iw^\infty$ with $v^\infty = x$ and $w^\infty = -\zeta v^\infty + f(v^\infty)^2$ is a solution of (4.2).

Proof. Multiplying (4.3) by w and (4.4) by v and adding up the resulting equations leads to

$$v^2 + w^2 = fv \quad (4.6)$$

and inserting this relation into (4.3) yields

$$w = -\zeta v + fv^2. \quad (4.7)$$

Inserting (4.6) and (4.7) into (4.4) gives

$$\begin{aligned} 0 &= -v + \zeta(-\zeta v + fv^2) - (-\zeta v + fv^2) \cdot fv + f \\ &= -f^2v^3 + 2\zeta fv^2 - (1 + \zeta^2)v + f \end{aligned}$$

and with $x := v$, we get (4.5). □

Next, we will calculate the solutions of (4.5).

Lemma 4.9. For $f^2 \in \left(\frac{2}{27}\zeta(\zeta^2 + 9) - \frac{2}{27}(\zeta^2 - 3)^{3/2}, \frac{2}{27}\zeta(\zeta^2 + 9) + \frac{2}{27}(\zeta^2 - 3)^{3/2}\right)$ and $\zeta > \sqrt{3}$ equation (4.5) has 3 real solutions.

Proof. To calculate these solutions, we will use Cardano's formula. First, we will reduce it to a depressed cubic equation. To do so, let $x := z + \beta$, where $\beta \in \mathbb{R} \setminus \{0\}$ will be chosen later. Inserting this into the equation for x yields

$$\begin{aligned} 0 &= (z + \beta)^3 - \frac{2\zeta}{f}(z + \beta)^2 + \frac{1 + \zeta^2}{f^2}(z + \beta) - \frac{1}{f} \\ &= z^3 + \left(3\beta - \frac{2\zeta}{f}\right)z^2 + \left(3\beta^2 - \frac{4\beta\zeta}{f} + \frac{1 + \zeta^2}{f^2}\right)z + \beta^3 - \frac{2\zeta}{f}\beta^2 + \frac{1 + \zeta^2}{f^2}\beta - \frac{1}{f}. \end{aligned}$$

Choosing $\beta := \frac{2\zeta}{3f}$ gives

$$\begin{aligned} 0 &= z^3 + \left(3\left(\frac{2\zeta}{3f}\right)^2 - \frac{4\zeta}{f}\frac{2\zeta}{3f} + \frac{1 + \zeta^2}{f^2}\right)z + \left(\left(\frac{2\zeta}{3f}\right)^3 - \frac{2\zeta}{f}\left(\frac{2\zeta}{3f}\right)^2 + \frac{1 + \zeta^2}{f^2}\frac{2\zeta}{3f} - \frac{1}{f}\right) \\ &= z^3 + \underbrace{\left(-\frac{4\zeta^2}{3f^2} + \frac{1 + \zeta^2}{f^2}\right)}_{=:p}z + \underbrace{\left(-\frac{16\zeta^3}{27f^3} + \frac{1^2 + \zeta^2}{f^2}\frac{2\zeta}{3f} - \frac{1}{f}\right)}_{=:q}. \end{aligned}$$

Now, we can apply Cardano's formula to the equation

$$z^3 + pz + q = 0.$$

It is well-known that there are three real solutions if and only if $\Delta := \frac{q^2}{4} + \frac{p^3}{27} < 0$, cf. [22]. Indeed,

$$\begin{aligned} \Delta &= \frac{q^2}{4} + \frac{p^3}{27} \\ &= \frac{(2\zeta^3 + 18\zeta - 27f^2)^2}{4 \cdot 27^2 f^6} + \frac{(3 - \zeta^2)^3}{27^2 f^6}, \end{aligned}$$

and hence, there are three real solutions of (4.5) if and only if

$$f^2 \in \left(\frac{2}{27}\zeta(\zeta^2 + 9) - \frac{2}{27}(\zeta^2 - 3)^{3/2}, \frac{2}{27}\zeta(\zeta^2 + 9) + \frac{2}{27}(\zeta^2 - 3)^{3/2} \right).$$

□

We notice, that

$$-\frac{q}{2}\sqrt{-\frac{27}{p^3}} = \frac{2\zeta^3 + 18\zeta - 27f^2}{2(\zeta^2 - 3)^{3/2}}$$

and

$$2\zeta^3 + 18\zeta - 27f^2 < 2(\zeta^2 - 3)^{3/2}$$

by the condition on the discriminant Δ as well as

$$2\zeta^3 + 18\zeta - 27f^2 \geq 0 \quad \text{and} \quad 2(\zeta^2 - 3)^{3/2} > 0$$

which are also true by the condition on the discriminant $f^2 \leq \frac{2}{27}\zeta(\zeta^2 + 9)$ and by definition. Consequently

$$0 \leq -\frac{q}{2}\sqrt{-\frac{27}{p^3}} \leq 1. \tag{4.8}$$

Hence, the solutions given in the following lemma are well-defined.

Lemma 4.10. *For ζ, f, p, q as before, the solutions of (4.5) are given by*

$$\begin{aligned} x_1 &= -\sqrt{-\frac{4}{3}}p \cos\left(\frac{1}{3} \arccos\left(-\frac{q}{2}\sqrt{-\frac{27}{p^3}}\right)\right) + \frac{2\zeta}{3f}, \\ x_2 &= +\sqrt{-\frac{4}{3}}p \cos\left(\frac{1}{3} \arccos\left(-\frac{q}{2}\sqrt{-\frac{27}{p^3}}\right) + \frac{\pi}{3}\right) + \frac{2\zeta}{3f}, \\ x_3 &= +\sqrt{-\frac{4}{3}}p \cos\left(\frac{1}{3} \arccos\left(-\frac{q}{2}\sqrt{-\frac{27}{p^3}}\right) - \frac{\pi}{3}\right) + \frac{2\zeta}{3f}. \end{aligned}$$

with $x_1 \leq x_2 \leq x_3$.

Proof. Cardano's formula now gives

$$\begin{aligned} z_1 &= -\sqrt{-\frac{4}{3}p} \cos\left(\frac{1}{3} \arccos\left(-\frac{q}{2}\sqrt{-\frac{27}{p^3}}\right)\right), \\ z_2 &= +\sqrt{-\frac{4}{3}p} \cos\left(\frac{1}{3} \arccos\left(-\frac{q}{2}\sqrt{-\frac{27}{p^3}}\right) + \frac{\pi}{3}\right), \\ z_3 &= +\sqrt{-\frac{4}{3}p} \cos\left(\frac{1}{3} \arccos\left(-\frac{q}{2}\sqrt{-\frac{27}{p^3}}\right) - \frac{\pi}{3}\right), \end{aligned}$$

with $z_1 \leq z_2 \leq z_3$ or equivalently with $x_i = z_i + \frac{2\zeta}{3f}$ for $i = 1, 2, 3$ as in Lemma 4.9, this proves the assertion. \square

4.3. Continuation via the Implicit Function Theorem

In this section, we analyze for which values of ζ, f solitons of (1.1) exist for fixed $d > 0$. There is a rescaled version given by

$$-du'' + (\tilde{\zeta} - \varepsilon i)u - |u|^2 u + i\tilde{f} = 0, \quad \text{on } \mathbb{R}. \quad (4.9)$$

Namely, u solves (4.9) with $\tilde{\zeta}, \tilde{f}$ if and only if $a(x) := \varepsilon^{-1/2}u(\varepsilon^{-1/2}x)$ solves (1.1) on \mathbb{R} with $\zeta = \tilde{\zeta}\varepsilon^{-1}$ and $f = \tilde{f}\varepsilon^{-3/2}$. In the following (Theorem 4.11), we will show that for given $\tilde{\zeta}, \tilde{f}$, (4.9) has soliton solutions for all $\varepsilon \in [0, \varepsilon_{max})$. Hence, we know that for the pair (ζ, f) with

$$\zeta \in \left(\frac{\tilde{\zeta}}{\varepsilon_{max}}, \infty\right), \quad f = \frac{\tilde{f}}{\tilde{\zeta}^{3/2}}\zeta^{3/2},$$

(1.1) has a soliton solution.

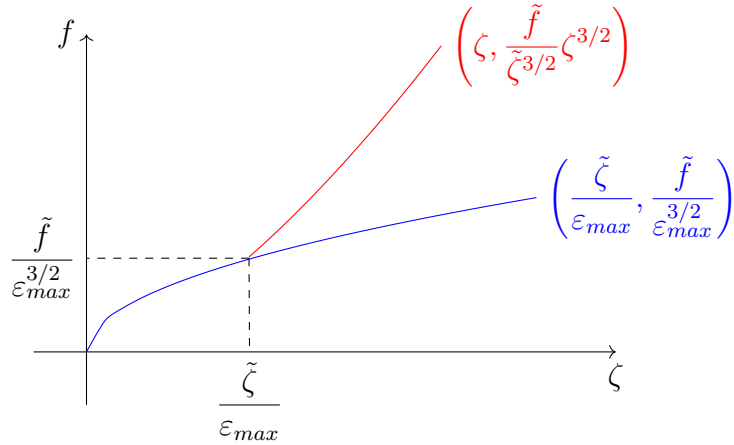


Figure 8: Illustration of lower envelope.

Varying $\tilde{\zeta}, \tilde{f}$, we get a lower envelope $\left(\frac{\tilde{\zeta}}{\varepsilon_{max}}, \frac{\tilde{f}}{\varepsilon_{max}^{3/2}}\right)$. Then our main result states that above this envelope solitons exist.

We first establish this result rigorously in Theorem 4.11. Afterwards, in Section 5, we show how to use this idea for a numerical algorithm to compute approximate soliton-type solutions.

If we define $g(x) := |x|^2 x$, we can rewrite (4.9) as

$$0 = -d\tilde{u}'' + \tilde{\zeta}\tilde{u} - \varepsilon i\tilde{u} - (g(\tilde{u} + u^\infty) - g(u^\infty)). \quad (4.10)$$

Now, we apply the Implicit Function Theorem to (4.10).

Theorem 4.11. *Let $d, \tilde{\zeta} > 0$ and $i\tilde{w}_i$ the purely imaginary solutions of Section 3 of (4.10) for $\varepsilon = 0$. Then there exist open neighborhoods U of $i\tilde{w}_i$ in \mathcal{H}_c , J of 0 in \mathbb{R} such that (4.10) is uniquely solvable for (\tilde{u}, ε) in $U \times J$.*

Proof. Define $H : \mathcal{H}_c \times \mathbb{R} \rightarrow \mathcal{L} = \{u \in L^2(\mathbb{R}; \mathbb{C}) : u(x) = u(-x)\}$ by

$$H(\tilde{u}, \varepsilon) := \left(-d\frac{d^2}{dx^2} + \tilde{\zeta}\right)\tilde{u} - \varepsilon i\tilde{u} - g(\tilde{u} + u^\infty) + g(u^\infty).$$

By definition of \tilde{w}_i , we have

$$H(i\tilde{w}_i, 0) = 0$$

and we define $L := D_{\tilde{u}}H(i\tilde{w}_i, 0) = -d\frac{d^2}{dx^2} + \tilde{\zeta} - Dg(i\tilde{w}_i + iw_i^\infty)$. By Remark 4.7,

$$\ker_{\mathcal{H}_c} \left(-d\frac{d^2}{dx^2} + \tilde{\zeta} - Dg(i\tilde{w}_i + iw_i^\infty)\right) = \{0\}.$$

Hence, $D_{\tilde{u}}H(i\tilde{w}_i, 0)$ is injective. Furthermore, L is self-adjoint and Fredholm of index 0 as a compact perturbation of an isomorphism, since $L_0 := -d\frac{d^2}{dx^2} + (\zeta - i - Dg(iw_i^\infty)) : H^2(\mathbb{R}) \rightarrow L^2(\mathbb{R})$ is an isomorphism and $K := Dg(i\tilde{w}_i) : H^2(\mathbb{R}) \rightarrow L^2(\mathbb{R})$ is compact. Indeed, consider $K_h : H^2(\mathbb{R}) \rightarrow L^2(\mathbb{R})$, $K_h\varphi := h\varphi$ for $h \in C_0^\infty(\mathbb{R})$. Then K_h is compact due to Sobolev embedding. By density, there exists a sequence $(h_n)_{n \in \mathbb{N}} \subset C_0^\infty(\mathbb{R})$ with $h_n \rightarrow Dg(i\tilde{w}_i)$ in $H^1(\mathbb{R})$. As $\|h_n - Dg(i\tilde{w}_i)\|_\infty \rightarrow 0$ for $n \rightarrow \infty$, this yields $\|(K_{h_n} - K)\varphi\| \leq \|h_n - Dg(i\tilde{w}_i)\|_\infty \|\varphi\|_{L^2}$ and hence $\|K_{h_n} - K\| \rightarrow 0$ and the

compactness of K . The self-adjointness follows as

$$\begin{aligned}
\langle Lz, \varphi \rangle &= \operatorname{Re} \int_{\mathbb{R}} (Lz) \bar{\varphi} \, dx \\
&= \operatorname{Re} \int_{\mathbb{R}} \left(-d \frac{d^2}{dx^2} z + \tilde{\zeta} z - Dg(i\tilde{w}_i + iw_i^\infty) z \right) \bar{\varphi} \, dx \\
&= \operatorname{Re} \int_{\mathbb{R}} \left(-d \frac{d^2}{dx^2} z + \tilde{\zeta} z - 2|i\tilde{w}_i + iw_i^\infty|^2 z + (i\tilde{w}_i + iw_i^\infty) \bar{z} \right) \bar{\varphi} \, dx \\
&= \operatorname{Re} \int_{\mathbb{R}} \left(-d \frac{d^2}{dx^2} \varphi + \tilde{\zeta} \varphi - 2|i\tilde{w}_i + iw_i^\infty|^2 \varphi + (i\tilde{w}_i + iw_i^\infty) \bar{\varphi} \right) \bar{z} \, dx \\
&= \operatorname{Re} \int_{\mathbb{R}} \left(-d \frac{d^2}{dx^2} \varphi + \tilde{\zeta} \varphi - Dg(i\tilde{w}_i + iw_i^\infty) \varphi \right) \bar{z} \, dx \\
&= \operatorname{Re} \int_{\mathbb{R}} (L\varphi) \bar{z} \, dx = \langle z, L\varphi \rangle.
\end{aligned}$$

Therefore, $L = D_{\tilde{u}}H(i\tilde{w}_i, 0) = L_0 - K$ has a bounded inverse and the statement follows from the Implicit Function Theorem. \square

Remark 4.12. Taking into account the rescaling $a(x) := \varepsilon^{-1/2}u(\varepsilon^{-1/2}x)$, the previous theorem proves in particular that for all $\varepsilon > 0$ sufficiently small, there are two even homoclinic solutions a of (4.9) with $\zeta = \tilde{\zeta}\varepsilon^{-1}$, $f = \tilde{f}\varepsilon^{-3/2}$ satisfying

$$\begin{aligned}
\left\| a - \lim_{|x| \rightarrow \infty} a(x) \right\|_{H^2} &= \left(\int_{\mathbb{R}} (a'')^2 + (a')^2 + (a - \lim_{|x| \rightarrow \infty} a(x))^2 \, dx \right)^{1/2} \\
&= \varepsilon^{-1/4} \left(\int_{\mathbb{R}} \frac{1}{\varepsilon^2} (u'')^2 + \frac{1}{\varepsilon} (u')^2 + (u - \lim_{|y| \rightarrow \infty} u(y))^2 \, dy \right)^{1/2} \\
&\geq \varepsilon^{-1/4} \left\| u - \lim_{|y| \rightarrow \infty} u(y) \right\|_{H^2} \rightarrow \infty
\end{aligned}$$

as $\varepsilon \rightarrow 0$.

Remark 4.13. The above theorem guarantees the existence of $\varepsilon_{max} > 0$ depending on $d, \tilde{\zeta}, \tilde{f}$ with the property that for $0 < \varepsilon < \varepsilon_{max}$ the parameter pair (ζ, f) with $\zeta = \tilde{\zeta}\varepsilon^{-1}$ and $f = \tilde{f}\varepsilon^{-3/2}$ allows for a localized solution of (4.9). Let us take $\varepsilon_{max} = \varepsilon_{max}(d, \tilde{\zeta}, \tilde{f})$ to be the largest value with the above property. Then we can consider the curve $(0, \varepsilon_{max}) \ni \varepsilon \mapsto (\tilde{\zeta}\varepsilon^{-1}, \tilde{f}\varepsilon^{-3/2})$ in the (ζ, f) -plane. By varying the parameters $\tilde{\zeta}$ and \tilde{f} these curves cover regions in the (ζ, f) -plane, such that above the lower envelope $(\tilde{\zeta}(\varepsilon_{max})^{-1}, \tilde{f}(\varepsilon_{max})^{-3/2})$ localized solutions of (1.1) exist.

The practical applicability of Theorem 4.11 is demonstrated in Section 5. However, at this point, we will give the brief idea how the proof of the theorem is the basis for a numerical continuation method with `pde2path`. The details on the implementation in `pde2path` can be found in Section 7.4. It is done by replacing the real line with the interval $[\pi, 2\pi]$ and by considering the rescaled version (4.9) of the Lugiato-Lefever equation

on $[\pi, 2\pi]$ with Neumann boundary conditions at the endpoints. Then, for a fixed value of $\tilde{\zeta}$ and $\tilde{f} = \varepsilon = 0$ the (shifted) approximate solution $i\sqrt{2\tilde{\zeta}} \left(\cosh \left((x - \pi)\sqrt{\tilde{\zeta}/d} \right) \right)^{-1}$ from Section 2 is continued first in \tilde{f} and then in ε , where we chose the purely imaginary solution due to Theorem 7.4. Rescaling $a(x) = \varepsilon^{-1/2}u(\varepsilon^{-1/2}(x - \pi))$ we obtain a function defined on $[\pi, (1 + \sqrt{\varepsilon})\pi]$ that we extend constantly to $[(1 + \sqrt{\varepsilon})\pi, 2\pi]$. The resulting function is mirrored on the vertical axis at $x = \pi$ so that an approximate 2π -periodic solution of (LLE) for parameter values $(\zeta, f) = (\tilde{\zeta}\varepsilon^{-1}, \tilde{f}\varepsilon^{-3/2})$ is found. Refining this solution with a Newton step yields a periodic soliton solution a solving (LLE) on $[0, 2\pi]$ for the parameters (ζ, f) . As an example, for fixed $d = 0.1$, $\tilde{\zeta} = 5$ we initially set $\tilde{f} = \varepsilon = 0$, and first continued the \cosh^{-1} -type soliton with respect to $\tilde{f} \in [0, 2.9]$. For fixed $\tilde{f} = 2.9$ the continuation is then done with respect to $\varepsilon \in [0, 1]$. The resulting solutions are shown in Figure 9. With $\varepsilon = 0.5$ the corresponding detuning and forcing values are $\zeta = \tilde{\zeta}\varepsilon^{-1} = 10$ and $f = \tilde{f}\varepsilon^{-3/2} = 8.20$. Similarly with $\varepsilon = 1$ the corresponding detuning and forcing values are $\zeta = \tilde{\zeta} = 5$ and $f = \tilde{f} = 2.9$.

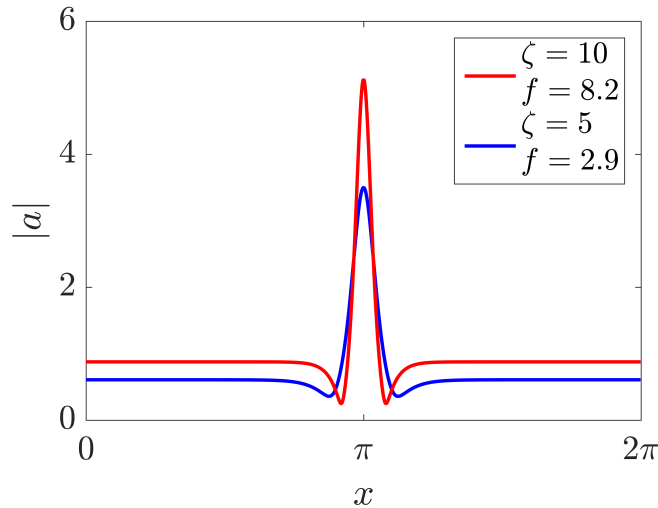


Figure 9: Solutions of (LLE).

We finish our discussion with a brief comment of the case $d < 0$ (normal dispersion), which we also discussed in [14]. Here, we also consider the rescaled equation and rewrite it in the form

$$-|d|u'' + (\varepsilon i - \tilde{\zeta})u + |u|^2 u - i\tilde{f} = 0 \quad \text{on } \mathbb{R}, \quad u(0) = 0. \quad (4.11)$$

For $\varepsilon = \tilde{f} = 0$ the solutions are given by $u(x) = e^{i\alpha}\varphi(x)$, where $\alpha \in [0, 2\pi)$ and

$$\varphi(x) = \sqrt{\tilde{\zeta}} \tanh \left(x\sqrt{\tilde{\zeta}(2|d|)^{-1}} \right).$$

Starting with $\varepsilon = 0$, we consider purely imaginary solutions for $|f| \geq 0$. The equilibria in the phase plane of Section 3.1 are the same as before, but due to $d < 0$ their character

changes. Now we have a center for $j = 2$ and two unstable saddles for $j = 1, 3$ and the unstable saddles are connected by two heteroclinic orbits. Going back to (4.11), we have for $\varepsilon = 0$ two heteroclinic solutions $u_1 = v_1 + iw_1, u_2 = v_2 + iw_2$ with $w'_1 > 0$ and $w'_2 < 0$ on \mathbb{R} . Moreover, $\lim_{x \rightarrow \infty} iw_1(x) = \lim_{x \rightarrow -\infty} iw_2(x) = iw^{(3)}$, $\lim_{x \rightarrow -\infty} iw_1(x) = \lim_{x \rightarrow \infty} iw_2(x) = iw^{(1)}$. For $\varepsilon > 0$ the unstable saddles persist and one might try to continue the heteroclinic solutions iw_1, iw_2 into the range $\varepsilon > 0$. Let us explain why the previous continuation argument fails in the case of iw_1 (the argument for iw_2 is the same). One could seek for heteroclinic solutions of the form

$$u = \tilde{u} + \psi_\varepsilon \quad \text{with } \tilde{u} \in H^2(\mathbb{R})$$

and where ψ_ε is a smooth given function of x , continuous in ε with

$$\psi_0 = iw_1 \quad \text{and} \quad \lim_{x \rightarrow \infty} \psi_\varepsilon(x) = u_\varepsilon^{(3)}, \quad \lim_{x \rightarrow -\infty} \psi_\varepsilon(x) = u_\varepsilon^{(1)},$$

where $u_\varepsilon^{(j)}$ are the equilibria of (4.11) for $\varepsilon > 0$. The implicit function continuation argument applied to

$$F(\tilde{u}, \varepsilon) = -|d|(\tilde{u} + \psi_\varepsilon)'' + \varepsilon i(\tilde{u} + \psi_\varepsilon) - g(\tilde{u} + \psi_\varepsilon)$$

would then provide \tilde{u} as a function of ε . Due to $\psi_0 = iw_1$, we have $F(0, 0) = 0$ and the linearized operator is given by $\frac{\partial F}{\partial \tilde{u}}(0, 0) = -|d|\frac{d^2}{dx^2} - \tilde{\zeta} + Dg(iw_1) : H^2(\mathbb{R}) \rightarrow L^2(\mathbb{R})$. Now there is the question of nondegeneracy of iw_1 . Since iw_1 is purely imaginary, $\frac{\partial F}{\partial \tilde{u}}(0, 0)$ decouples into two real-valued, self-adjoint operators

$$L_1 := \left(-|d|\frac{d^2}{dx^2} - \tilde{\zeta} + w_1^2(x) \right) : H^2(\mathbb{R}) \rightarrow L^2(\mathbb{R}), \quad (4.12)$$

$$L_2 := \left(-|d|\frac{d^2}{dx^2} - \tilde{\zeta} + 3w_1^2(x) \right) : H^2(\mathbb{R}) \rightarrow L^2(\mathbb{R}). \quad (4.13)$$

As $w^{(j)}$ solves $(-\tilde{\zeta} + w^2)w = f > 0$ for $j = 1, 2, 3$ and $w^{(1)} < 0 < w^{(3)}$, we see that $-\tilde{\zeta} + \lim_{x \rightarrow -\infty} w_1^2(x) = -\tilde{\zeta} + (w^{(1)})^2 < 0$ and $-\tilde{\zeta} + \lim_{x \rightarrow \infty} w_1^2(x) = -\tilde{\zeta} + (w^{(3)})^2 > 0$. Hence, we get for the essential spectrum of L_1 the relation

$$\sigma_{ess}(L_1) = [-\tilde{\zeta} + (w^{(1)})^2, \infty)$$

and $0 \in \sigma_{ess}(L_1)$. Unlike in the case of $d > 0$, L_1 is not a Fredholm operator and the nondegeneracy of the heteroclinic solution fails for $d < 0$.

5. Numerical experiments

In this section, we use numerical path continuation in a way as already foreshadowed in Section 4.3. The goal is to numerically calculate 2π -periodic solutions of (LLE) using the results of Sections 2 - 4. To do so, we need to replace the real line by the interval $[\pi, 2\pi]$ and consider the rescaled version (4.9) on $[\pi, 2\pi]$ with Neumann boundary conditions at the endpoints. Then for $d > 0$, set $\tilde{\zeta} > 0$ for $\tilde{f} = \varepsilon = 0$ and continue the approximate (shifted) solution $i\sqrt{2\tilde{\zeta}} \left(\cosh \left((x - \pi)\sqrt{\tilde{\zeta}/d} \right) \right)^{-1}$ of the NLS numerically in $\tilde{f} \in [0, \tilde{f}_0]$. Subsequently, we take all solutions for $\tilde{f} \in [0, \tilde{f}_0]$ and continue them in $\varepsilon \in [0, \varepsilon_0]$. This procedure is then repeated for all $\tilde{\zeta} \in (0, \tilde{\zeta}_0]$. Finally, all solutions are rescaled according to Section 4 by $a(x) := \varepsilon^{-1/2}u(\varepsilon^{-1/2}(x - \pi))$ and we obtain solutions of

$$-da'' + (\zeta - i)a - |a|^2 a + if = 0, \quad a'((1 - \sqrt{\varepsilon})\pi) = a'(\pi) = 0$$

with $\zeta = \frac{\tilde{\zeta}}{\varepsilon}$ and $f = \frac{\tilde{f}}{\varepsilon^{3/2}}$. Extending these solutions as constants to $[(1 + \sqrt{\varepsilon})\pi, 2\pi]$ and vertically reflecting at $x = \pi$ then yields approximate periodic solutions of (LLE). In Figure 10, the continuation routine for $\tilde{\zeta} = 5$ is shown. First the approximate solution on the NLS is continued in \tilde{f} . Subsequently fixing $\tilde{f} = 0.5$, we continue in ε .

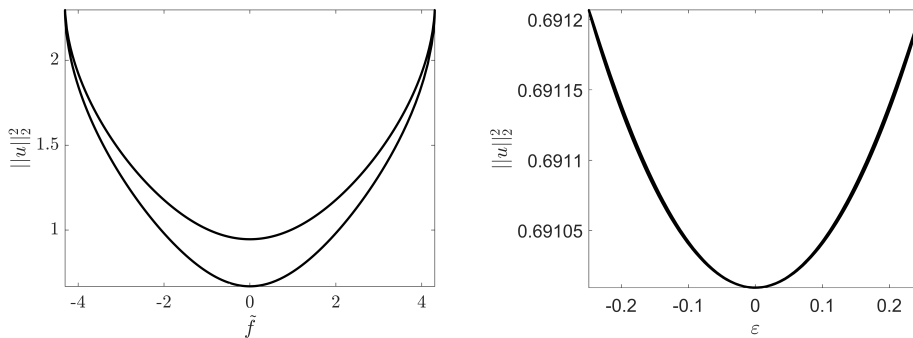


Figure 10: Continuation of the approximate solution in \tilde{f} and then in ε .

The approximate solutions found by this method are post-processed by a Newton step and spectral stability is checked. The results for $d = 0.01$ can be seen in Figure 12. Observe, that we can find spectrally stable soliton solutions as well as spectrally unstable soliton solutions, cf. Figure 11. In [42], orbital asymptotic stability of 2π -periodic solutions was investigated. This result particularly yields stability of our spectrally stable solutions and instability of our spectrally unstable solutions.

Let us briefly comment the shape of the continuation in \tilde{f} in Figure 10. Obviously for each \tilde{f} (with $\varepsilon = 0$), we find two solutions with different L^2 -norm. This is due to the phase plane analysis in Section 3.1, where, in the absence of damping, we always find two homoclinic orbits corresponding to one single $\tilde{f} < \frac{2\sqrt{3}}{9}\tilde{\zeta}^{3/2}$. These homoclinic orbits

serve as separatrices, with periodic solutions inside and outside. Our procedure described above uses the homoclinic orbits as an approximation to a 2π -periodic solution inside the homoclinic orbits. However, there is always another 2π -periodic solution outside the homoclinic orbit. These solutions can be found on the upper curve.

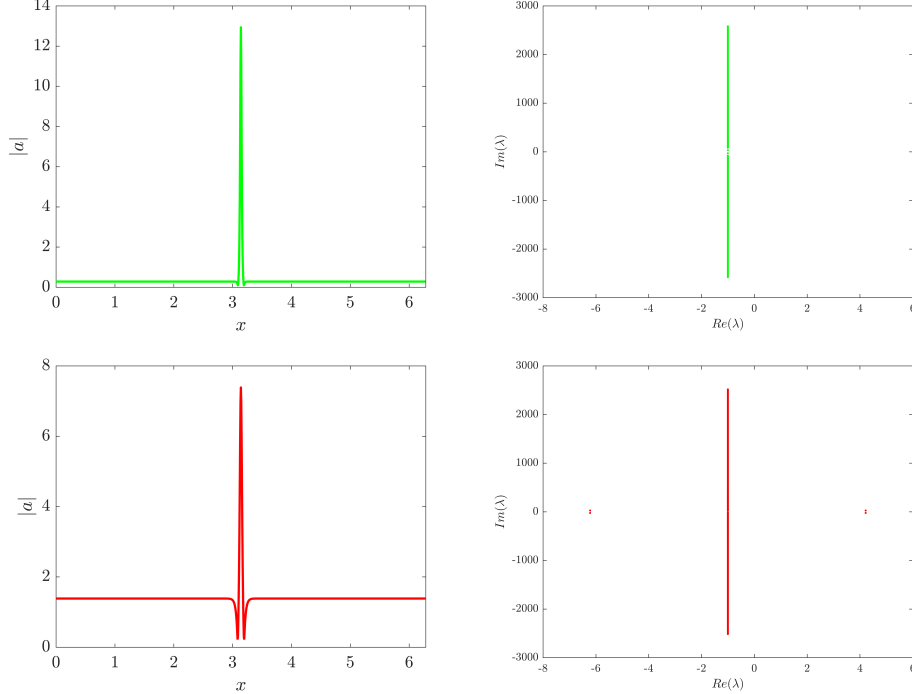


Figure 11: Top: Stable solution together with the spectrum of the linearization for $\zeta = \tilde{\zeta}\varepsilon^{-1} = 80$ and $f = \tilde{f}\varepsilon^{-3/2} = 23$. Bottom: Unstable solution together with the spectrum of the linearization for $\zeta = \tilde{\zeta}\varepsilon^{-1} = 20$ and $f = \tilde{f}\varepsilon^{-3/2} = 25$.

Our analysis in Section 4 was only valid for $\zeta > \sqrt{3}$ and

$$f^2 \in \left(\frac{2}{27}\zeta(\zeta^2 + 9) - \frac{2}{27}(\zeta^2 - 3)^{3/2}, \frac{2}{27}\zeta(\zeta^2 + 9) + \frac{2}{27}(\zeta^2 - 3)^{3/2} \right).$$

A result from [19] states that highly localized solutions on \mathbb{R} serve as good approximations for solutions of (LLE). Therefore, one could assume that f^2 should not exceed the region given above and we included these bounds as blue curves in Figure 12. Indeed, we observe that the upper bound coincides with our numerical results. However, the lower bound does not seem to be as good.

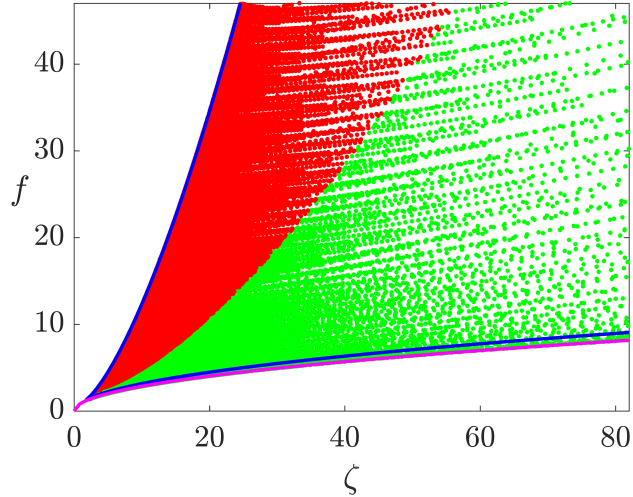


Figure 12: Soliton solutions found by continuation of an approximate solution of the NLS. The unstable solutions are marked in red, the stable solutions in green.

Yet, there is another lower bound

$$f^2 > \frac{8\zeta}{\pi^2} \quad \Leftrightarrow \quad \zeta < \frac{f^2\pi^2}{8}, \quad (5.1)$$

suggested in [19], which is only valid for large values of $\frac{f}{\sqrt{d}}$, as discussed in Section 8. This bound is also included in magenta in Figure 12 and seems to be more consistent with our numerical results.

In [29], a bound for non-existence of nontrivial solutions is given. For

$$\zeta > 6f^2(1 + 12f^2\pi^2d^{-1})^2 \quad (5.2)$$

nontrivial solutions cease to exist. As $\frac{f^2\pi^2}{8} < 6f^2(1 + 12f^2\pi^2d^{-1})^2$, these two bounds are compatible.

5.A. Details on the implementation

In this appendix, we comment some details on the implementation for the computation of the (ζ, f) -plane of this section. The idea is to consider the rescaled version

$$-du'' + (\tilde{\zeta} - \varepsilon i)u + |u|^2 u + i\tilde{f} = 0$$

on $[0, \pi]$ with homogeneous Neumann boundary conditions. For $\varepsilon = \tilde{f} = 0$ the approximate solutions $i\sqrt{2\tilde{\zeta}} \left(\cosh \left((x - \pi)\sqrt{\tilde{\zeta}/d} \right) \right)^{-1}$ of the NLS are first continued in \tilde{f} and then in ε in a systematic way, which leads to large areas in the (ζ, f) -planes with solutions of (LLE) by using the rescaling $\zeta = \tilde{\zeta}\varepsilon^{-1}$ and $f = \tilde{f}\varepsilon^{-3/2}$.

Algorithm 1 Computation of stable and unstable bright solitons

Input: $d = 0.01$, $\tilde{\zeta} > 0$, $\tilde{f} = \varepsilon = 0$

while $\tilde{\zeta} \leq \tilde{\zeta}_0$ **do**

 continue $i\sqrt{2\tilde{\zeta}} \left(\cosh \left((x - \pi)\sqrt{\tilde{\zeta}/d} \right) \right)^{-1}$ in f until fold point is found

 continue each of these solutions in ε until fold point is found

 rescale solutions and parameters

 extend solutions constantly and reflect at $x = \pi$

 Newton step

 check spectral stability

end while

indicate solutions in (ζ, f) -plane

Part III.
Bifurcation

6. Outline

In this third part, we will discuss (LLE) numerically using the `Matlab`-based toolbox `pde2path` for numerical path continuation and bifurcation.

In Section 7, we briefly discuss the functionality of `pde2path` based on numerical path continuation and present the main routines for continuation, switching of branches and fold continuation. Moreover, we implement the equation as a system in `pde2path` and present a first bifurcation diagram computed by the software. Furthermore we give some details on the implementation.

The results of Section 8 are published in [13] together with Philipp Trocha, Rainer Mandel, Christian Koos, Tobias Jahnke and Wolfgang Reichel. For anomalous dispersion $d > 0$ and for normal dispersion $d < 0$, we develop a heuristics in order to find the most localized soliton solutions using the bifurcation diagrams. Bright single solitons for $d > 0$ are found on the last bifurcating branch, when we number the bifurcation successively along the curve of constant solutions. Dark solitons for $d < 0$ are found on the first bifurcating branch. Using these heuristics, we define the properties *comb bandwidth* and *power conversion efficiency* for the corresponding frequency combs, which allows us to compare solitons for different values of d and f . For $d > 0$, we can compare our results to some known approximation formulas. This global study provides an overview on the structure of nontrivial solutions. We observe that for bright and for dark solitons the bandwidth increases with f whereas the power conversion efficiency decreases. Furthermore, we obtain that with $d \rightarrow 0$ the combwidth increases whereas the power conversion efficiency decreases. In direct comparison of bright and dark solitons, we will observe, that the bright solitons have a decreased combwidth along with a higher conversion efficiency for the same values of f . The approach presented within this parts, can also be extended to include additional effects as two photon absorption. These results allow a targeted design of soliton comb generators for specific applications.

7. pde2path and Numerical Path Continuation

The `Matlab` toolbox `pde2path` (cf. [10],[44]) is designed to numerically treat continuation and bifurcation of PDE systems.

For the discussion of numerical path continuation and bifurcation detection, the following definitions from [30] are very useful to discuss a discretized and therefore finite-dimensional problem.

Definition 7.1. *Let $F : \mathbb{R}^n \times \mathbb{R} \rightarrow \mathbb{R}^n$ be a C^1 -map.*

- *A point $(u_0, \lambda_0) \in \mathbb{R}^n \times \mathbb{R}$ is called regular, if $\text{rank}(DF(x)) = n$. Otherwise (u_0, λ_0) is called singular.*
- *$w \in \mathbb{R}^n$ is called a regular value of F , if (u_0, λ_0) is a regular point of F for all $(u_0, \lambda_0) \in F^{-1}(w)$. Otherwise w is called a singular value.*

Definition 7.2. *Let A be an $n \times (n + 1)$ -matrix with $\text{rank}(A) = n$. The unique vector $t = t(A) \in \mathbb{R}^{n+1}$ satisfying*

- $At = 0$,
- $\|t\| = 1$,
- $\det \begin{pmatrix} A \\ t^T \end{pmatrix} > 0$,

is called the tangent vector induced by A .

There are different ways to parametrize the set of regular solutions

$$\mathcal{L} := \{(u, \lambda) \in \mathbb{R}^n \times \mathbb{R} : F(u, \lambda) = 0, \text{rank}(DF(u, \lambda)) = n\}.$$

In `pde2path`, the so-called pseudo-arclength parametrization is used. If we assume that $(u_0, \lambda_0) \in \mathbb{R}^n \times \mathbb{R}$ is a regular solution of $F(u, \lambda) = 0$, then the Implicit Function Theorem yields the existence of a unique continuously differentiable function $s \mapsto c(s)$ such that $c(0) = (u_0, \lambda_0)$ and

$$\begin{aligned} F(c(s)) &= 0 \\ c(0) &= (u_0, \lambda_0) \end{aligned}$$

and $\|\dot{c}(s)\| \equiv 1$. According to [44], we choose a differentiable function $p : \mathbb{R}^n \times \mathbb{R} \times \mathbb{R} \rightarrow \mathbb{R}$, $(u, \lambda, s) \mapsto p(u, \lambda, s)$ such that

$$p(u_0, \lambda_0, 0) = 0 \tag{7.1}$$

and the extended Jacobian

$$\begin{pmatrix} DF(u_0, \lambda_0) \\ D_{(u,\lambda)}p(u_0, \lambda_0, 0)^T \end{pmatrix} \in \mathbb{R}^{(n+1) \times (n+1)} \quad \text{is not singular.} \quad (7.2)$$

In this case, the equation

$$p(u, \lambda, s) = 0$$

defines a parametrization of the solutions of $F(u, \lambda) = 0$ close to (u_0, λ_0) . This is described in the following lemma (cf. [30]).

Lemma 7.3. *Assume zero is a regular value of F and $(u_0, \lambda_0) \in \mathbb{R}^n \times \mathbb{R}$ is a solution of $F(u, \lambda) = 0$. Then under conditions (7.1) and (7.2), there exists an open neighborhood $J \subset \mathbb{R}$ of 0 and a uniquely defined function $c : J \rightarrow \mathbb{R}^n \times \mathbb{R}$, such that*

$$\begin{aligned} F(c(s)) &= 0, \\ p(c(s), s) &= 0. \end{aligned} \quad (7.3)$$

Remark 7.4. • *The parameter s is called pseudo-arclength.*

- *Lemma 7.3 yields a local parametrization of the solution curve.*

The question now is how to choose the function p in a way suitable for numerical path continuation. Differentiating (7.3) by s yields

$$\begin{aligned} DF(c(s)) \cdot \dot{c}(s) &= 0 \\ D_{(u,\lambda)}p(c(s), s) \cdot \dot{c}(s) + D_s p(c(s), s) &= 0 \end{aligned}$$

and the lower equation can be rewritten

$$-\frac{D_{(u,\lambda)}p(c(s), s)}{D_s p(c(s), s)} \cdot \dot{c}(s) = 1$$

if $D_s p(c(s), s) \neq 0$. Therefore, c is a solution of the initial value problem

$$\dot{c} = \begin{pmatrix} DF(c) \\ -\frac{D_{(u,\lambda)}p(c,\cdot)}{D_s p(c,\cdot)} \end{pmatrix}^{-1} \begin{pmatrix} 0 \\ 1 \end{pmatrix}, \quad c(0) = (u_0, \lambda_0). \quad (7.4)$$

If we consider the initial value problem

$$\dot{\tilde{c}} = t(DF(\tilde{c})) = \begin{pmatrix} DF(c) \\ -t(DF(c))^T \end{pmatrix}^{-1} \begin{pmatrix} 0 \\ 1 \end{pmatrix}, \quad \tilde{c}(0) = (u_0, \lambda_0), \quad (7.5)$$

the solution curve $s \mapsto c(s)$ parametrized by pseudo-arclength is indeed a valid approximation to the solution curve $s \mapsto \tilde{c}(s)$ parametrized by arclength due to Theorems 3 and 4 in [3].

For a given s_0 , a point $(u_0, \lambda_0) := (u(s_0), \lambda(s_0))$ and additionally knowing a tangent vector $\tau_0 := (\dot{u}_0, \dot{\lambda}_0) := \frac{d}{ds}(u(s), \lambda(s))|_{s=s_0}$, `pde2path` uses the following pseudo-arclength parametrization for s near s_0

$$p(u, \lambda, s) := \xi[\dot{u}_0 \cdot (u - u_0)] + (1 - \xi)\dot{\lambda}_0(\lambda - \lambda_0) - (s - s_0) = 0$$

with weight $0 < \xi < 1$.

7.1. cont

The main routine concerning numerical path continuation in `pde2path` is `cont`. Using this routine, one can perform a predefined number of path continuation steps `msteps`. Given a starting point (u_0, λ_0) and a tangent direction τ_0 , `pde2path` performs a predictor corrector algorithm to compute further points on this branch. Here an Euler predictor with tangent vector τ_0 is used, i.e.,

$$(\tilde{u}_{l+1}, \tilde{\lambda}_{l+1}) = (u_l, \lambda_l) + ds \cdot \tau_0$$

with stepsize ds . Subsequently, a Newton-corrector is performed, i.e.,

$$\begin{pmatrix} u_{l+1} \\ \lambda_{l+1} \end{pmatrix} = \begin{pmatrix} \tilde{u}_{l+1} \\ \tilde{\lambda}_{l+1} \end{pmatrix} - A(\tilde{u}_{l+1}, \tilde{\lambda}_{l+1})^{-1} H(\tilde{u}_{l+1}, \tilde{\lambda}_{l+1}) \quad (7.6)$$

with

$$A := DH = \begin{pmatrix} D_u F & D_\lambda F \\ \xi \dot{u}_0 & (1 - \xi) \dot{\lambda}_0 \end{pmatrix}.$$

Theoretically, this is only possible if A is not singular. Therefore, this routine does not work at possible bifurcation points. However, in principle, path continuation methods shoot past singular points of A . Therefore, for the detection of bifurcation points, we use the following criterion: We will call $(u(s_0), \lambda(s_0)) = (u_0, \lambda_0)$ a simple bifurcation point if $\det(A)$ changes sign in (u_0, λ_0) and implicitly assume that this happens if a simple eigenvalue of A crosses zero.

If the user sets `p.sw.bifcheck=1`, `cont` calls the function `bifdetec` which checks whether a simple bifurcation point was crossed during the last predictor corrector step, i.e., whether $\det(A)$ changed sign. This excludes fold points, where an eigenvalue of A reaches zero but does not change sign, see [23]. If a bifurcation point is detected, the location is refined using a bisection method.

Finally, depending on the residual, the step size is adapted and subsequently, the new tangent in (u_{l+1}, λ_{l+1}) is calculated.

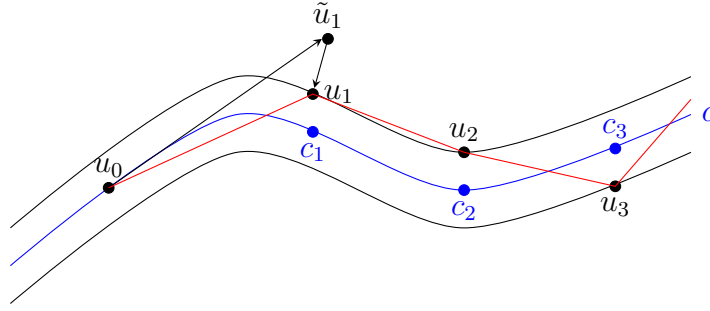


Figure 13: Idea of predictor corrector method: The red curve is the numerical approximation to the true solution curve c . Starting from u_0 the Euler predictor calculates a first approximation \tilde{u}_1 and the Newton corrector yields u_1 .

Algorithm 2 cont

Input: (u_0, λ_0, τ_0) , `msteps`

while `steps < msteps` **do**

 Predictor: $(u_1, \lambda_1) = (u_0, \lambda_0) + ds \cdot \tau_0$

 Corrector: Iterate (7.6) until convergence

if `p.sw.bifcheck=1` **then**

 Call `bifdetec`

end if

 Adapt step size

 Calculate new tangent τ_1 and set $(u_0, \lambda_0, \tau_0) = (u_1, \lambda_1, \tau_1)$

end while

7.2. swibra

Calling the function `swibra`, the user can switch to the bifurcating branch. Hence, one has to compute the new tangent τ_0 . In order to do this, one needs to differentiate the unknown bifurcating branch with respect to the pseudo-arclength s . `pde2path` uses "Method I" from [23] (Section 5.26) as this method does not need the parametrization of the bifurcating branch. We will briefly recall this method.

Having found a simple bifurcation point $(u(s_0), \lambda(s_0)) = (u_0, \lambda_0)$, assume that $\phi \in \ker D_u F(u_0, \lambda_0)$. Now choose $\phi_0 \in \mathbb{R}^n$ such that

$$D_u F(u_0, \lambda_0) \phi_0 + D_\lambda F(u_0, \lambda_0) = 0 \tag{7.7}$$

with $\phi^T \phi_0 = 0$. With this, we split $\text{ran}(D_u F(u_0, \lambda_0))$ in two orthogonal complements. Differentiating F twice with respect to s yields

$$\begin{aligned} \frac{d^2}{ds^2} F(u(s), \lambda(s)) \Big|_{s=s_0} &= D_u F(u_0, \lambda_0) \ddot{u}_0 + D_\lambda F(u_0, \lambda_0) \ddot{\lambda}_0 + D_{uu} F(u_0, \lambda_0) [\dot{u}_0, \dot{u}_0] \\ &\quad + 2D_{u\lambda} F(u_0, \lambda_0) \dot{u}_0 \dot{\lambda}_0 + D_{\lambda\lambda} F(u_0, \lambda_0) \dot{\lambda}_0^2 = 0. \end{aligned} \quad (7.8)$$

Splitting \dot{u}_0 into a component in $\ker(D_u F(u_0, \lambda_0))$ and a component in $\text{ran}(D_u F(u_0, \lambda_0))$, the ansatz

$$\begin{aligned} \dot{\lambda}_0 &= \beta \\ \dot{u}_0 &= \alpha \phi + \beta \phi_0 \end{aligned}$$

with $\alpha, \beta \in \mathbb{R}$ is chosen. Inserting this in (7.8) and multiplying the resulting equation from the left by ψ^T where $\psi \in \ker((D_u F(u_0, \lambda_0))^*)$, we obtain

$$\begin{aligned} 0 &= \psi^T D_{uu} F(u_0, \lambda_0) [\phi, \phi] \alpha^2 + 2\psi^T (D_{uu} F(u_0, \lambda_0) [\phi_0, \phi] + D_{u\lambda} F(u_0, \lambda_0) \phi) \alpha \beta \\ &\quad + \psi^T (D_{uu} F(u_0, \lambda_0) [\phi_0, \phi_0] + 2D_{u\lambda} F(u_0, \lambda_0) \phi_0 + D_{\lambda\lambda} F(u_0, \lambda_0)) \beta^2, \end{aligned}$$

where $\psi^T D_u F(u_0, \lambda_0) \ddot{u}_0 = 0$ as $\psi \in \ker((D_u F(u_0, \lambda_0))^*)$ and $\psi^T D_\lambda F(u_0, \lambda_0) \ddot{\lambda}_0 = 0$ due to (7.7) together with $\psi \in \ker((D_u F(u_0, \lambda_0))^*)$.

From this equation, **swibra** approximates α, β and hence $\dot{u}_0, \dot{\lambda}_0$. Finally, we get an approximation for the tangential vector τ_0 of the bifurcating branch.

7.3. Fold continuation

As turning points (=fold points, where $\dot{\lambda}(s_0) = 0$) in bifurcation diagrams are of special interest, we used fold continuation a lot during the computation of the results presented in the following sections. Thus, we will give a short introduction. In order to perform a fold continuation, one needs an additional free parameter, e.g. $\Lambda := (\lambda, \mu)$. We consider the extended system

$$H(u, \phi, \Lambda) = \begin{pmatrix} F(u, \Lambda) \\ D_u F(u, \Lambda) \phi \\ \|\phi\|_{L^2}^2 - 1 \\ p(u, \phi, \Lambda, s) \end{pmatrix} = 0 \quad (7.9)$$

and its Jacobian

$$DH(u, \phi, \Lambda) = \begin{pmatrix} D_u F & 0 & D_\Lambda F \\ D_{uu} F \phi & D_u F & D_{\Lambda u} F \phi \\ 0 & 2\phi^T & 0 \\ \xi \dot{u}^T & \xi \dot{\phi}^T & (1 - (\xi + \xi_q)/2) \dot{\Lambda} \end{pmatrix},$$

where $\phi \in \ker(D_u F)$ with $\|\phi\|_{L^2} = 1$ by the third equation of (7.9) and the fourth equation yields the pseudo-arclength equation

$$\begin{aligned} p(u, \phi, \Lambda, s) &:= \xi[\dot{u}_0 \cdot (u - u_0)] + \xi_q[\dot{\phi}_0 \cdot (\phi - \phi_0)] + \left(1 - \frac{\xi + \xi_q}{2}\right) \dot{\Lambda}_0(\Lambda - \Lambda_0) - (s - s_0) \\ &= 0 \end{aligned}$$

with weights ξ and ξ_q . The matrices $D_u F$ and $D_{uu} F \phi$ can either be calculated numerically or assembled by the user. However, as the calculation is very costly and admits numerical errors, we assembled it by hand in our cases, cf. Section 7.4. The derivatives with respect to Λ are calculated by the toolbox via finite differences.

Having found a fold point, calling `spcontini`, the user can start a fold continuation. After a predefined number of steps with the function `cont`, calling `spcontexit`, one can switch back to regular continuation.

7.4. First example of bifurcation diagrams of LLE

In this section, we will explain how the Lugiato-Lefever equation is implemented. The goal is to numerically find the bifurcation points and bifurcating branches, described in [29]. We will consider the Lugiato-Lefever equation as the system

$$\begin{aligned} -dv'' &= -w - \zeta v + (v^2 + w^2)v, \\ -dw'' &= v - \zeta w + (v^2 + w^2)w - f, \end{aligned}$$

on $[0, \pi]$ with homogeneous Neumann boundary conditions. For the implementation in `pde2path`, we rewrite the system in the form

$$F(U, \zeta) = F(v, w, \zeta) = 0 \tag{7.10}$$

where $U = (v, w)$ and

$$F(v, w, \zeta) := \begin{pmatrix} -dv'' + w + \zeta v - (v^2 + w^2)v \\ -dw'' - v + \zeta w - (v^2 + w^2)w + f \end{pmatrix}.$$

The nonlinearity

$$g = g(v, w, \zeta) := \begin{pmatrix} -w - \zeta v + (v^2 + w^2)v \\ v - \zeta w + (v^2 + w^2)w - f \end{pmatrix}$$

is implemented in `nodalf.m` with $v(\cdot) = \mathbf{u}(1:p.np)$, $w(\cdot) = \mathbf{u}(p.np+1:2*p.np)$.

We present a simple example, where we use ζ as the active continuation and bifurcation parameter for fixed values of $d = 0.1$ and $f = 2$. These parameters have been chosen due to illustrative reasons. We start the continuation procedure from a constant approximate

solution (v_0, w_0) for $\zeta = -0.5$. Given this starting point, `pde2path` begins with the continuation algorithm and checks whether a bifurcation point is crossed.

The constant solution branch is indicated in black in Figure 14. During the continuation process, we find 16 bifurcation points. Switching to the bifurcating branches and starting another continuation routine, we observe that some of the bifurcating branches return to the constant solution branch at some other bifurcation point and some branches return to another branch of nontrivial solutions.

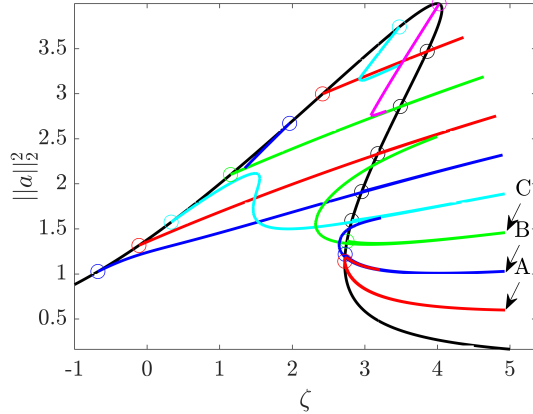


Figure 14: Bifurcation diagram for $d = 0.1$, $f = 2$.

This observation is proven in part (c) of Theorem 1 in [29] and follows from Rabinowitz' global bifurcation theorem from [39] together with a priori bounds. Furthermore, this theorem guarantees that we have found all bifurcation points. In Figure 14, a complete picture of all branches bifurcating from the trivial branch is shown and the bifurcating branches are illustrated as colored lines. The solutions at labels A, B and C can be seen in Figure 15.

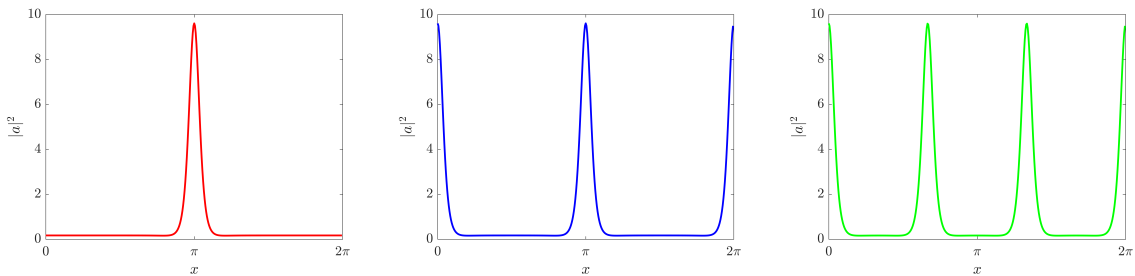


Figure 15: 1-soliton, 2-soliton and 3-soliton found at labels A, B and C in Figure 14.

8. Soliton Quality

Based on Section 7.4, we present a global bifurcation study of the LLE, covering a large parameter range for d and f . The results of this section have been published in [13]. Our analysis comprises both bright-soliton states in resonators with anomalous group-velocity dispersion (GVD) [19] as well as dark solitons that form in the presence of normal GVD [46]. For both types of combs, we classify branches associated with single and multi-soliton states and characterize the broadest frequency combs by their optical bandwidth as well as by the pump-to-comb power transfer efficiency. Our bifurcation analysis hence allows determining and systematically optimizing the performance of Kerr comb generators in integrated photonic systems, which is of significant importance for industrial adoption of these devices. As in Section 7.4, we consider solutions $a : [0, \pi] \rightarrow \mathbb{C}$ of the Lugiato-Lefever equation on $[0, \pi]$ of LLE with Neumann boundary conditions

$$-da'' + (\zeta - i)a - |a|^2 a + if = 0, \quad a'(0) = a'(\pi) = 0 \quad (8.1)$$

and reflecting a solution in an even way around $x = \pi$ yields a 2π -periodic solution. In Fourier modes the solution is represented as $a(x) = \sum_{k \in \mathbb{Z}} \hat{a}_k e^{ikx}$ with $\hat{a}_{-k} = \hat{a}_k$. The intracavity power of the field is given by the square of the L^2 -norm $\|a\|_2^2 := \sum_{k \in \mathbb{Z}} |\hat{a}_k|^2 = \frac{1}{2\pi} \int_0^{2\pi} |a|^2 dx$.

For simplicity of the presentation, we assume that the trivial solution a_0 can be parametrized (locally) as $a_0 = a_0(\zeta)$. However, as discussed in [29], this fails only at the turning points of the trivial curve, which does not lead to any undesirable effect.

The analysis of this section, particularly Theorem 8.1, is based on Theorem 10.1 in Part IV in the case $\kappa = 0$.

8.1. Bifurcation analysis for the LLE

We will prove in Lemma 10.5 in Part IV with $\kappa = 0$ that bifurcation can only occur if there is an integer $k \in \mathbb{N}$ such that

$$(\zeta_0 + dk^2)^2 - 4|a_0(\zeta_0)|^2(\zeta_0 + dk^2) + 1 + 3|a_0(\zeta_0)|^4 = 0. \quad (8.2)$$

Solving (8.2) yields

$$k_{1,2} := \sqrt{\frac{2|a_0(\zeta_0)|^2 - \zeta_0 \pm \sqrt{|a_0(\zeta_0)|^4 - 1}}{d}}. \quad (8.3)$$

The k -value obtained by evaluating the expression on the right side of (8.3) defines the periodicity $2\pi/k$ of the solutions on the bifurcating branch close to the bifurcation point. Equations (8.2) and (8.3) naturally occur in bifurcation studies of the Lugiato-Lefever equation. In [16], for instance, bifurcations are considered from the point of

view of spatial dynamics both for normal and anomalous dispersion, and parameter regimes are determined where patterned soliton states bifurcate from trivial solutions. In [35], a similar approach is taken to study bifurcation of dark solitons from trivial solutions in the normal dispersion regime. In both of these works bifurcations with respect to the forcing parameter f are studied and 2π -periodicity of the solutions is neglected. In contrast, our work takes into account 2π -periodicity and our goal is to find a global picture of all branches bifurcating with respect to the detuning ζ , whose physical accessible parameter space is usually larger than the parameter space for f . With the help of (8.3), we formulate the following version of the bifurcation result Theorem 10.1 for $\kappa = 0$. The curve $(\zeta, a_0(\zeta))$ of constant solutions is shown in black in Figure 16(a) and (d) for $f = 2$.

Theorem 8.1. *For a point $P = (\zeta_0, a_0(\zeta_0))$ on the curve of trivial solutions the following is true:*

- (i) *If exactly one of the two numbers $k_{1,2}$ from (8.3) is an integer and if the transversality condition*

$$2|a_0(\zeta_0)|^4(|a_0(\zeta_0)|^2 - \zeta_0) \mp (1 + \zeta_0^2 - |a_0(\zeta_0)|^4)\sqrt{|a_0(\zeta_0)|^4 - 1} \neq 0 \quad (8.4)$$

holds with “−” if $k_1 \in \mathbb{N}$ and “+” if $k_2 \in \mathbb{N}$, then P is a bifurcation point for (8.1).

- (ii) *If neither k_1 nor k_2 is an integer, then P is not a bifurcation point for (8.1), and near P only trivial solutions of (8.1) exist.*

In the remaining cases, where either the condition (8.4) fails or both k_1 and k_2 are integers, no statement is made.

For the cases $f = 2$, $d = \pm 0.1$, we have computed the bifurcation points determined by (8.2) with `pde2path`, as explained in Section 7. The computed bifurcation points are marked by circles in Figure 16(a) and (d) for $d = 0.1$ and $d = -0.1$ respectively. In case (i) of the above theorem, we may apply Rabinowitz’ global bifurcation theorem from [39]. It says not only that $(\zeta_0, a_0(\zeta_0))$ is a bifurcation point, but that we can obtain a branch of nontrivial solutions bifurcating from the trivial branch at the bifurcation point $(\zeta_0, a_0(\zeta_0))$ and returning either to the trivial branch at some other bifurcation point or to another branch of nontrivial solutions, cf. [29]. We also checked for all bifurcation points which one of the numbers $k_{1,2}$ in (8.3) is an integer and whether the transversality condition (8.4) holds, cf. Table 1.

In Figure 16(a), a complete picture of all branches bifurcating from the trivial branch is shown for $d = 0.1$. The branches were computed by the `pde2path` (cf. [44, 10]). For the example given in Figure 16, all bifurcation points were reproduced by `pde2path`. Bifurcation branches determined by `pde2path` are shown additionally in Figure 16(a) as colored lines. Here, the single soliton branch ($k = 1$) is highlighted in red. Blue branches

are related to higher order soliton frequency combs ($k = 2 \dots 8$). In Figure 16(d), the same procedure is performed for $d = -0.1$ and the single dark soliton branch is again marked in red.

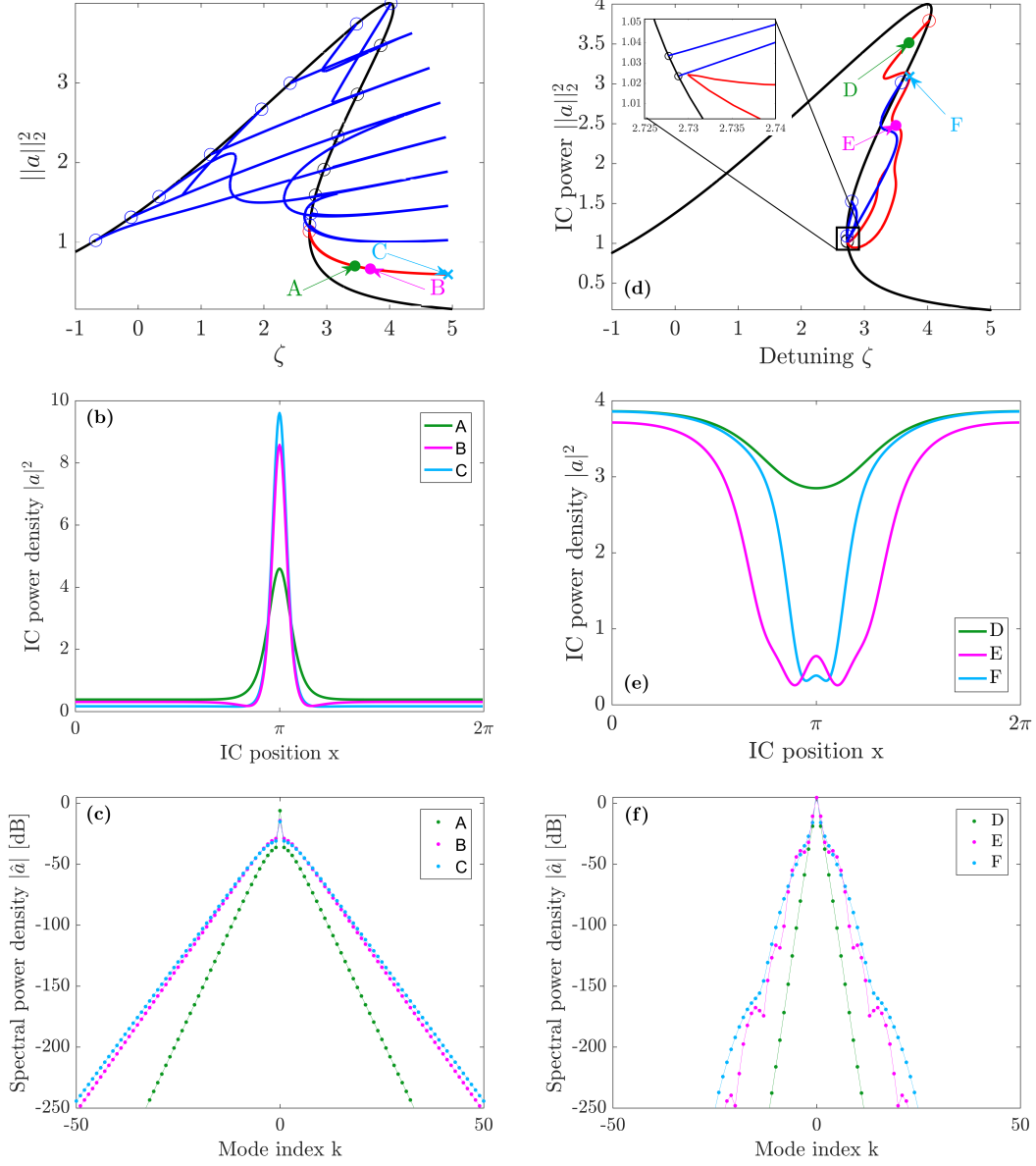


Figure 16: Bifurcation diagram of (8.1) for $f = 2$ and $d = 0.1$ (left) and for $f = 2$ and $d = -0.1$ (right), corresponding solutions and frequency combs.

ζ_0	$a_0(\zeta_0)$	k_1	k_2	Transv.
-0.6770	0.51 + 0.87i	5.44	5	3.67
-0.1117	0.66 + 0.94i	6	4.35	5.56
0.3325	0.79 + 0.98i	6.35	4	4.49
1.1508	1.05 + 1.00i	7	3.47	12.26
1.9646	1.34 + 0.94i	7.65	3	4.44
2.4179	1.50 + 0.87i	8	2.74	16.42
3.4759	1.87 + 0.49i	8.72	2	4.12
4.0242	2.00 - 0.05i	8.85	1	3.85
3.8603	1.73 - 0.68i	8	1.56i	-22.26
3.4893	1.43 + 0.90i	7	2.13i	-23.74
3.1793	1.17 - 0.99i	6	2.49i	-21.14
2.9576	0.96 - 1.00i	5	2.76i	-17.57
2.8218	0.80 - 0.98i	4	2.96i	-14.19
2.7541	0.68 - 0.95i	3	3.09i	-11.41
2.7293	0.61 - 0.92i	2	3.14i	-9.32
2.7239	0.57 - 0.90i	1	3.15i	-8.00

Table 1: Bifurcation points on the trivial branch for $d = 0.1$, $f = 2$.

8.2. Solitons along bifurcating branches

`pde2path` was explored in depth to cover much more extensive parameter regions for the detection of single soliton states on bifurcating branches. Based on a large number of numerical experiments, heuristics concerning the branches associated with single soliton states as well as the location of the solitons with the strongest localization on these branches could be developed.

Starting from the bifurcation point with the smallest detuning value, let us number the bifurcation points and bifurcating branches successively along the trivial branch. We observe the following

- (i) For $d > 0$, bright single solitons occur on the last bifurcating branch. The most localized single solitons occur near the first turning point of this branch (locally maximizing ζ), cf. Figure 16(a).
- (ii) For $d < 0$, dark single solitons occur on the first bifurcating branch. The most localized single solitons occur near the second turning point of this branch (locally maximizing ζ), cf. Figure 16(d).

Both for normal and anomalous dispersion, the common feature of the most localized single solitons is their occurrence at maximal possible detuning values within all turning points of the bifurcating branch.

For quantification of localization, we need the following definition.

Definition 8.2. Let a be a solution of (LLE) as in Figure 17 and $x_{min}, x_{max} \in [0, 2\pi]$ such that $|a(x_{min})|^2 \leq |a(x)|^2 \leq |a(x_{max})|^2$ for all $x \in [0, 2\pi]$. Furthermore let

$$x_1 := \min \left\{ x \in [0, \pi] : \left| |a(x)|^2 - |a(x_{min})|^2 + \frac{1}{2} (|a(x_{max})|^2 - |a(x_{min})|^2) \right| \right\}.$$

- For anomalous dispersion $d > 0$, assume w.l.o.g. that $|a(0)|^2 = |a(2\pi)|^2 \leq |a(\pi)|^2$. Then we define the full width half maximum

$$FWHM_a := 2 |\pi - x_1|.$$

- For normal dispersion $d < 0$, assume w.l.o.g. that $|a(0)|^2 = |a(2\pi)|^2 \geq |a(\pi)|^2$. Then we define the full width half minimum

$$FWHM_i := 2 |\pi - x_1|.$$

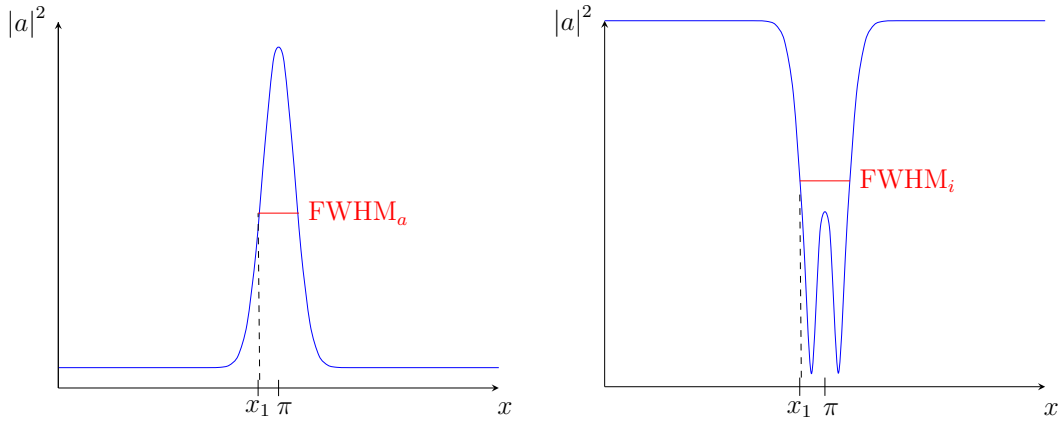


Figure 17: Illustration of $FWHM_a$ for $d > 0$ and $FWHM_i$ for $d < 0$.

These heuristics are illustrated in Figure 18, where $FWHM_a$ of the solution for $d > 0$ and $FWHM_i$ of the solution for $d < 0$ is plotted along the bifurcating branch starting from the bifurcation point. Note that the soliton at label C in Figure 16(a) ($FWHM_a=0.3330$) has slightly smaller $FWHM_a$ than the soliton at label B ($FWHM_a=0.3393$).

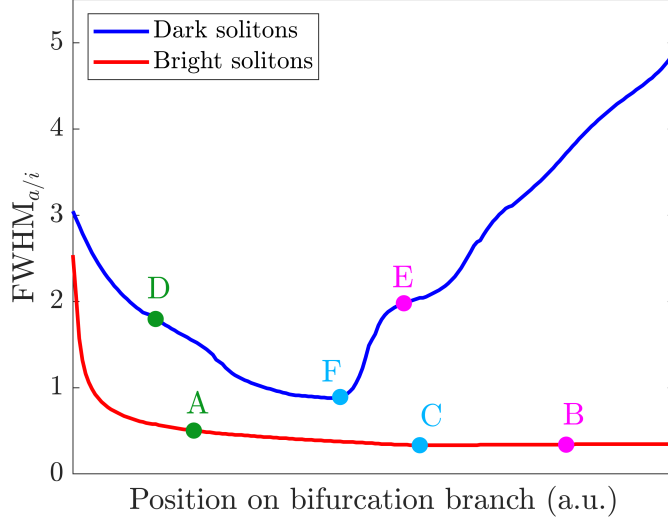


Figure 18: $\text{FWHM}_{a/i}$ along the bifurcating branch for anomalous dispersion ($d = 0.1$) and normal dispersion ($d = -0.1$) for $f = 2$.

For different points A, B, C along the bright single soliton branch and D, E, F along the dark single soliton branch respectively, comb states are depicted in the spatial and frequency domain in Figure 16(b), (c) and (e), (f). The comb states identified by using the aforementioned criteria, i.e., the states located at the points C and F, show the strongest localization in the spatial domain. We can see that in the case of anomalous dispersion, there is no other state on the branch $k = 1$ for the same value of ζ . However, in the case of normal dispersion, we find another dark soliton state with equal detuning marked by point D in Figure 16(d), as e.g. discussed in [16]. Point F in Figure 16(d) corresponds to a deeper intensity drop in the spatial domain and has the broader comb, making it the state of interest compared to point D. In this example, the soliton character of the solutions, i.e., their strong localization in the spatial domain, at the turning point is visible but not yet very pronounced due to the moderate value of f . With increasing f the soliton localization as well as the comb power and comb bandwidth will be much enhanced. At the same time, the graphs of the bifurcation branches will be less illustrative due to a steeply increasing number and density of bifurcation points. Therefore, $f = 2$ is chosen merely for illustrative reasons, and much larger ranges of f are covered in Section 8.3.

8.3. Quantitative characterization of soliton frequency combs

8.3.1. Characteristics of soliton frequency combs

Using the heuristics from the previous subsection, we are able to identify single soliton solutions with the smallest $\text{FWHM}_{a/i}$ for a certain forcing both in the normal as well as in the anomalous dispersion regime. Based on this approach, we now characterize these comb states $a(x) = \sum_{k \in \mathbb{Z}} \hat{a}_k e^{ikx}$ by their comb bandwidth $2k^*$ and their power conversion efficiency η , defined next.

Definition 8.3. *We define the following characteristics of soliton frequency combs.*

- (i) *The comb bandwidth is $2k^*$, where k^* is the minimal value such that $|\hat{a}_{k^*}|^2 \leq \frac{1}{2}|\hat{a}_1|^2$,*
- (ii) *The power conversion efficiency η is defined as $\eta := f^{-2} \sum_{k \in \mathbb{Z} \setminus \{0\}} |\hat{a}_k|^2$.*

This means that the power conversion efficiency is the ratio between the intracavity comb power $\sum_{k \in \mathbb{Z} \setminus \{0\}} |\hat{a}_k|^2$ and the pump power f^2 . The intracavity comb power does not contain the zero mode, since $|\hat{a}_0|$ mostly stems from the pump and is therefore nonzero even if no comb is formed in the microresonator.

8.3.2. Approximation formulas

For bright solitons, under the assumption of high forcing, approximation formulas for the comb bandwidth as well as the power conversion efficiency exist, cf. [1],[5]. Assuming a detuning set to its maximum value $\zeta_{\text{BS,max}} = \pi^2 f^2 / 8$, they read as

$$2k_{\text{BS,max}}^* \approx \sqrt{2} \ln(1 + \sqrt{2}) \frac{f}{\sqrt{d}}, \quad (8.5a)$$

$$\eta_{\text{BS,max}} \approx \frac{1}{f} \sqrt{\frac{d}{2}} \quad (8.5b)$$

and will be motivated in the following.

For bright solitons, a closed form approximation [1],[19],[34],[33] of the intracavity field is given by

$$a(x) = a^\infty + \tilde{a}(x) \approx a^\infty + \sqrt{2\zeta} \left(\cosh \left(x \sqrt{\zeta/d} \right) \right)^{-1} e^{i\varphi_0} \quad (8.6)$$

with $a^\infty = \text{const.}$ and $\varphi_0 \approx \arccos \left(\frac{\sqrt{8\zeta}}{\pi f} \right)$ is the relative phase of the soliton with respect to a^∞ . For highly localized solitons, we approximate $a(x) \approx \tilde{a}(x)$. For a given forcing,

the maximal detuning $\zeta_{\text{BS,max}} = \frac{\pi^2 f^2}{8}$ can be derived by the condition on argument of the arccos

$$\frac{\sqrt{8\zeta}}{\pi f} \leq 1,$$

cf. supplementary information in [19]. For a maximal detuning, the intracavity field reads

$$a \approx \frac{\pi f}{2} \left(\cosh \left(\frac{\pi f}{2\sqrt{2d}} x \right) \right)^{-1}. \quad (8.7)$$

Given this expression, the power conversion efficiency at the maximum detuning for bright solitons can be expressed as

$$\eta_{\text{BS,max}} \approx \frac{1}{2\pi f^2} \int_{-\pi}^{\pi} \left| \frac{\pi f}{2} \left(\cosh \left(\frac{\pi f}{2\sqrt{2d}} x \right) \right)^{-1} \right|^2 dx = \frac{1}{f} \sqrt{\frac{d}{2}} \tanh \left(\frac{\pi f}{2\sqrt{2d}} \pi \right) \approx \frac{1}{f} \sqrt{\frac{d}{2}} \quad (8.8)$$

for large values of $\frac{f}{\sqrt{d}}$.

In order to determine the formula for the comb bandwidth, we calculate an approximation of the Fourier coefficients

$$\begin{aligned} |\hat{a}_k|^2 &= \left| \frac{1}{2\pi} \int_{-\pi}^{\pi} \frac{\pi f}{2} \left(\cosh \left(\frac{\pi f}{2\sqrt{2d}} x \right) \right)^{-1} e^{-ikx} dx \right|^2 \\ &\approx \left| \frac{1}{2\pi} \int_{-\infty}^{\infty} \frac{\pi f}{2} \left(\cosh \left(\frac{\pi f}{2\sqrt{2d}} x \right) \right)^{-1} e^{-ikx} dx \right|^2 = \frac{d}{2} \left(\cosh \left(\frac{\sqrt{2d}}{f} k \right) \right)^{-2}. \end{aligned} \quad (8.9)$$

In particular $|\hat{a}_1|^2 \approx \frac{d}{2} \left(\cosh \left(\frac{\sqrt{2d}}{f} \right) \right)^{-2} \approx \frac{d}{2}$ for large values of $\frac{f}{\sqrt{d}}$. Hence, k^* from Definition 8.3 fulfills

$$\left(\cosh \left(\frac{\sqrt{2d}}{f} k^* \right) \right)^{-2} \approx \frac{1}{2}, \quad (8.10)$$

and finally

$$2k_{\text{BS,max}}^* \approx \sqrt{2} \ln(1 + \sqrt{2}) \frac{f}{\sqrt{d}}. \quad (8.11)$$

Expressions for the approximation of dark solitons are given in [35]. They are valid near the bifurcation point and are obtained using multiple scale asymptotics. However, this kind of solitons, indicated in Figure 16(d) by point D, is of less interest due to its lower comb power compared to the dark soliton at point F. For dark solitons of the latter type, no formula for bandwidth or power conversion efficiency is available to the best of our knowledge.

8.3.3. Results

For dispersion parameters $d \in \{\pm 0.1, \pm 0.15, \pm 0.2, \pm 0.25\}$ and $f > 1$, we have carried out a large parameter study. For $d > 0$ we computed the last bifurcation point and its corresponding bifurcating branch. Based on the heuristics in Section 8.2, we stopped the computation as soon as we reached the first turning point, i.e., point C in Figure 16(a), where the most localized bright soliton is found. In the same manner the strongest localized dark solitons in the case $d < 0$ are at the second turning point of the first bifurcating branch, i.e., point F in Figure 16(d). For all of the above values of the dispersion d and the pump power f the corresponding solitons at the turning point were investigated and their comb bandwidth as well as their power conversion efficiency were evaluated.

The results are plotted in Figure 19. For bright solitons, gray lines corresponding to the approximate expressions in (8.5a) and (8.5b) are also shown (a) and (c). Overall, the approximate and the numerically computed values are quite similar except for small values of f .

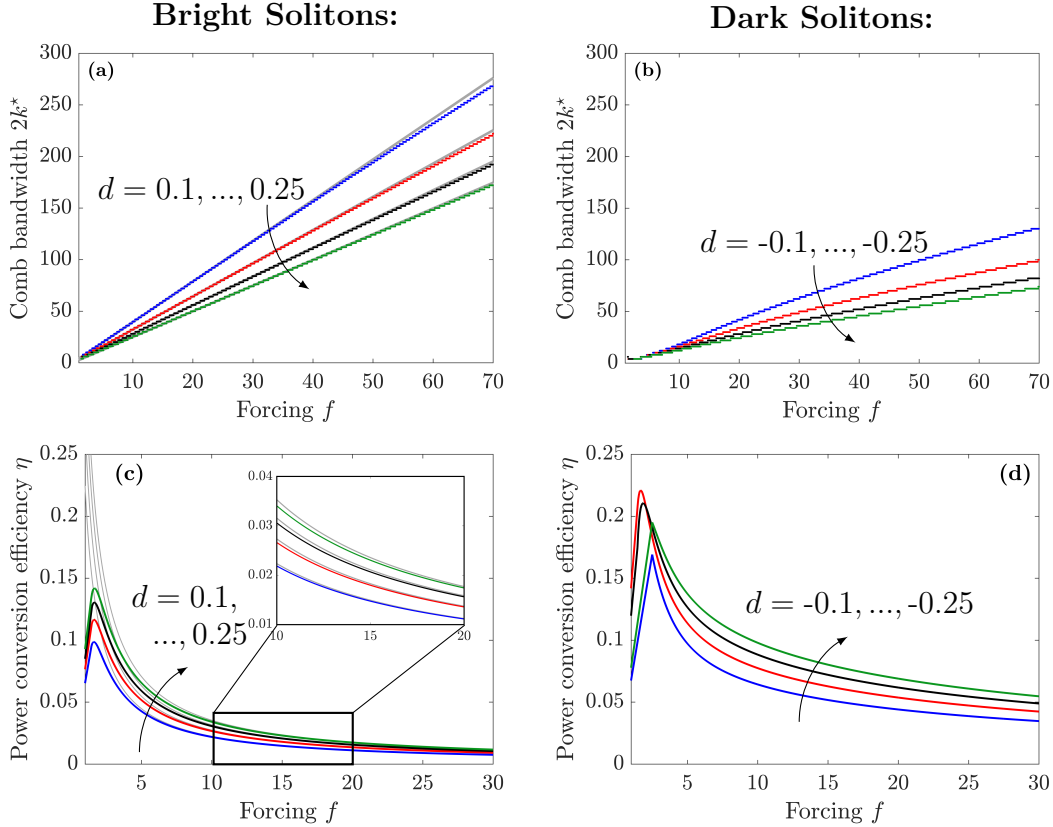


Figure 19: Comb bandwidths and power conversion efficiencies for bright and dark solitons.

8.3.4. Conclusion

The comb bandwidth increases with an increasing f at the expense of a decreasing conversion efficiency. Additionally, one can see that with $d \rightarrow 0$ the comb bandwidth increases whereas the power conversion efficiency decreases. The overall dependence of the conversion efficiency and comb bandwidth of dark solitons shows the same trends for bright solitons, see Figure 19(b) and (d). In direct comparison, dark solitons have a decreased bandwidth along with a higher conversion efficiency for the same values of f and $|d|$. We relate this to their increased width, which enables a stronger power transfer from the pumped continuous-wave background to the soliton, thereby increasing the conversion efficiency. However, a solution with higher $\text{FWHM}_{a,i}$ is also linked to a narrower comb in frequency domain.

We note that the comb bandwidth of both bright and dark solitons does not increase strictly linearly with an increasing forcing as suggested by the approximation formula in the case $d > 0$.

Our approach can be further extended to include additional effects such as two photon absorption and to study their impact on the stationary comb states. Our results allow for targeted design of soliton comb generators for specific applications. In this context, power conversion efficiency and comb bandwidth are key performance characteristics that need to be optimized under technical restrictions such as limited optical input power.

8.A. Details on the implementation

In this appendix, we comment some details on the implementation for the routines used in the previous subsections. As already explained, the primary continuation and bifurcation parameter is ζ . As soon as we have found the first bifurcation point for normal dispersion or the last bifurcation point for anomalous dispersion, we switch to the bifurcating branch and continue this branch until we reach the second fold point in the case of normal dispersion or the first fold point in the case of anomalous dispersion. Subsequently, we perform a fold point continuation. As explained in Section 7.3, we need an additional free parameter, where we choose f . However, to reduce numerical errors, we regularly restart the calculation of bifurcation point and bifurcating branches.

Algorithm 3 Computation of combwidth and power conversion efficiency

Input: d

$f := 1.01$

while $f \leq 100$ **do**

 initialize problem

 find bifurcation point

 switch to bifurcating branch

 continue bifurcating branch till the fold point

 perform fold point continuation till $f + 2.5$

 save solutions in fold points

$f := f + 2.5$

end while

compute combwidth and power conversion efficiency

Part IV.
LLE with Two-Photon-Absorption

9. Outline

We will now consider the Lugiato-Lefever equation with an additional nonlinear damping term. The results of this chapter are published in [14] together with Rainer Mandel and Wolfgang Reichel. This additional term in the Lugiato-Lefever equation is due to two photon absorption (TPA) which occurs for semiconductor based optical devices such as silicon. Their nonlinear Kerr effect is much higher than for other materials and hence, they are interesting for applications. During TPA two photons are absorbed and electrons from the valence band are excited into the conducting band and hence, free carriers are generated which leads to nonlinear loss. The other affect which occurs in semiconductor based devices is free carrier absorption (FCA) where free carriers are excited from one state to another within the same band. To our knowledge, there are no rigorous mathematical studies dealing with TPA and FCA

$$\begin{aligned} -da'' + (\zeta - i)a - (1 + i\kappa)|a|^2a + if - s(i - \mu)na &= 0, \\ n' &= \kappa|a|^4 - \frac{n}{\tau} \end{aligned}$$

with $\kappa, s, \mu, \tau \geq 0$. Following [18] and [26], the stationary Lugiato-Lefever equation in the presence of TPA and absence of FCA, by assuming $s = 0$, is given by

$$-da'' + (\zeta - i)a - (1 + i\kappa)|a|^2a + if = 0, \quad a(\cdot) = a(\cdot + 2\pi), \quad (9.1)$$

with $\kappa > 0$ and where the spatial period given by the circular nature of the resonator is normalized to 2π .

We prove that the bifurcating branches described in [13] and [29] for $\kappa = 0$ persist for sufficiently small values of $\kappa \in (0, \kappa_*)$. Moreover, if κ exceeds a critical value κ_* , then bifurcation points on the trivial curve disappear. This can also be seen numerically in the bifurcation diagrams. We observe, that with increasing values of κ more and more bifurcation points vanish and that they cease to exist, if we exceed a certain threshold κ_*^{num} . Comparing them with the analytically obtained values κ_* of our Theorem, we discover, that they are very similar.

Furthermore, we investigate what happens to the entire set of solutions when κ increases. Using a priori bounds on solutions of (9.1) on the torus $\mathbb{T} := \mathbb{R}/2\pi\mathbb{Z}$, we prove that there is a second critical value κ^* such that all solutions of (9.1) are constant provided $\kappa > \kappa^*$. Hence, Kerr comb formation is prohibited for large TPA. However, we find a second bound, which guarantees the absence of nontrivial solutions of (9.1). Studying the time-dependent problem, we show that there are no nontrivial solutions provided $\kappa > \frac{1}{\sqrt{3}}$. Combining this bound with the one obtained by the a priori bounds, we obtain the constancy of all solutions for $\kappa > \min\{\kappa^*, \frac{1}{\sqrt{3}}\}$.

Additionally, we consider solutions of

$$-da'' + (\zeta - i)a - (1 + i\kappa)|a|^2a + if = 0, \quad \text{on } \mathbb{R}, \quad a'(0) = 0, \quad (9.2)$$

in the case of anomalous dispersion $d > 0$. As soliton-like stationary solutions of (9.2) are of utmost importance in applications, we consider the formation of bright solitary combs for anomalous dispersion in the presence of small TPA using the Implicit Function Theorem. The results concerning (9.2) are in the spirit of Section 4.3. As in Section 4.3, we prove together with an appropriate rescaling, that there exists a lower envelope (ζ, f) such that above this envelope, localized solutions of (9.2) exist.

10. Bifurcation

Let us start with the discussion of (9.1) on the torus \mathbb{T} by investigating bifurcation from the curve of trivial solution with respect to ζ . The following results provide nontrivial solutions via bifurcation theory for $\kappa \in (0, \kappa_*)$, i.e., the bifurcating branches described in [29] for $\kappa = 0$ persist for small $\kappa > 0$. The natural question, what happens to the bifurcating branches when κ gets larger, is also answered in part (iii) of the theorem: bifurcation points disappear at latest when κ exceeds κ_* . In Figure 20 the vanishing of bifurcation points and nontrivial solutions for increasing κ is illustrated for anomalous dispersion $d = 0.1$ and $f = 1.6$. Black curves indicate the line of trivial solutions, colored curves show bifurcation branches. With increasing nonlinear damping, more and more bifurcation branches vanish, until all have disappeared.

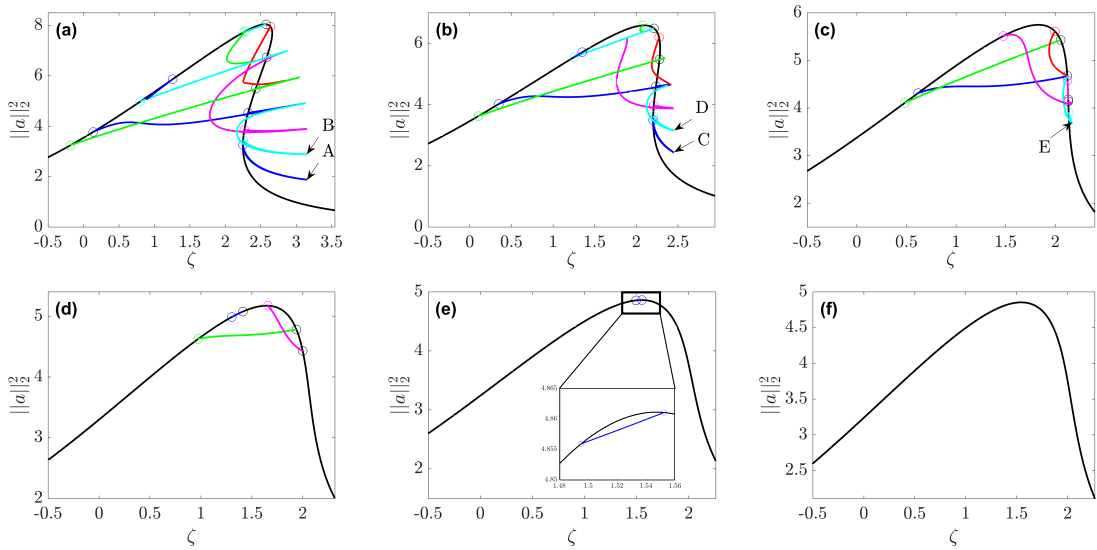


Figure 20: Bifurcation diagrams for $d = 0.1$, $f = 1.6$. Subfigure (a) corresponds to $\kappa = 0$, (b) to $\kappa = 0.05$, (c) to $\kappa = 0.1$, (d) to $\kappa = 0.15$, (e) to $\kappa = 0.185$ and (f) to $\kappa = 0.186$. Solutions at turning points A, B in (a), C, D in (b) and E in (c) are shown in Figure 21.

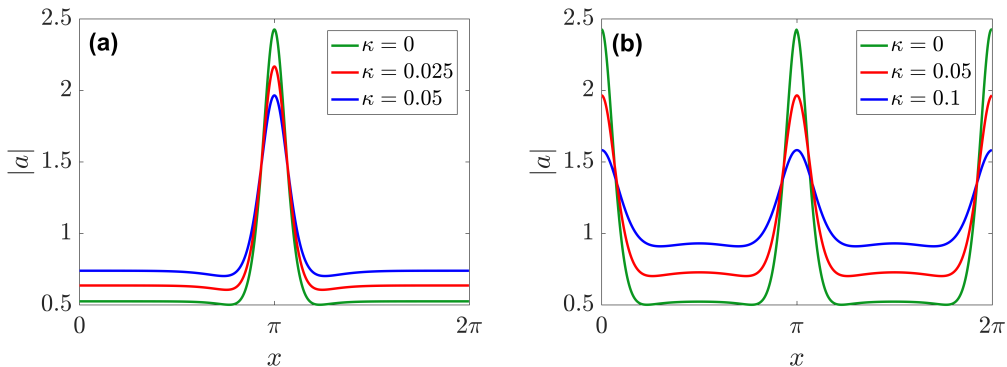


Figure 21: Subfigure (a) shows 1-solitons and subfigure (b) 2-solitons of (9.1) for increasing values of κ .

In Figure 22, the vanishing of bifurcation points and nontrivial solutions for increasing κ is illustrated for normal dispersion $d = -0.1$, $f = 1.6$. Black curves indicate again the line of trivial solutions, colored curves show bifurcation branches.

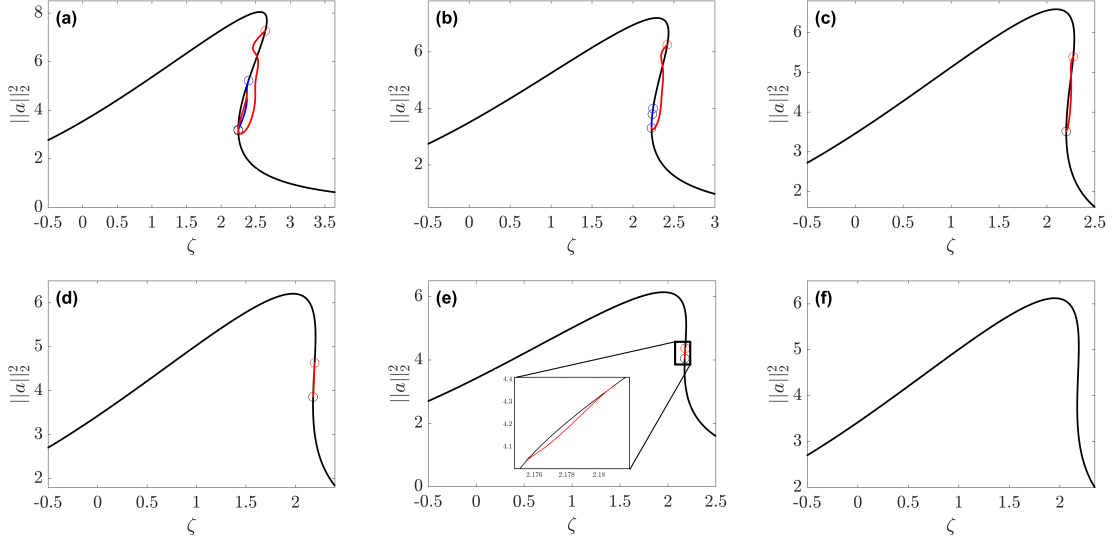


Figure 22: Bifurcation diagrams for $d = -0.1$, $f = 1.6$. Subfigure (a) corresponds to $\kappa = 0$, (b) to $\kappa = 0.025$, (c) to $\kappa = 0.05$, (d) to $\kappa = 0.07$, (e) to $\kappa = 0.074$ and (f) to $\kappa = 0.075$.

Theorem 10.1. For $f \neq 0, \kappa > 0$ the following holds:

- (i) All constant solutions of (9.1) form a smooth unbounded curve in $H^2(\mathbb{T}) \times \mathbb{R}$.
- (ii) A point (ζ, a_0) on the curve of constant solutions is a bifurcation point provided exactly one of the two numbers

$$k_{1,2} := \sqrt{\frac{2|a_0|^2 - \zeta \pm \sqrt{(1 - 3\kappa^2)|a_0|^4 - 4\kappa|a_0|^2 - 1}}{d}} \quad (10.1)$$

is in \mathbb{N} and

$$2(3\kappa^2 - |a_0|^4)(|a_0|^2 - \zeta) - 4\kappa|a_0|^2(3|a_0|^2 - \zeta) \pm \sqrt{(1 - 3\kappa^2)|a_0|^4 - 4\kappa|a_0|^2 - 1} \left(1 + \zeta^2 - |a_0|^4 - 4\kappa|a_0|^2 + 3\kappa^2\right) \neq 0 \quad (10.2)$$

with “+” if $k_1 \in \mathbb{N}$ and “-” if $k_2 \in \mathbb{N}$.

- (iii) The curve of constant solutions does not contain bifurcation points provided $\kappa > \kappa_*$ where

$$\kappa_* := \max \left\{ \kappa \in \left(0, \frac{1}{\sqrt{3}}\right) : \frac{2\kappa + \sqrt{1 + \kappa^2}}{(1 - 3\kappa^2)^3} (1 - \kappa^2 + \kappa\sqrt{1 + \kappa^2})^2 \leq f^2 \right\} \text{ if } f^2 > 1,$$

$$\kappa_* := 0 \text{ if } f^2 \leq 1.$$

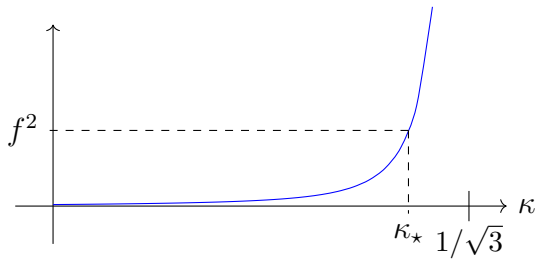
Remark 10.2. • Necessarily, we have $\kappa < \sqrt{3}$ in case (ii) since otherwise the values $k_{1,2}$ in (10.1) will not be real. Moreover, in case (ii) we may apply Rabinowitz' global bifurcation theorem from [39]. It says not only that (ζ, a_0) is a bifurcation point, but that there is a global branch of non-trivial solutions that either returns to the trivial branch at some other bifurcation point or becomes unbounded in the ζ -direction or in the $H^2(\mathbb{T})$ -direction.

- Notice that by strict monotonicity, the value κ_* is the uniquely determined solution of

$$\frac{2\kappa + \sqrt{1 + \kappa^2}}{(1 - 3\kappa^2)^3} (1 - \kappa^2 + \kappa\sqrt{1 + \kappa^2})^2 = f^2, \quad (10.3)$$

cf. Figure 23.

- For $|f| \searrow 1$, we have $\kappa_* \rightarrow 0$. This is consistent with [29], where for $\kappa = 0$ it was shown that no bifurcations occur in the case $|f| \leq 1$.
- By running `pde2path` for increasing values of $\kappa > 0$ we can determine numerically when bifurcations cease to exist. The values for κ_* from Theorem 10.1 and these numerically determined values from `pde2path` are very similar, cf Table 2.



f	κ_*	κ_*^{num}
1.1	0.045	0.042
1.6	0.185	0.185
2	0.248	0.245
4	0.380	0.378
10	0.474	0.473
20	0.513	0.513

Figure 23: Illustration of (10.3).

Table 2: κ_* from Theorem 10.1 and numerical values from `pde2path`.

In the following, we prove Theorem 10.1 .

Proof. (i) is proved in Lemma 10.3 below together with the following remark.

Proof of (ii) – simplicity of the kernel of the linearization:

Notice that $\ker L$ is either two-dimensional or four-dimensional, since αe^{ikx} belonging to $\ker L$ always implies that αe^{-ikx} also belongs to $\ker L$. The two-dimensional case happens if exactly one of the two numbers $k_{1,2}$ from (10.1) is an integer and the four-dimensional case happens if both $k_1, k_2 \in \mathbb{N}$.

In order to achieve simple instead of multiple eigenvalues, we need to change the setting for (9.1) by additionally requiring $a'(0) = 0$, i.e., solutions need to be even around $x = 0$. Together with 2π -periodicity this implies $a'(\pi) = 0$, i.e., we consider (9.1) with vanishing Neumann boundary conditions at $x = 0$ and $x = \pi$. If we define $H_{even}^2(\mathbb{T})$ and $L_{even}^2(\mathbb{T})$ as the subspaces of $H^2(\mathbb{T})$ and $L^2(\mathbb{T})$ with even symmetry around $x = 0$ then $L, L^* : H_{even}^2(\mathbb{T}) \rightarrow L_{even}^2(\mathbb{T})$ are again Fredholm operators, and Lemma 10.5 still holds. In this way we halve the dimension of $\ker L$ for every k satisfying (10.21) since instead of both αe^{ikx} and αe^{-ikx} only $\alpha \cos(kx)$ remains in the kernel of L . In particular, we get a one-dimensional kernel of L if and only if exactly one of the numbers $k_{1,2}$ from (10.1) belongs to \mathbb{N} . The same is true for the kernel of L^* .

Proof of (ii) - computing the kernel of the linearization:

Under the condition that exactly one of the numbers $k_{1,2}$ from (10.1) belongs to \mathbb{N} , let us compute $\ker L$ and $\ker L^*$. In Lemma 10.5, we prove the bifurcation equation. To describe the matrix $N - dk^2 \text{Id}$ with N from the proof of Lemma 10.5, let us introduce the real numbers $\alpha_j, \tilde{\alpha}_j, \alpha_j^*, \tilde{\alpha}_j^*$ for $j = 1, 2$ as follows

$$\begin{aligned} N - dk^2 \text{Id} &= \begin{pmatrix} -\alpha_2 & \alpha_1 \\ \tilde{\alpha}_2 & -\tilde{\alpha}_1 \end{pmatrix} = \begin{pmatrix} -\tilde{\alpha}_2^* & \alpha_2^* \\ \tilde{\alpha}_1^* & -\alpha_1^* \end{pmatrix} \\ &= \begin{pmatrix} -\zeta - dk^2 + (\text{Re } a_0)^2 + 2|a_0|^2 - \kappa \text{Im}(a_0^2) & \text{Im}(a_0^2) - 1 - 2\kappa|a_0|^2 + \kappa \text{Re}(a_0^2) \\ \text{Im}(a_0^2) + 1 + \kappa \text{Re}(a_0^2) + 2\kappa|a_0|^2 & -\zeta - dk^2 + 2|a_0|^2 - \text{Re}(a_0^2) + \kappa \text{Im}(a_0^2) \end{pmatrix}. \end{aligned} \quad (10.4)$$

In the matrix $N - dk^2 \text{Id}$ the off-diagonal elements have the property that

$$\alpha_1 < \text{Im}(a_0^2) < \tilde{\alpha}_2$$

and hence, they cannot be zero simultaneously. Therefore, if $\text{Im}(a_0^2) \leq 0$ we can define

$$\alpha := (\alpha_1, \alpha_2)^T, \quad \alpha^* := (\alpha_1^*, \alpha_2^*)^T \quad (10.5)$$

and obtain eigenvectors of $N - dk^2 \text{Id}$, $N^T - k^2 \text{Id}$, respectively, so that $\ker L = \text{span}\{\alpha e^{ikx}\}$, $\ker L^* = \text{span}\{\alpha^* e^{ikx}\}$. Likewise, if $\text{Im}(a_0^2) \geq 0$ then

$$\tilde{\alpha} := (\tilde{\alpha}_1, \tilde{\alpha}_2)^T, \quad \tilde{\alpha}^* := (\tilde{\alpha}_1^*, \tilde{\alpha}_2^*)^T \quad (10.6)$$

are the eigenvectors of $N - dk^2 \text{Id}$, $N^T - k^2 \text{Id}$ leading to $\ker L = \text{span}\{\tilde{\alpha} e^{ikx}\}$, $\ker L^* = \text{span}\{\tilde{\alpha}^* e^{ikx}\}$.

Proof of (ii) - tangent direction to the trivial branch of solutions:

Let us assume that the curve of trivial solutions of (9.1) is parametrized by $t \mapsto (\zeta(t), a_0(t))$ as in Lemma 10.3, and that $(\zeta, a_0) = (\zeta(t_0), a_0(t_0))$ is a specific bifurcation point. Let us compute the tangent $(\dot{\zeta}, \dot{a}_0) = \frac{d}{dt}(\zeta(t), a_0(t))|_{t=t_0}$. As explained in Remark 10.6 we can ignore turning points where $\dot{\zeta} = 0$. Differentiating the equation $(i - \zeta(t))a_0(t) + g(a_0(t)) = 0$ with respect to t and evaluating the derivative at t_0 we get

$$(Dg(a_0) + i - \zeta)\dot{a}_0 = \dot{\zeta}a_0.$$

Inserting $Dg(a_0)z = (1 + i\kappa)(2|a_0|^2z + a_0^2\bar{z})$, we find

$$(2(1 + i\kappa)|a_0|^2 + i - \zeta)\dot{a}_0 + (1 + i\kappa)a_0^2\bar{\dot{a}}_0 = \dot{\zeta}a_0$$

and hence,

$$\dot{a}_0 = \tau\dot{\zeta}a_0 \quad \text{with} \quad \tau = \frac{(1 - 3i\kappa)|a_0|^2 - \zeta - i}{3(1 + \kappa^2)|a_0|^4 + 4(\kappa - \zeta)|a_0|^2 + \zeta^2 + 1}. \quad (10.7)$$

Proof of (ii) – sufficient condition for bifurcation:

According to the Theorem of Crandall-Rabinowitz, see Theorem 3.4 or [6] or Theorem I.5.1 in [24], two conditions are sufficient for bifurcation. The first is that $\ker L$ is simple, i.e., one-dimensional. In part (ii) above, we proved this to hold provided $k_1 \in \mathbb{N}$, $k_2 \notin \mathbb{N}$ or vice versa with $k_{1,2}$ from (10.1). In the following, we write k for the one which is the integer. In view of the statement of (ii), it therefore remains to show that the second condition, the so-called transversality condition, is satisfied provided (10.2) holds. To verify this we bring our problem into the form used in [6]. Nontrivial solutions of (9.1), which are even around $x = 0$ may be written as $a(\cdot) = a_0(t) + b(\cdot)$ with $b'(0) = b'(\pi) = 0$. From (9.1), we derive the equation for the function b in the form

$$F(t, b) := -db'' - (i - \zeta(t))(a_0(t) + b) - g(a_0(t) + b) = 0 \quad (10.8)$$

where $F : \mathbb{R} \times H_{even}^2(\mathbb{T}) \rightarrow L_{even}^2(\mathbb{T})$. Notice that $F(t, 0) = 0$ for all t , i.e., the curve of trivial solutions $(\zeta(t), a_0(t))$ for (9.1) has now become the line of zero solutions $(t, 0)$ for (10.8). Let us write $D_{bt}F(t_0, 0)$ for the mixed second derivative of F with respect to (t, ζ) at the point $(t_0, 0)$. According to [6], the transversality condition is expressed by

$$D_{bt}F(t_0, 0)\phi \notin \text{ran } D_bF(t_0, 0),$$

with ϕ such that $\ker D_bF(t_0, 0) = \text{span}\{\phi\}$. In our case, $D_bF(t_0, 0) = L$, where L is the linearized operator given in (10.22). By the Fredholm alternative, $\text{ran } L = (\ker L^*)^\perp = \text{span}\{\phi^*\}^\perp$, and $\phi(x) = \alpha \cos(kx)$, $\phi^*(x) = \alpha^* \cos(kx)$ if $\text{Im}(a_0^2) \leq 0$, cf. (10.5), or $\phi(x) = \tilde{\alpha} \cos(kx)$, $\phi^*(x) = \tilde{\alpha}^* \cos(kx)$ with $\tilde{\alpha}, \tilde{\alpha}^*$ if $\text{Im}(a_0^2) \geq 0$, cf. (10.6). The components of α, α^* and $\tilde{\alpha}, \tilde{\alpha}^*$ can be read from (10.4). Since orthogonality of two functions u, v in the real Hilbert space $L_{even}^2(\mathbb{T})$ means vanishing of the inner product $\langle u, v \rangle = \text{Re} \int_0^\pi u(x)\bar{v}(x) dx$, we find that transversality is expressed as

$$\langle D_{bt}F(t_0, 0)\phi, \phi^* \rangle = \text{Re} \int_0^\pi (D_{bt}F(t_0, 0)\phi)\bar{\phi}^* dx \neq 0. \quad (10.9)$$

Using $D^2g(a_0)(z, w) = 2(1 + i\kappa)(\bar{a}_0zw + a_0z\bar{w} + a_0\bar{z}w)$, we find for the second derivative

$$\begin{aligned} D_{bt}F(t_0, 0)\phi &= \dot{\zeta}\phi - D^2g(a_0)(\phi, \dot{a}_0) \\ &= \dot{\zeta}\phi - 2(1 + i\kappa)(\bar{a}_0\phi\dot{a}_0 + a_0\phi\bar{\dot{a}}_0 + a_0\bar{\phi}\dot{a}_0) \end{aligned} \quad (10.10)$$

with $\dot{a}_0 = \tau \dot{\zeta} a_0$, τ from (10.7). As explained in Remark 10.6, we can ignore the turning points where $\dot{\zeta} = 0$. Hence, inserting (10.10) into the transversality condition (10.9) we get in case $\text{Im}(a_0^2) \leq 0$,

$$\text{Re}\left(\alpha\bar{\alpha}^* - 2(1 + i\kappa)(2 \text{Re } \tau |a_0|^2 \alpha\bar{\alpha}^* + \tau a_0^2 \bar{\alpha}\bar{\alpha}^*)\right) \neq 0 \quad (10.11)$$

and in case $\text{Im}(a_0^2) \geq 0$, we replace α, α^* by $\tilde{\alpha}, \tilde{\alpha}^*$. Let us first consider the case $\text{Im}(a_0^2) \leq 0$. Here we obtain

$$\begin{aligned} \alpha\bar{\alpha}^* &= (\alpha_1 + i\alpha_2)(\alpha_1^* - i \underbrace{\alpha_2^*}_{=\alpha_1}) = \alpha_1(\alpha_1^* + \alpha_2) + i(\underbrace{\alpha_2\alpha_1^*}_{=\alpha_1\tilde{\alpha}_1^*} - \alpha_1^2) \\ &= \alpha_1 \left(2\zeta_0 + 2dk^2 - 4|a_0|^2 + i(2 + 4\kappa|a_0|^2) \right). \end{aligned} \quad (10.12)$$

Likewise, we use (10.4) and $\det(N - dk^2 \text{Id}) = 0$ to compute

$$\begin{aligned} \bar{\alpha}\bar{\alpha}^* &= (\alpha_1 - i\alpha_2)(\alpha_1^* - i \underbrace{\alpha_2^*}_{=\alpha_1}) = \alpha_1(\alpha_1^* - \alpha_2) - i(\alpha_1^2 + \underbrace{\alpha_2\alpha_1^*}_{=\alpha_1\tilde{\alpha}_1^*}) \\ &= \alpha_1 2(1 - i\kappa)\bar{a}_0^2. \end{aligned} \quad (10.13)$$

Taking the expressions for $\alpha\bar{\alpha}^*$ and $a_0^2 \bar{\alpha}\bar{\alpha}^*$ into the transversality condition (10.11) finally leads to

$$\begin{aligned} &\text{Re}\left(\alpha\bar{\alpha}^*(1 - 4(1 + i\kappa) \text{Re } \tau |a_0|^2)\right) - \text{Re}\left(\bar{\alpha}\bar{\alpha}^* 2(1 + i\kappa)\tau a_0^2\right) \\ &= (1 - 4 \text{Re } \tau |a_0|^2) \text{Re}(\alpha\bar{\alpha}^*) + 4\kappa \text{Re } \tau |a_0|^2 \text{Im}(\alpha\bar{\alpha}^*) - 4\alpha_1(1 + \kappa^2)|a_0|^4 \text{Re } \tau \\ &= \alpha_1 \left(2\zeta_0 + 2dk^2 - 4|a_0|^2 - 4 \text{Re } \tau |a_0|^2 (2\zeta_0 + 2dk^2 - 3|a_0|^2(1 + \kappa^2) - 2\kappa) \right) \neq 0. \end{aligned} \quad (10.14)$$

Since $\text{Im}(a_0^2) \leq 0$ implies that α_1 is non-zero, the non-vanishing of the expression in brackets amounts to (after inserting $\text{Re } \tau$ from (10.7))

$$(\zeta - dk^2)(|a_0|^4 - 3\kappa^2) + (\zeta^2 + 1)(\zeta + dk^2 - 2|a_0|^2) - 4\kappa|a_0|^2(|a_0|^2 + dk^2) \neq 0.$$

Using (10.1), we obtain the transversality condition (10.2).

Changes in case $\text{Im}(a_0^2) \geq 0$ amount to replacing α_1 in (10.12), (10.13) and (10.14) by $\tilde{\alpha}_2$, which is non-zero in this case. Therefore, the final transversality condition (10.2) is the same as before.

Proof of (iii) – nonexistence of bifurcations:

We assume that bifurcation for (9.1) occurs at some trivial solution (ζ, a_0) so that the claim is proved once we show $\kappa \leq \kappa_*$. By Lemma 10.5, we know that the quadratic equation in $\zeta + dk^2$ from (10.21) holds for some $k \in \mathbb{N}_0$. In particular, the discriminant is nonnegative and we obtain

$$0 \leq (4|a_0|^2)^2 - 4 \cdot (3(1 + \kappa^2)|a_0|^4 + 4\kappa|a_0|^2 + 1) = 4\left((1 - 3\kappa^2)|a_0|^4 - 4\kappa|a_0|^2 - 1\right). \quad (10.15)$$

For $\kappa \geq \frac{1}{\sqrt{3}}$ this inequality is unsolvable, so we necessarily have $\kappa \in [0, \frac{1}{\sqrt{3}})$ as well as

$$|a_0|^2 \geq \frac{2\kappa + \sqrt{1 + \kappa^2}}{1 - 3\kappa^2}. \quad (10.16)$$

On the other hand, the inequality (10.20) from the proof of (i) gives $|a_0|^2 \leq f^2\tau$ where τ is the unique value such that $\tau(1 + \kappa f^2\tau)^2 = 1$. Therefore,

$$\tilde{\tau} := \frac{2\kappa + \sqrt{1 + \kappa^2}}{(1 - 3\kappa^2)f^2} \leq \frac{|a_0|^2}{f^2} \leq \tau. \quad (10.17)$$

Since $z \mapsto z(1 + \kappa f^2 z)^2$ is increasing on $[0, \infty)$, we deduce from the definition of τ the inequality

$$\tilde{\tau}(1 + \kappa f^2 \tilde{\tau})^2 \leq \tau(1 + \kappa f^2 \tau)^2 = 1.$$

Inserting $\tilde{\tau}$ from (10.17), this is equivalent to

$$\frac{2\kappa + \sqrt{1 + \kappa^2}}{(1 - 3\kappa^2)^3} (1 - \kappa^2 + \kappa\sqrt{1 + \kappa^2})^2 \leq f^2,$$

which implies $\kappa \leq \kappa_*$ by definition of κ_* . This finishes the proof of (iii). \square

The following lemma, which proves part (i) of the theorem above, provides a parametrization of the curve of constant solutions.

Lemma 10.3. *Let $\tau \in (0, 1)$ be the unique value such that $\tau(1 + \kappa f^2\tau)^2 = 1$. For $t \in (-\sqrt{\tau}, \sqrt{\tau})$ define*

$$A(t) := t \left(\frac{1 + 4\kappa f^2\tau + 3\kappa^2 f^4\tau^2 + t^2(-3\kappa^2 f^4\tau - 2\kappa f^2) + t^4 \kappa^2 f^4}{\tau - t^2} \right)^{1/2}.$$

Then $t \mapsto (\zeta(t), a_0(t))$ parametrizes the curve of trivial solutions with

$$\begin{aligned} \zeta(t) &:= f^2(\tau - t^2) + A(t), \\ a_0(t) &:= f(\tau - t^2) \left(1 + \kappa f^2(\tau - t^2) - iA(t) \right). \end{aligned}$$

Proof. Constant solutions (a_0, ζ) of (9.1) satisfy

$$(\zeta - i)a_0 - (1 + i\kappa)|a_0|^2 a_0 + if = 0 \quad (10.18)$$

and in particular

$$|a_0|^2 \left((\zeta - |a_0|^2)^2 + (1 + \kappa|a_0|^2)^2 \right) = f^2. \quad (10.19)$$

Let us successively parametrize $|a_0|^2$, ζ and a_0 . Since $(\zeta - |a_0|^2)^2 \geq 0$, we obtain from (10.19) that

$$0 < |a_0|^2 f^{-2} \leq \tau, \quad (10.20)$$

for $\tau \in (0, 1)$ as in the statement of the lemma. Equation (10.19) suggests the following parametrization of $|a_0|^2$ by $t \mapsto |a_0|^2(t) := f^2(\tau - t^2)$ for $t \in (-\sqrt{\tau}, \sqrt{\tau})$. The sign of t is chosen according to $\text{sign}(t) = \text{sign}(\zeta - |a_0|^2)$. Due to (10.19), the value ζ can be written as follows:

$$\begin{aligned}\zeta &= f^2(\tau - t^2) + \zeta - |a_0|^2 \\ &= f^2(\tau - t^2) + \text{sign}(t)|\zeta - |a_0|^2| \\ &\stackrel{(10.19)}{=} f^2(\tau - t^2) + \text{sign}(t)\sqrt{f^2|a_0|^{-2} - (1 + \kappa|a_0|^2)^2}.\end{aligned}$$

Inserting the parametrization of $|a_0|^2(t)$ yields the following parametrization of ζ

$$\zeta(t) = f^2(\tau - t^2) + \text{sign}(t)\sqrt{\frac{1}{\tau - t^2} - (1 + \kappa f^2(\tau - t^2))^2} = f^2(\tau - t^2) + A(t).$$

Next, we rearrange (10.18) to express a_0 in terms of $f, \kappa, \zeta, |a_0|^2$ and use (10.19) to find

$$\begin{aligned}a_0 &= \frac{if}{|a_0|^2 - \zeta + i(1 + \kappa|a_0|^2)} \\ &= \frac{-if(i(1 + \kappa|a_0|^2) + \zeta - |a_0|^2)}{(1 + \kappa|a_0|^2)^2 + (\zeta - |a_0|^2)^2} \\ &\stackrel{(10.19)}{=} \frac{|a_0|^2}{f} \left(1 + \kappa|a_0|^2 + i(|a_0|^2 - \zeta)\right).\end{aligned}$$

If we insert $|a_0|^2(t) = f^2(\tau - t^2)$ and $\zeta(t) = f^2(\tau - t^2) + A(t)$ into the previous expression we finally arrive at

$$a_0(t) = f(\tau - t^2) \left(1 + \kappa f^2(\tau - t^2) - iA(t)\right).$$

□

Remark 10.4. *The curve $(\zeta, a_0) : (-\sqrt{\tau}, \sqrt{\tau}) \rightarrow \mathbb{R} \times \mathbb{R}^2$ is smooth and unbounded in the ζ -component. The same is true if we consider (ζ, a_0) as a map from $(-\sqrt{\tau}, \sqrt{\tau})$ into $\mathbb{R} \times H^2(\mathbb{T})$.*

The following result is a generalization of Proposition 4.3 in [29]. It provides the necessary condition for bifurcation.

Lemma 10.5. *All bifurcation points (ζ, a_0) for (9.1) with respect to the curve of trivial solutions satisfy*

$$(\zeta + dk^2)^2 - 4|a_0|^2(\zeta + dk^2) + 3(1 + \kappa^2)|a_0|^4 + 4\kappa|a_0|^2 + 1 = 0 \quad (10.21)$$

for some $k \in \mathbb{N}$.

Proof. By the Implicit Function Theorem, we know that a necessary condition for bifurcation is that the linearized operator

$$L = -d \frac{d^2}{dx^2} - (i - \zeta) - Dg(a_0) : H^2(\mathbb{T}) \rightarrow L^2(\mathbb{T}) \quad (10.22)$$

has a nontrivial kernel. Here $g(a) = (1 + i\kappa)|a|^2 a - if$ stands for the nonlinearity and $Dg(a)z := \frac{d}{dt}g(a + tz)|_{t=0} = 2(1 + i\kappa)|a|^2 z + (1 + i\kappa)a^2 \bar{z}$ with $a, z \in \mathbb{C}$ for the derivative of g at a . The derivative $Dg(a)$ can also be written in the form

$$Dg(a)z = \begin{pmatrix} \operatorname{Re}(a^2) + 2|a|^2 - \kappa \operatorname{Im}(a^2) & \operatorname{Im}(a^2) - 2\kappa|a|^2 + \kappa \operatorname{Re}(a^2) \\ \operatorname{Im}(a^2) + \kappa \operatorname{Re}(a^2) + 2\kappa|a|^2 & 2|a|^2 - (\operatorname{Re} a^2) + \kappa \operatorname{Im}(a^2) \end{pmatrix} \begin{pmatrix} \operatorname{Re} z \\ \operatorname{Im} z \end{pmatrix}. \quad (10.23)$$

L is Fredholm of index 0, since $-d \frac{d^2}{dx^2} - (i - \zeta) : H^2(\mathbb{T}) \rightarrow L^2(\mathbb{T})$ is an isomorphism and $K : H^2(\mathbb{T}) \rightarrow L^2(\mathbb{T})$, $\varphi \mapsto Dg(a_0)\varphi$ is compact due to compact Sobolev embedding. Therefore, the space $\ker L$ is finite dimensional, and the adjoint operator

$$L^* = -d \frac{d^2}{dx^2} + (i + \zeta) - \overline{Dg(a_0)} : H^2(\mathbb{T}) \rightarrow L^2(\mathbb{T}) \quad (10.24)$$

has a kernel with the same finite dimension as $\ker L$. Any element $\phi \in \ker L$ can be expanded in the form $\phi(x) = \sum_{l \in \mathbb{Z}} \alpha_l e^{ilx}$. The condition that $\phi \in \ker L$ means that there is at least one integer $k \in \mathbb{Z}$ such that $L(\alpha e^{ikx}) = (dk^2 - i + \zeta - Dg(a_0))\alpha e^{ikx} = 0$ for some $\alpha \in \mathbb{C} \setminus \{0\}$. In other words, dk^2 is an eigenvalue of the matrix

$$N = Dg(a_0) + \begin{pmatrix} -\zeta & -1 \\ 1 & -\zeta \end{pmatrix}$$

with $Dg(a_0)$ in matrix representation given by (10.23). Non-zero elements in $\ker L$ exist if $\det(-dk^2 \operatorname{Id} + N) = 0$ and computing this determinant yields (10.21). Solving for k leads to $k_{1,2}$ given by (10.1). Likewise, non-zero elements in $\ker L^*$ exist if $\det(-d\tilde{k}^2 \operatorname{Id} + N^T) = 0$ for some integer $\tilde{k} \in \mathbb{N}_0$. Solving $\det(-d\tilde{k}^2 \operatorname{Id} + N^T) = \det(-d\tilde{k}^2 \operatorname{Id} + N) = 0$ leads to the same formula (10.1) as for k . Consequently, (10.1) is equivalent to both L and L^* having nontrivial kernels. If neither k_1 or k_2 are in \mathbb{N} then $\ker L = \ker L^* = \{0\}$, and in this case the Implicit Function Theorem, cf. Theorem I.1.1 in [24], implies that solutions nearby the point (ζ, a_0) are unique, i.e., trivial, and hence (ζ, a_0) cannot be a bifurcation point. Therefore, k_1 or k_2 in \mathbb{N} is a necessary condition for bifurcation. \square

Remark 10.6. *We exclude the case $k_1 = 0$ or $k_2 = 0$ in the bifurcation condition (10.21). It happens exactly at the turning points of the curve of trivial solutions and corresponds to the non-injectivity of $\zeta(t)$. Since it creates only artificial bifurcation points as explained in Section 4.2 in [29], we omit it.*

11. Nonexistence of Nontrivial Solutions

11.1. A priori bounds and nonexistence of nontrivial solutions I

Here, we calculate a priori bounds in $L^\infty(\mathbb{T})$ for solutions of (9.1), following the discussion in [29].

Theorem 11.1. *Let $d \neq 0$, $\kappa > 0$ and $\zeta, f \in \mathbb{R}$. Then every solution $a \in C^2(\mathbb{T})$ of (9.1) satisfies*

$$\|a\|_\infty \leq \left(1 + 2\pi^2 f^2 |d|^{-1}\right) \min \left\{ |f|, \left(\frac{|f|}{\kappa}\right)^{1/3} \right\}. \quad (11.1)$$

Proof. Let $a \in H^2(\mathbb{T})$ be a solution of (9.1). Then we define the 2π -periodic function $r := -d \operatorname{Im}(a'\bar{a})'$. Using (9.1) we obtain

$$\begin{aligned} r &= -d \operatorname{Im}(a''\bar{a}) \\ &= \operatorname{Im}\left((i - \zeta)|a|^2 + (1 + i\kappa)|a|^4 - if\bar{a}\right) \\ &= |a|^2 + \kappa|a|^4 - f \operatorname{Re} a. \end{aligned} \quad (11.2)$$

Using the fact that r is 2π -periodic together with Hölder's inequality, we get from the previous identity

$$\begin{aligned} 0 &= \int_0^{2\pi} r \, dx = \int_0^{2\pi} (|a|^2 + \kappa|a|^4 - f \operatorname{Re} a) \, dx \\ &\geq \kappa \|a\|_4^4 + \|a\|_2^2 - \sqrt{2\pi} |f| \|a\|_2 \\ &\geq \|a\|_2 \left(\frac{\kappa}{2\pi} \|a\|_2^3 + \|a\|_2 - \sqrt{2\pi} |f| \right). \end{aligned} \quad (11.3)$$

Neglecting once the $\|a\|_2^3$ and once the $\|a\|_2$ term, we obtain the L^2 -bound

$$\|a\|_2 \leq \sqrt{2\pi} \tilde{C}_\kappa \quad \text{with} \quad \tilde{C}_\kappa = \min \left\{ |f|, \left(\frac{|f|}{\kappa}\right)^{1/3} \right\}. \quad (11.4)$$

Next, we derive a bound for $\|a'\|_2$. First, the differential equation (9.1) yields the identity

$$\begin{aligned} \|a'\|_2^2 &= \operatorname{Re} \int_0^{2\pi} \left(-ida'' - i\zeta a + (i - \kappa)|a|^2 a + f\right)' \bar{a}' \, dx \\ &= \operatorname{Re} \int_0^{2\pi} -ida''' \bar{a}' + i(|a|^2 a)' \bar{a}' - \kappa(|a|^2 a)' \bar{a}' \, dx \\ &= \operatorname{Re} \int_0^{2\pi} i(|a|^2)' a \bar{a}' \, dx - \kappa \int_0^{2\pi} |a|^2 |a'|^2 \, dx - \kappa \operatorname{Re} \int_0^{2\pi} (|a|^2)' a \bar{a}' \, dx \\ &= -\operatorname{Im} \int_0^{2\pi} (|a|^2)' a \bar{a}' \, dx - \kappa \int_0^{2\pi} |a|^2 |a'|^2 \, dx - \frac{\kappa}{2} \int_0^{2\pi} (|a|^2)' (|a|^2)' \, dx \\ &\leq -\operatorname{Im} \int_0^{2\pi} (|a|^2)' a \bar{a}' \, dx. \end{aligned} \quad (11.5)$$

Then, we set $R := -d\operatorname{Im}(a'\bar{a}) = d\operatorname{Im}(\bar{a}'a)$ so that $R' = r$ as well as $R(0) = R(2\pi)$. Using the identity (11.2) we get the pointwise estimate $r \geq -\frac{f^2}{4}$ on $[0, 2\pi]$ from which we deduce

$$\begin{aligned} R(x) - R(0) &= \int_0^x r(t) dt \geq -\frac{\pi}{2}f^2 \quad (x \in [0, 2\pi]) \quad \text{and} \\ R(x) - R(2\pi) &= -\int_x^{2\pi} r(t) dt \leq \frac{\pi}{2}f^2 \quad (x \in [0, 2\pi]). \end{aligned} \tag{11.6}$$

Using the definition of R and (11.6) we deduce from (11.5)

$$\begin{aligned} |d| \|a'\|_2^2 &\leq \left| d\operatorname{Im} \left(\int_0^{2\pi} (|a|^2)'\bar{a}'a dx \right) \right| = \left| \int_0^{2\pi} (|a|^2)'R dx \right| \\ &\leq \int_0^{2\pi} (|a|^2)'|R - R(0)| dx \\ &\leq \frac{\pi f^2}{2} \int_0^{2\pi} |(a|^2)'| dx = \pi f^2 \int_0^{2\pi} |a| |a'| dx \\ &\leq \pi f^2 \|a\|_2 \|a'\|_2 \\ &\leq \sqrt{2}\pi^{3/2} f^2 \tilde{C}_\kappa \|a'\|_2 \end{aligned}$$

with \tilde{C}_κ from (11.4). So we find

$$|d| \|a'\|_2 \leq \sqrt{2}\pi^{3/2} f^2 \tilde{C}_\kappa. \tag{11.7}$$

Finally, we combine the previous estimates for $\|a\|_2, \|a'\|_2$ to deduce an L^∞ -estimate. From (11.4), we obtain that there is a $x_1 \in [0, 2\pi]$ satisfying $|a(x_1)| \leq \tilde{C}_\kappa$. Together with (11.7), this implies

$$\begin{aligned} \|a\|_\infty &\leq |a(x_1)| + \|a - a(x_1)\|_\infty \\ &\leq \tilde{C}_\kappa + \|a'\|_1 \\ &\leq \tilde{C}_\kappa + \sqrt{2\pi} \|a'\|_2 \\ &\leq \left(1 + 2\pi^2 f^2 |d|^{-1}\right) \tilde{C}_\kappa. \end{aligned} \tag{11.8}$$

□

Remark 11.2. *One can obtain a more refined version of the bound (11.1) of the form $\|a\|_\infty \leq \left(1 + 2\pi^2 f^2 |d|^{-1}\right) C_\kappa$ where*

$$C_\kappa = \sqrt[3]{\frac{|f|}{2\kappa} + \sqrt{\frac{f^2}{4\kappa^2} + \frac{1}{27\kappa^3}}} - \sqrt[3]{-\frac{|f|}{2\kappa} + \sqrt{\frac{f^2}{4\kappa^2} + \frac{1}{27\kappa^3}}}. \tag{11.9}$$

This follows from Cardano's formula applied to (11.3). We did not make further use of the refined value of C_κ , since (11.1) already provides a meaningful a priori bound

both for small as well as for large values of κ . However, observe that C_κ from (11.9) is non-singular in κ , indeed

$$\sqrt[3]{A + \sqrt{B}} - \sqrt[3]{-A + \sqrt{B}} = \frac{2A}{(A + \sqrt{B})^{2/3} + (A + \sqrt{B})^{1/3}(-A + \sqrt{B})^{1/3} + (-A + \sqrt{B})^{2/3}}$$

where $A := \frac{|f|}{2\kappa}$ and $B := \frac{f^2}{4\kappa^2} + \frac{1}{27\kappa^3}$. Hence,

$$\lim_{\kappa \rightarrow 0} C_\kappa = |f|,$$

which recovers a similar bound as in Theorem 1 in [29], which reads for $\kappa = 0$

$$\|a\|_\infty \leq |f| (1 + 12\pi^2 f^2 |d|^{-1}).$$

With the L^∞ -bound (11.1), the constancy of solutions for large κ is proved along the lines of the proof of Theorem 2 in [29]. However, from a technical point of view, several partial results from the proof presented in [29] break down and new difficulties have to be overcome so that the proof given next contains several new aspects.

Theorem 11.3. *Let $d \neq 0$, $\kappa > 0$, $\zeta, f \in \mathbb{R}$ and let κ^* be given by*

$$\kappa^* := 6\sqrt{6} \left(1 + 2\pi^2 f^2 |d|^{-1}\right)^3 f^2.$$

Then all solutions of (9.1) are constant provided $\kappa > \kappa^$.*

Proof. We equip the real Hilbert space $H^1(\mathbb{T})$ with the inner product generated by the norm

$$\|\phi\|_{H^1}^2 := \gamma \|\phi'\|_2^2 + \|\phi\|_2^2 \quad \text{for } \phi \in H^1(\mathbb{T}), \quad (11.10)$$

where $\gamma > 0$ will be suitably chosen later. We observe that a solution $a : [0, 2\pi] \rightarrow \mathbb{C}$ of (9.1) is constant if and only if the function $A = a'$ is trivial. Since a solves (9.1), the function A is a 2π -periodic solution of the differential equation

$$-dA'' = (i - \zeta)A + 2(1 + i\kappa)|a|^2 A + (1 + i\kappa)a^2 \bar{A}. \quad (11.11)$$

We introduce the differential operator $L_\kappa : H^2(\mathbb{T}) \subset L^2(\mathbb{T}) \rightarrow L^2(\mathbb{T})$ by

$$L_\kappa B := -dB'' - (i - \zeta)B - 2i\kappa|a|^2 B - i\kappa a^2 \bar{B} \quad (11.12)$$

so that (11.11) may be rewritten as

$$L_\kappa A = 2|a|^2 A + a^2 \bar{A}. \quad (11.13)$$

The fact that $L_\kappa^{-1} : L^2(\mathbb{T}) \rightarrow H^1(\mathbb{T})$ exists as a bounded linear operator will follow from the injectivity of L_κ , since L_κ is a Fredholm operator of index 0. The injectivity is a

consequence of the following estimate. For $g \in L^2(\mathbb{T})$ let $B \in H^2(\mathbb{T})$ satisfy $L_\kappa B = g$. Testing with \bar{B} yields

$$\int_0^{2\pi} \left(d|B'|^2 - (i - \zeta)|B|^2 - 2i\kappa|a|^2|B|^2 - i\kappa a^2 \bar{B}^2 \right) dx = \int_0^{2\pi} g \bar{B} dx.$$

Taking the real and imaginary part of this equation implies

$$d \|B'\|_2^2 + \zeta \|B\|_2^2 + \kappa \operatorname{Im} \int_0^{2\pi} a^2 \bar{B}^2 dx = \operatorname{Re} \int_0^{2\pi} g \bar{B} dx, \quad (11.14)$$

$$\|B\|_2^2 + \kappa \int_0^{2\pi} \underbrace{\left(2|a|^2|B|^2 + \operatorname{Re}(a^2 \bar{B}^2) \right)}_{\geq |a|^2|B|^2} dx = -\operatorname{Im} \int_0^{2\pi} g \bar{B} dx. \quad (11.15)$$

From (11.15) and $\kappa \geq 0$, we get $\|B\|_2 \leq \|g\|_2$. Together with (11.14), (11.15), we obtain

$$\begin{aligned} |d| \|B'\|_2^2 + \operatorname{sign}(d)\zeta \|B\|_2^2 - \kappa \int_0^{2\pi} |a|^2|B|^2 dx &\leq \|g\|_2^2, \\ \|B\|_2^2 + \kappa \int_0^{2\pi} |a|^2|B|^2 dx &\leq \|g\|_2^2. \end{aligned}$$

Multiplying the second equation with $\sigma \geq 1$ and summing up both equations, we finally get

$$|d| \|B'\|_2^2 + (\sigma + \operatorname{sign}(d)\zeta) \|B\|_2^2 \leq (\sigma + 1) \|g\|_2^2.$$

Choosing σ sufficiently large and γ from (11.10) sufficiently small, we obtain $\|B\|_{H^1}^2 \leq 4\|g\|_2^2$. This implies in particular the injectivity of L_κ , consequently the boundedness of $L_\kappa^{-1} : L^2(\mathbb{T}) \rightarrow H^1(\mathbb{T})$ and finally also the norm bound $\|L_\kappa^{-1}\| \leq 2$ uniformly in $\kappa > 0$.

Having proven this bound, we turn to the task to prove that solutions A of (11.11) are trivial for $\kappa > \kappa^*$. In view of (11.13), we define the bounded linear operator

$$K_a B := L_\kappa^{-1} \left(2|a|^2 B + a^2 \bar{B} \right) : L^2(\mathbb{T}) \rightarrow L^2(\mathbb{T}).$$

It remains to show that its operator norm is smaller than 1, because then K_a is a contraction and therefore admits a unique fixed point A , which must be the trivial one. Since

$$\|2|a|^2 B + a^2 \bar{B}\|_2^2 = \int_0^{2\pi} \left(5|a|^4|B|^2 + 2|a|^2 \bar{a}^2 B^2 + 2|a|^2 a^2 \bar{B}^2 \right) dx \leq 9\|a\|_\infty^4 \|B\|_2^2,$$

we find that

$$\|K_a\| \leq 3\|L_\kappa^{-1}\| \|a\|_\infty^2 \stackrel{(11.8),(11.4)}{\leq} 6 \left(1 + 2\pi^2 f^2 |d|^{-1} \right)^2 \left(\frac{f^2}{\kappa} \right)^{2/3},$$

which is smaller than 1 for $\kappa > \kappa^*$. □

11.2. Nonexistence of nontrivial solutions II

A second threshold for the nonexistence of nontrivial solutions may be obtained by studying the time-dependent Lugiato-Lefever equation

$$i\partial_t a = -(i - \zeta)a - da_{xx} - (1 + i\kappa)|a|^2 a + if. \quad (11.16)$$

Modifying slightly the proof by Jahnke, Mikl and Schnaubelt [21], who considered (11.16) for $\kappa = 0$, we first derive the global well-posedness of the initial value problem for (11.16) with initial data $a(0) = \phi \in H^4(\mathbb{T})$. In [21], the corresponding well-posedness result for $\kappa = 0$ is based on the observation that the flow remains bounded in $L^2(\mathbb{T})$ and that the $H^1(\mathbb{T})$ -norm grows at most like \sqrt{t} as $t \rightarrow \infty$. It is not known whether infinite time blow-up or convergence occurs in this case. We show that for sufficiently strong nonlinear damping $\kappa \geq \frac{1}{\sqrt{3}}$ the solutions converge to a constant solution regardless of the initial datum. Combining Theorem 11.3 and Theorem 11.4 below, we obtain that for $\kappa > \min\{\kappa^*, \frac{1}{\sqrt{3}}\}$ only constant solutions exist. Notice that all weak solutions of (9.1) are smooth and in particular lie in $H^4(\mathbb{T})$.

Let us first recall a global existence and uniqueness results in the case $\kappa = 0$. It is shown in Theorem 2.1 in [21] that (11.16) with $a(0) = \phi \in H^4(\mathbb{T})$ and $\kappa = 0$ has a unique solution $a \in C(\mathbb{R}_+, H^4(\mathbb{T})) \cap C^1(\mathbb{R}_+, H^2(\mathbb{T})) \cap C^2(\mathbb{R}_+, L^2(\mathbb{T}))$. The proof of this result may be adapted to the case $\kappa > 0$ since the crucial estimate (6) in that paper is even better when $\kappa > 0$ given that the damping effect is stronger. The remaining parts of the proof need not be modified so that we get the same estimates and global well-posedness result as in [21] also in the case $\kappa > 0$.

Theorem 11.4. *Let $d \neq 0$, $\zeta, f \in \mathbb{R}$ and $\kappa \geq \frac{1}{\sqrt{3}}$. If $a(0) = \phi \in H^4(\mathbb{T})$ then the solution of (11.16) is in $C(\mathbb{R}_+; H^4(\mathbb{T}))$ and converges in $H^1(\mathbb{T})$ to a constant as $t \rightarrow \infty$. In particular, all solutions of (9.1) are constant.*

Proof. Since we will need the inequality $\|a(t)\|_2 \leq \max\{\sqrt{2\pi}|f|, \|a(0)\|_2\}$ in the proof of our convergence results, let us prove this first. For notational convenience we suppress the spatial variable in our notation.

For any given solution a of (11.16) the following estimate holds

$$\begin{aligned} \frac{d}{dt} \left(\frac{\|a(t)\|_2^2}{2} \right) &= \operatorname{Re} \left(\int_0^{2\pi} a_t(t) \overline{a(t)} dx \right) \\ &\stackrel{(11.16)}{=} \operatorname{Re} \left(\int_0^{2\pi} \left((-1 - i\zeta + (i - \kappa)|a(t)|^2)a(t) + f + ida_{xx}(t) \right) \overline{a(t)} dx \right) \\ &= -\|a(t)\|_2^2 - \kappa\|a(t)\|_4^4 + f \int_0^{2\pi} \operatorname{Re}(a(t)) dx \\ &\leq -\|a(t)\|_2^2 - \frac{\kappa}{2\pi}\|a(t)\|_2^4 + \sqrt{2\pi}|f|\|a(t)\|_2. \end{aligned}$$

So $\|a(t)\|_2$ decreases provided the last term is negative. Since this is true is precisely for $\|a(t)\|_2 \geq \sqrt{2\pi}\tilde{C}_\kappa$ by (11.3) (11.4), we conclude

$$\|a(t)\|_2 \leq \max\{\sqrt{2\pi}\tilde{C}_\kappa, \|a(0)\|_2\} \stackrel{(11.4)}{\leq} \max\{\sqrt{2\pi}|f|, \|a(0)\|_2\} \quad \text{for all } t \geq 0. \quad (11.17)$$

Furthermore, using the equation for a and integration by parts we get

$$\begin{aligned} \frac{d}{dt} \left(\frac{\|a_x(t)\|_2^2}{2} \right) &= \operatorname{Re} \left(\int_0^{2\pi} a_{xt}(t) \overline{a_x(t)} dx \right) \\ &= -\operatorname{Re} \left(\int_0^{2\pi} a_t(t) \overline{a_{xx}(t)} dx \right) \\ &\stackrel{(11.16)}{=} -\operatorname{Re} \left(\int_0^{2\pi} \left((-1 - i\zeta + (i - \kappa)|a(t)|^2)a(t) + f + ida_{xx}(t) \right) \overline{a_{xx}(t)} dx \right) \\ &= -\int_0^{2\pi} |a_x(t)|^2 dx - \kappa \int_0^{2\pi} |a(t)|^2 |a_x(t)|^2 dx - 2\kappa \int_0^{2\pi} \operatorname{Re} \left(a(t) \overline{a_x(t)} \right)^2 dx \\ &\quad - 2 \int_0^{2\pi} \operatorname{Im} \left(a(t) \overline{a_x(t)} \right) \operatorname{Re} \left(a(t) \overline{a_x(t)} \right) dx. \end{aligned}$$

Writing $a\bar{a}_x = s + ir$ and using the scalar inequality

$$-\kappa(s^2 + r^2) - 2\kappa s^2 - 2sr \leq \underbrace{(-2\kappa + \sqrt{1 + \kappa^2})}_{=:\alpha_\kappa} (s^2 + r^2), \quad (s, r \in \mathbb{R}), \quad (11.18)$$

we get the estimate

$$\frac{d}{dt} \left(\frac{\|a_x(t)\|_2^2}{2} \right) \leq -\|a_x(t)\|_2^2 + \alpha_\kappa \int_0^{2\pi} |a(t)|^2 |a_x(t)|^2 dx \quad \text{for all } t \geq 0.$$

Since we assumed $\kappa \geq \frac{1}{\sqrt{3}}$, we have $\alpha_\kappa \leq 0$ so that $\|a_x(t)\|_2^2$ decays exponentially to 0. The Poincaré-Wirtinger inequality (cf. 5.8.1 in [12]) implies $\|a(t) - \frac{1}{2\pi} \int_0^{2\pi} a(t) dx\|_2$ decays exponentially as $t \rightarrow \infty$. The L^2 -boundedness of $a(t)$ derived in (11.17) now implies that the sequence $\int_0^{2\pi} a(t) dx$ is bounded, hence $a(t_m)$ converges in $L^2(\mathbb{T})$ for some sequence $t_m \nearrow \infty$ to some constant solution a^* of (9.1). It remains to prove that this actually implies the convergence of the whole sequence.

By the fundamental theorem of calculus, we get

$$\|a(t) - a^*\|_\infty \leq \|a_x(t)\|_1 + \min_{[0, 2\pi]} |a(t) - a^*| \leq \sqrt{2\pi} \|a_x(t)\|_2 + \frac{1}{\sqrt{2\pi}} \|a(t) - a^*\|_2. \quad (11.19)$$

In particular, the subsequence $a(t_m)$ converges uniformly to the constant a^* . So for any given $\delta \in (0, 1)$, we can find an $\varepsilon > 0$ such that all $h \in \mathbb{C}$ with $|h| < \varepsilon$ satisfy the

inequality

$$\begin{aligned}
& \operatorname{Re} \left((i - \kappa) \left(|a^* + h|^2 (a^* + h) - |a^*|^2 a^* \right) \bar{h} \right) \\
&= -\kappa |a^*|^2 |h|^2 - 2\kappa \left(\operatorname{Re} (a^* \bar{h}) \right)^2 - 2 \operatorname{Im} (a^* \bar{h}) \operatorname{Re} (a^* \bar{h}) + O(|h|^3) \\
&\stackrel{(11.18)}{\leq} \alpha_\kappa |a^*|^2 |h|^2 + O(|h|^3) \\
&\leq \delta |h|^2.
\end{aligned} \tag{11.20}$$

Here we used $\alpha_\kappa \leq 0$. Choosing t_m large enough, we can achieve

$$\|a(t_m) - a^*\|_2 \leq \frac{\sqrt{2\pi}}{4} \varepsilon \quad \text{and} \quad \|a_x(t)\|_2 \leq \frac{1}{4\sqrt{2\pi}} \varepsilon \quad \text{for all } t \geq t_m. \tag{11.21}$$

So the function $h(t) := a(t) - a^*$ satisfies for $t \geq t_m$ the following differential inequality provided $\|h(t)\|_\infty \leq \varepsilon$

$$\begin{aligned}
\frac{d}{dt} \left(\frac{\|h(t)\|_2^2}{2} \right) &= \operatorname{Re} \left(\int_0^{2\pi} \partial_t h(t) \bar{h}(t) dx \right) \\
&\stackrel{(11.16)}{=} -\|h(t)\|_2^2 + \operatorname{Re} \left((i - \kappa) \int_0^{2\pi} \left(|a^* + h(t)|^2 (a^* + h(t)) - |a^*|^2 a^* \right) \bar{h}(t) dx \right) \\
&\stackrel{(11.20)}{\leq} (-1 + \delta) \|h(t)\|_2^2.
\end{aligned}$$

Given that $\|h(t_m)\|_\infty \leq \frac{\sqrt{2\pi}}{4} \varepsilon < \varepsilon$, we infer that $\|h(t)\|_2 = \|a(t) - a^*\|_2$ decreases on some maximal interval $(t_m, t_m + T)$ and we want to show $T = \infty$. From (11.21), we infer

$$\|h(t)\|_2 \leq \frac{\sqrt{2\pi}}{4} \varepsilon, \quad \|h_x(t)\|_2 \leq \frac{1}{4\sqrt{2\pi}} \varepsilon \quad \text{for all } t \in [t_m, t_m + T]$$

so that (11.19) implies

$$\|h(t)\|_\infty \leq \sqrt{2\pi} \cdot \frac{1}{4\sqrt{2\pi}} \varepsilon + \frac{1}{\sqrt{2\pi}} \cdot \frac{\sqrt{2\pi}}{4} \varepsilon \leq \frac{\varepsilon}{2} < \varepsilon \quad \text{for all } t \in [t_m, t_m + T].$$

As shown above, this implies that $\|h(t)\|_2$ is decreasing on a right neighborhood of $t_m + T$. So we conclude that there cannot be a finite maximal T with the property mentioned above. As a consequence, $T = \infty$, $\|h(t)\|_2$ is decreasing on $[t_m, \infty)$ and we obtain $\|a(t) - a^*\|_{H^1(\mathbb{T})} = \|h(t)\|_{H^1(\mathbb{T})} \rightarrow 0$ as claimed. \square

We add an extension of this result that covers damping parameters $\kappa < \frac{1}{\sqrt{3}}$. In this case we may obtain the convergence of the flow provided the initial condition $\phi = a(0)$ has the property that $\|\phi_x\|_2$ and $\|\phi\|_2$ are not too large.

Lemma 11.5. *Assume $d \neq 0, \zeta, f \in \mathbb{R}$ and $\kappa < \frac{1}{\sqrt{3}}$. Assume that the initial condition $a(0) = \phi \in H^4(\mathbb{T})$ satisfies*

$$2\pi\|\phi_x\|_2 + \max\{\sqrt{2\pi}|f|, \|\phi\|_2\} < \sqrt{\frac{2\pi}{\alpha_\kappa}}. \quad (11.22)$$

Then the uniquely determined solution $a \in C(\mathbb{R}_+, H^4(\mathbb{T}))$ of (11.16) converges in $H^1(\mathbb{T})$ to a constant.

Proof. We argue as above. Using the same estimate as in the above proof, we get now for $\alpha_\kappa > 0$

$$\begin{aligned} \frac{d}{dt} \left(\frac{\|a_x(t)\|_2^2}{2} \right) &\leq -\|a_x(t)\|_2^2 + \alpha_\kappa \int_0^{2\pi} |a(t)|^2 |a_x(t)|^2 \\ &\leq (-1 + \alpha_\kappa \|a(t)\|_\infty^2) \|a_x(t)\|_2^2 \\ &\stackrel{(11.19)}{\leq} \left(-1 + \alpha_\kappa (\sqrt{2\pi} \|a_x(t)\|_2 + \frac{1}{\sqrt{2\pi}} \|a(t)\|_2)^2 \right) \|a_x(t)\|_2^2 \\ &\stackrel{(11.17)}{\leq} \left(-1 + \alpha_\kappa (\sqrt{2\pi} \|a_x(t)\|_2 + \frac{1}{\sqrt{2\pi}} \max\{\sqrt{2\pi}|f|, \|a(0)\|_2\})^2 \right) \|a_x(t)\|_2^2. \end{aligned}$$

So the prefactor is negative for small $t > 0$ by assumption (11.22). Hence, by monotonicity, it remains negative for all $t > 0$ and we conclude as above. \square

We do not know whether the above convergence result is sharp in the sense that there are initial data causing non-convergence or even blow-up in infinite time. As above we moreover infer that all nonconstant stationary solutions a for $\kappa < \frac{1}{\sqrt{3}}$ satisfy

$$2\pi\|a_x\|_2 + \max\{\sqrt{2\pi}|f|, \|a\|_2\} \geq \sqrt{\frac{2\pi}{\alpha_\kappa}}.$$

12. Continuation

Following the discussion of Section 4.3, we prove the existence of nontrivial solutions of (9.2) in a neighborhood of solutions for $(\varepsilon, \kappa) = (0, 0)$ found in Section 3. Similarly, we will use a rescaled version of (9.2) given by

$$-du'' + (\tilde{\zeta} - \varepsilon i)u - (1 + i\kappa)|u|^2 u + i\tilde{f} = 0 \quad \text{on } \mathbb{R} \quad (12.1)$$

for $d, \tilde{\zeta} > 0$, $|\tilde{f}| < \frac{2\sqrt{3}}{9}\tilde{\zeta}^{3/2}$ and $\varepsilon, \kappa \geq 0$ and rewrite it in the form

$$-d\tilde{u}'' + \tilde{\zeta}\tilde{u} - \varepsilon i\tilde{u} - (1 + i\kappa)(g(\tilde{u} + u^\infty) - g(u^\infty)) = 0 \quad (12.2)$$

where $u = \tilde{u} + u^\infty$. Again, u solves (12.1) with $\tilde{\zeta}, \tilde{f}$ if and only if $a(x) := \varepsilon^{-1/2}u(\varepsilon^{-1/2}x)$ solves (9.2) with $\zeta = \tilde{\zeta}\varepsilon^{-1}$ and $f = \tilde{f}\varepsilon^{-3/2}$ on \mathbb{R} . As before, \mathcal{H}_c and \mathcal{H}_r denote the complex and real-valued Hilbert spaces.

In particular, we prove the following result

Theorem 12.1. *Let $d, \tilde{\zeta} > 0$ and $|\tilde{f}| < \frac{2\sqrt{3}}{9}\tilde{\zeta}^{3/2}$. Then for all $\varepsilon, \kappa > 0$ sufficiently small, there are two even homoclinic solutions a of (9.2) with $\zeta = \tilde{\zeta}\varepsilon^{-1}$, $f = \tilde{f}\varepsilon^{-3/2}$ satisfying $\|a - \lim_{|x| \rightarrow \infty} a(x)\|_{H^2} \rightarrow \infty$ as $\varepsilon \rightarrow 0$ uniformly with respect to κ .*

Remark 12.2. *As in the remark after Theorem 4.11, the above theorem guarantees that above the lower envelope $(\tilde{\zeta}\varepsilon_0^{-1}, \tilde{f}\varepsilon_0^{-3/2})$ localized solutions of (9.2) exist.*

Theorem 12.1 is demonstrated in the following. We have continued the soliton solution with $d = 0.1, \tilde{\zeta} = 5, \tilde{f} = 2.9, \varepsilon = 0.5$ in κ . As in Section 4.3, for three different values of κ , the resulting solutions are shown in Figure 24. With $\varepsilon = 0.5$ the corresponding detuning and forcing values are $\zeta = \tilde{\zeta}\varepsilon^{-1} = 10$ and $f = \tilde{f}\varepsilon^{-3/2} = 8.20$. We observe, that with increasing values of κ the amplitude of the solution decreases.

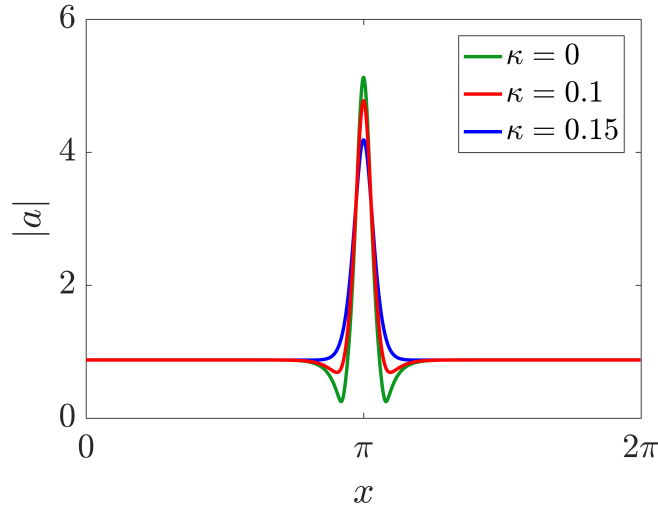


Figure 24: Solutions of (9.1) for $d = 0.1$, $\zeta = 10$, $f = 8.2$ and different values of κ .

Theorem 12.1 and Remark 12.2 are a direct consequence of the following result.

Theorem 12.3. *Let $u_i = iw_i$ for $i = 1, 2$ be the solutions of (12.1) for $(\varepsilon, \kappa) = (0, 0)$ from Section 3. Then there exist open neighborhoods U of iw_i in \mathcal{H}_c , J of $(0, 0)$ in $\mathbb{R} \times \mathbb{R}$ such that (12.2) is uniquely solvable for $(\tilde{u}, \varepsilon, \kappa)$ in $U \times J$.*

Proof. We define $F : \mathcal{H}_c \times \mathbb{R} \times \mathbb{R} \rightarrow \mathcal{L} = \{u \in L^2(\mathbb{R}; \mathbb{C}) : u(x) = u(-x)\}$ by

$$F(\tilde{u}, \varepsilon, \kappa) := -d\tilde{u}'' + \tilde{\zeta}\tilde{u} - \varepsilon i\tilde{u} - (1 + i\kappa)(g(\tilde{u} + u^\infty) - g(u^\infty)).$$

Then we have $F(i\tilde{w}_i, 0, 0) = 0$ by definition of $i\tilde{w}_i$ and $D_{\tilde{u}}F(i\tilde{w}_i, 0, 0) = -d\frac{d^2}{dx^2} + \tilde{\zeta} - Dg(u_i) : \mathcal{H}_c \rightarrow \mathcal{L}$. Due to Remark 4.7 we know that $\ker_{\mathcal{H}_c}(D_{\tilde{u}}F(i\tilde{w}_i, 0, 0)) = \{0\}$ for $i = 1, 2$. Since $D_{\tilde{u}}F(i\tilde{w}_i, 0, 0)$ is a Fredholm operator of index 0 (cf. proof of Theorem 4.11), it has a bounded inverse and thus the statement of the theorem follows from the Implicit Function Theorem. \square

Remark 12.4. *Taking into account the rescaling $a(x) = \varepsilon^{-1/2}u(\varepsilon^{-1/2}x)$, we have as in the remark after the proof of Theorem 4.11*

$$\left\| a - \lim_{|x| \rightarrow \infty} a(x) \right\|_{H^2} \geq \varepsilon^{-1/4} \left\| u - \lim_{|x| \rightarrow \infty} u(x) \right\|_{H^2} \rightarrow \infty$$

for $\varepsilon \rightarrow 0$ uniformly with respect to κ .

Part V.
Outlook and Further Results

13. A Priori Estimate

In this section, we will give an a priori estimate on the homoclinic and purely imaginary solutions w_i in the absence of damping, provided by the phase plane analysis in Lemma 3.1 for $i = 1, 2$. It will be used in Section 14.

Decomposing w_i into $w_i = \tilde{w}_i + w_i^\infty$, where $\tilde{w}_i \in \mathcal{H}_r$, we have $\lim_{|x| \rightarrow \infty} w_i = w_i^\infty := w^{(2)}$ from Section 3.1, $\lim_{|x| \rightarrow \infty} \tilde{w}_i' = 0$ and hence the constant of the first integral in (3.4) reads

$$c = \zeta(w_i^\infty)^2 - \frac{1}{2}(w_i^\infty)^4 + 2fw_i^\infty.$$

Inserting this into the first integral and using (3.5) yields

$$\begin{aligned} 0 &= -d\tilde{w}_i'^2 + \zeta\tilde{w}_i^2 + 2\zeta\tilde{w}_i w_i^\infty - \frac{1}{2}\tilde{w}_i^4 - 2\tilde{w}_i^3 w_i^\infty - 3\tilde{w}_i^2 (w_i^\infty)^2 - 2\tilde{w}_i (w_i^\infty)^3 + 2f\tilde{w}_i \\ &= -d\tilde{w}_i'^2 + \zeta\tilde{w}_i^2 - \frac{1}{2}\tilde{w}_i^4 - 2\tilde{w}_i^3 w_i^\infty - 3\tilde{w}_i^2 (w_i^\infty)^2 \end{aligned}$$

or equivalently

$$\tilde{w}_i'^2 = \frac{1}{d} \left(\zeta\tilde{w}_i^2 - \frac{1}{2}\tilde{w}_i^4 - 2\tilde{w}_i^3 w_i^\infty - 3\tilde{w}_i^2 (w_i^\infty)^2 \right). \quad (13.1)$$

Lemma 13.1. *Let $d, \zeta > 0$, $|f| < \frac{2\sqrt{3}}{9}\zeta^{3/2}$ and consider the homoclinic and purely imaginary solutions w_i of Lemma 3.1. Then $\|\tilde{w}_i\|_{H_1}$ can be estimated by*

$$\begin{aligned} \|\tilde{w}_i\|_{H_1}^2 &\leq 2\sqrt{2d} \left[-\sqrt{2\zeta - \tilde{w}_i(0)^2 - 4w_i^\infty \tilde{w}_i(0) - 6(w_i^\infty)^2} + \sqrt{2\zeta - 6(w_i^\infty)^2} \right. \\ &\quad \left. - 2w_i^\infty \arctan \left(\frac{2w_i^\infty + \tilde{w}_i(0)}{\sqrt{2\zeta - \tilde{w}_i(0)^2 - 4w_i^\infty \tilde{w}_i(0) - 6(w_i^\infty)^2}} \right) + 2w_i^\infty \arctan \frac{2w_i^\infty}{\sqrt{2\zeta - 6(w_i^\infty)^2}} \right] \\ &\quad + \max \left\{ \frac{4(\zeta - 3(w_i^\infty)^2)\tilde{w}_i(0)^2 - \tilde{w}_i(0)^4}{2\sqrt{4d(\zeta - 3(w_i^\infty)^2) - 2d\tilde{w}_i(0)^2}}, \frac{4(\zeta - 3w_{0,f}^\infty{}^2 - 2w_{0,f}^\infty \tilde{w}_{0,f}(0))\tilde{w}_{0,f}(0)^2 - \tilde{w}_{0,f}(0)^4}{2\sqrt{4d(\zeta - 3w_{0,f}^\infty{}^2 - 2w_{0,f}^\infty \tilde{w}_{0,f}(0)) - 2d\tilde{w}_{0,f}(0)^2}} \right\}. \end{aligned}$$

with

$$\tilde{w}_i(0) = -2w_i^\infty \pm \sqrt{2(\zeta - (w_i^\infty)^2)}, \quad (13.2)$$

where "−" holds for the symmetrically increasing homoclinic solution and "+" holds for the symmetrically decreasing homoclinic solution.

Proof. Using the substitution $\tilde{w}_i(x) = y$, we calculate

$$\begin{aligned}
& \int_{-\infty}^0 \tilde{w}_i(x)^2 dx \\
&= \int_0^{\tilde{w}_i(0)} \frac{y^2}{\tilde{w}'_i(\tilde{w}_i^{-1}(y))} dy \\
&\stackrel{(13.1)}{=} \sqrt{d} \int_0^{\tilde{w}_i(0)} \frac{y^2}{\sqrt{\zeta y^2 - \frac{y^4}{2} - 2w_i^\infty y^3 - 3(w_i^\infty)^2 y^2}} dy \\
&= \sqrt{2d} \int_0^{\tilde{w}_i(0)} \frac{y}{\sqrt{2\zeta - y^2 - 4w_i^\infty y - 6(w_i^\infty)^2}} dy \\
&= \sqrt{2d} \left[-\sqrt{2\zeta - y^2 - 4w_i^\infty y - 6(w_i^\infty)^2} - 2w_i^\infty \arctan \left(\frac{2w_i^\infty + y}{\sqrt{2\zeta - y^2 - 4w_i^\infty y - 6(w_i^\infty)^2}} \right) \right]_0^{\tilde{w}_i(0)} \\
&= \sqrt{2d} \left[-\sqrt{2\zeta - \tilde{w}_i(0)^2 - 4w_i^\infty \tilde{w}_i(0) - 6(w_i^\infty)^2} + \sqrt{2\zeta - 6(w_i^\infty)^2} \right. \\
&\quad \left. - 2w_i^\infty \arctan \left(\frac{2w_i^\infty + \tilde{w}_i(0)}{\sqrt{2\zeta - \tilde{w}_i(0)^2 - 4w_i^\infty \tilde{w}_i(0) - 6(w_i^\infty)^2}} \right) + 2w_i^\infty \arctan \frac{2w_i^\infty}{\sqrt{2\zeta - 6(w_i^\infty)^2}} \right],
\end{aligned}$$

and $\tilde{w}_i(0)$ satisfies

$$\zeta \tilde{w}_i^2 - \frac{1}{2} \tilde{w}_i^4 - 2\tilde{w}_i^3 w_i^\infty - 3\tilde{w}_i^2 (w_i^\infty)^2 = 0,$$

which shows

$$\tilde{w}_i(0) = -2w_i^\infty \pm \sqrt{2(\zeta - (w_i^\infty)^2)}$$

where "-" holds for the symmetrically increasing homoclinic solution and "+" holds for the symmetrically decreasing homoclinic solution.

Now we estimate $\int_{-\infty}^0 \tilde{w}'_i(x)^2 dx$. Using again the substitution $\tilde{w}_i(x) = y$ together with the estimate $|y| \sqrt{\alpha - y^2} \leq \frac{|y|(\alpha - |y|^2)}{\sqrt{\alpha - |y|_{max}^2}}$, we get if $\tilde{w}_i w_i^\infty \geq 0$,

$$\begin{aligned}
\int_{-\infty}^0 \tilde{w}'_i(x)^2 dx &= \int_0^{\tilde{w}_i(0)} \tilde{w}'_i(\tilde{w}_i^{-1}(y)) dy \\
&= \frac{1}{\sqrt{d}} \int_0^{\tilde{w}_i(0)} y \sqrt{\zeta - \frac{y^2}{2} - 2w_i^\infty y - 3(w_i^\infty)^2} dy \\
&\leq \frac{1}{\sqrt{2d}} \int_0^{\tilde{w}_i(0)} y \sqrt{2(\zeta - 3(w_i^\infty)^2) - y^2} dy
\end{aligned}$$

$$\begin{aligned}
&\leq \frac{1}{\sqrt{2d}} \int_0^{\tilde{w}_i(0)} \frac{y(2(\zeta - 3(w_i^\infty)^2) - y^2)}{\sqrt{2(\zeta - 3(w_i^\infty)^2) - \tilde{w}_i(0)^2}} dy \\
&= \frac{[(\zeta - 3(w_i^\infty)^2)y^2 - \frac{1}{4}y^4]_0^{\tilde{w}_i(0)}}{\sqrt{4d(\zeta - 3(w_i^\infty)^2) - 2d\tilde{w}_i(0)^2}} \\
&= \frac{4(\zeta - 3(w_i^\infty)^2)\tilde{w}_i(0)^2 - \tilde{w}_i(0)^4}{4\sqrt{4d(\zeta - 3(w_i^\infty)^2) - 2d\tilde{w}_i(0)^2}}.
\end{aligned}$$

Similarly if $\tilde{w}_i w_i^\infty \leq 0$,

$$\begin{aligned}
&\int_{-\infty}^0 \tilde{w}'_{0,f}(x)^2 dx \\
&\leq \frac{1}{\sqrt{2d}} \int_0^{\tilde{w}_{0,f}(0)} y \sqrt{2(\zeta - 3w_{0,f}^{\infty 2} - 2w_{0,f}^\infty \tilde{w}_{0,f}(0)) - y^2} dy \\
&\leq \frac{1}{\sqrt{2d}} \int_0^{\tilde{w}_{0,f}(0)} \frac{y(2(\zeta - 3w_{0,f}^{\infty 2} - 2w_{0,f}^\infty \tilde{w}_{0,f}(0)) - y^2)}{\sqrt{2(\zeta - 3w_{0,f}^{\infty 2} - 2w_{0,f}^\infty \tilde{w}_{0,f}(0)) - \tilde{w}_{0,f}(0)^2}} dy \\
&= \frac{[(\zeta - 3w_{0,f}^{\infty 2} - 2w_{0,f}^\infty \tilde{w}_{0,f}(0))y^2 - \frac{1}{4}y^4]_0^{\tilde{w}_{0,f}(0)}}{\sqrt{4d(\zeta - 3w_{0,f}^{\infty 2} - 2w_{0,f}^\infty \tilde{w}_{0,f}(0)) - 2d\tilde{w}_{0,f}(0)^2}} \\
&= \frac{4(\zeta - 3w_{0,f}^{\infty 2} - 2w_{0,f}^\infty \tilde{w}_{0,f}(0))\tilde{w}_{0,f}(0)^2 - \tilde{w}_{0,f}(0)^4}{4\sqrt{4d(\zeta - 3w_{0,f}^{\infty 2} - 2w_{0,f}^\infty \tilde{w}_{0,f}(0)) - 2d\tilde{w}_{0,f}(0)^2}}.
\end{aligned}$$

Finally, we obtain

$$\begin{aligned}
\|\tilde{w}_i\|_{H^1}^2 &\leq 2\sqrt{2d} \left[-\sqrt{2\zeta - \tilde{w}_i(0)^2 - 4w_i^\infty \tilde{w}_i(0) - 6(w_i^\infty)^2} + \sqrt{2\zeta - 6(w_i^\infty)^2} \right. \\
&\quad \left. - 2w_i^\infty \arctan \left(\frac{2w_i^\infty + \tilde{w}_i(0)}{\sqrt{2\zeta - \tilde{w}_i(0)^2 - 4w_i^\infty \tilde{w}_i(0) - 6(w_i^\infty)^2}} \right) + 2w_i^\infty \arctan \frac{2w_i^\infty}{\sqrt{2\zeta - 6(w_i^\infty)^2}} \right] \\
&\quad + \max \left\{ \frac{4(\zeta - 3(w_i^\infty)^2)\tilde{w}_i(0)^2 - \tilde{w}_i(0)^4}{2\sqrt{4d(\zeta - 3(w_i^\infty)^2) - 2d\tilde{w}_i(0)^2}}, \frac{4(\zeta - 3w_{0,f}^{\infty 2} - 2w_{0,f}^\infty \tilde{w}_{0,f}(0))\tilde{w}_{0,f}(0)^2 - \tilde{w}_{0,f}(0)^4}{2\sqrt{4d(\zeta - 3w_{0,f}^{\infty 2} - 2w_{0,f}^\infty \tilde{w}_{0,f}(0)) - 2d\tilde{w}_{0,f}(0)^2}} \right\}.
\end{aligned}$$

□

14. Spectral Properties of the Linearization

In this section, we will calculate the spectrum of the linearized operator $L : \mathcal{H}_c \rightarrow L^2(\mathbb{R})$,

$$L := -d \frac{d^2}{dx^2} + \zeta - Dg(iw_i),$$

where iw_i are the homoclinic and purely imaginary solutions of Lemma 3.1 and $g(a) = |a|^2 a - if$, $Dg(a)z := \left. \frac{d}{dt} g(a + tz) \right|_{t=0} = 2|a|^2 z + a^2 \bar{z}$. The spectral analysis of this chapter only applies for w_1 symmetrically increasing if $f > 0$ and w_2 symmetrically decreasing if $f < 0$.

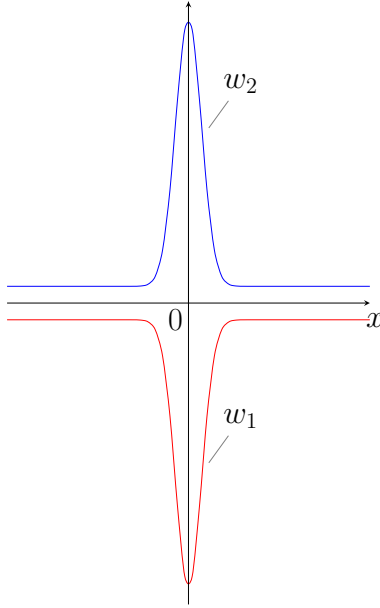


Figure 25: w_1 for $f > 0$ and w_2 for $f < 0$.

Splitting the linearized operator into real and imaginary part yields $L_j : \mathcal{H}_r \rightarrow L^2(\mathbb{R})$ for $j = 1, 2$ from Section 4.1. Then, $\lambda := \lambda_1 + i\lambda_2 \in \rho(L)$ whenever $(L - \lambda)^{-1} : L^2(\mathbb{R}) \rightarrow \mathcal{H}_c$ exists as a bounded linear operator. This is true if and only if $(L_1 - \lambda_1)^{-1} : L^2(\mathbb{R}) \rightarrow \mathcal{H}_r$ and $(L_2 - \lambda_2)^{-1} : L^2(\mathbb{R}) \rightarrow \mathcal{H}_r$ exist as bounded linear operators and thus, $\lambda \in \rho(L_1) \cap \rho(L_2)$. Hence,

$$\sigma(L) = \mathbb{R} \setminus \rho(L) = \sigma(L_1) \cup \sigma(L_2).$$

In the following, we will calculate the spectrum of the operator L , or L_1 and L_2 , respectively. By Section 4.1, we already know, that $0 \notin \sigma(L)$.

We start by calculating the essential spectra of L_1 and L_2 in the next lemma.

Lemma 14.1. *Let $d, \zeta > 0$ and $|f| < \frac{2\sqrt{3}}{9}\zeta^{3/2}$. The essential spectrum of L is given by $\sigma_{ess}(L) = [\zeta - 3(w_i^\infty)^2, \infty)$.*

Proof. Define

$$L_0 := -d \frac{d^2}{dx^2} + \zeta - 3(w_i^\infty)^2$$

Then $\sigma_{ess}(L_0) = [\zeta - 3(w_i^\infty)^2, \infty)$. We note that

$$L_2 = L_0 - 3\tilde{w}_i^2 - 6\tilde{w}_i w_i^\infty.$$

As $3\tilde{w}_i^2 + 6\tilde{w}_i w_i^\infty$ is a relatively compact perturbation (see Corollary 2 in Section XIII.4 in [40]), we infer that $\sigma_{ess}(L_2) = \sigma_{ess}(L_0) = [\zeta - 3(w_i^\infty)^2, \infty)$. Similarly, $\sigma_{ess}(L_1) = \sigma_{ess}(L_0) = [\zeta - (w_i^\infty)^2, \infty)$ and hence, as $\zeta - 3(w_i^\infty)^2 \leq \zeta - (w_i^\infty)^2$, we infer that $\sigma_{ess}(L) = [\zeta - 3(w_i^\infty)^2, \infty)$. \square

Lemma 14.2. *Let $d, \zeta > 0$, $|f| < \frac{2\sqrt{3}}{9}\zeta^{3/2}$. Then $\sigma(L_1) \subset [-\frac{f}{w_2^\infty + \tilde{w}_2(0)}, \infty)$ for $f < 0$ and $\sigma(L_1) \subset [\frac{f}{w_1^\infty + \tilde{w}_1(0)}, \infty)$ for $f > 0$.*

Proof. We will prove the assertion only for $f < 0$. However, a similar proof applies for $f > 0$. Observe that

$$L_1(w_2^\infty + \tilde{w}_2) = -f.$$

Hence, for all $\eta \in C_c^\infty(\mathbb{R})$,

$$\begin{aligned} - \int_{\mathbb{R}} f \frac{\eta^2}{w_2^\infty + \tilde{w}_2} dx &= \int_{\mathbb{R}} L_1(w_2^\infty + \tilde{w}_2) \cdot \frac{\eta^2}{w_2^\infty + \tilde{w}_2} dx \\ &= \int_{\mathbb{R}} d\eta'^2 + (\zeta - (w_2^\infty + \tilde{w}_2)^2)\eta^2 - d \left(\frac{\eta' \tilde{w}_2'}{w_2^\infty + \tilde{w}_2} - \eta' \right)^2 dx \\ &\leq \int_{\mathbb{R}} d\eta'^2 + (\zeta - (w_2^\infty + \tilde{w}_2)^2)\eta^2 dx. \end{aligned}$$

This leads to

$$\int_{\mathbb{R}} d\eta'^2 + (\zeta - (w_2^\infty + \tilde{w}_2)^2)\eta^2 dx \geq - \int_{\mathbb{R}} f \frac{\eta^2}{w_2^\infty + \tilde{w}_2} dx \geq - \frac{f}{w_2^\infty + \tilde{w}_2(0)} \int_{\mathbb{R}} \eta^2 dx$$

for all $\eta \in C_c^\infty(\mathbb{R})$ and by density, this is also true for all $\eta \in H^1(\mathbb{R})$ and thus

$$\sigma(L_1) \subset \left[-\frac{f}{w_2^\infty + \tilde{w}_2(0)}, \infty \right).$$

\square

Lemma 14.3. *Let $d, \zeta > 0$, $|f| < \frac{2\sqrt{3}}{9}\zeta^{3/2}$. Then L_2 has exactly one negative eigenvalue with*

$$\lambda_1(L_2) \leq - \frac{\sqrt{d}}{\sqrt{\zeta - 3(w_i^\infty)^2}} \tilde{w}_i(0)^4 \|\tilde{w}_i\|_{L^2}^{-2},$$

where $\|\tilde{w}_i\|_{L^2}$ as in the proof of Lemma 13.1.

Proof. The quadratic form is given by

$$b_{L_1}(\phi) := \int_{\mathbb{R}} d\phi'^2 + (\zeta - 3(w_i^\infty + \tilde{w}_i)^2)\phi^2 dx$$

and testing

$$\begin{aligned} 0 &= -d\tilde{w}_i'' + \zeta(\tilde{w}_i + w_i^\infty) - (\tilde{w}_i + w_i^\infty)^3 + f \\ &= -d\tilde{w}_i'' + \zeta\tilde{w}_i - \tilde{w}_i^3 - 3\tilde{w}_i^2w_i^\infty - 3\tilde{w}_i(w_i^\infty)^2 + \zeta w_i^\infty - (w_i^\infty)^3 + f \\ &= -d\tilde{w}_i'' + \zeta\tilde{w}_i - \tilde{w}_i^3 - 3\tilde{w}_i^2w_i^\infty - 3\tilde{w}_i(w_i^\infty)^2 \end{aligned}$$

by \tilde{w}_i , yields

$$\int_{\mathbb{R}} d\tilde{w}_i'^2 + \zeta\tilde{w}_i^2 - \tilde{w}_i^4 - 3\tilde{w}_i^3w_i^\infty - 3\tilde{w}_i^2(w_i^\infty)^2 dx = 0.$$

Hence,

$$\begin{aligned} b_{L_1}(\tilde{w}_i) &:= \int_{\mathbb{R}} d\tilde{w}_i'^2 + (\zeta - 3(w_i^\infty + \tilde{w}_i)^2)\tilde{w}_i^2 dx \\ &= \int_{\mathbb{R}} d\tilde{w}_i'^2 + \zeta\tilde{w}_i^2 - \tilde{w}_i^4 - 3\tilde{w}_i^3w_i^\infty - 3\tilde{w}_i^2(w_i^\infty)^2 - 2\tilde{w}_i^4 - 3\tilde{w}_i^3w_i^\infty dx \\ &= - \int_{\mathbb{R}} 2\tilde{w}_i^4 + 3\tilde{w}_i^3w_i^\infty dx \\ &\leq -2 \int_{\mathbb{R}} \tilde{w}_i^4 dx = -4 \int_{-\infty}^0 \tilde{w}_i^4 dx = -4 \int_0^{\tilde{w}_i(0)} \frac{y^4}{\tilde{w}_i'(\tilde{w}_i^{-1}(y))} dy \\ &\stackrel{(13.1)}{=} -4\sqrt{d} \int_0^{\tilde{w}_i(0)} \frac{y^4}{\sqrt{\zeta y^2 - \frac{y^4}{2} - 2w_i^\infty y^3 - 3(w_i^\infty)^2 y^2}} dy \\ &= -4\sqrt{2d} \int_0^{\tilde{w}_i(0)} \frac{y^3}{\sqrt{2\zeta - y^2 - 4w_i^\infty y - 6(w_i^\infty)^2}} dy \\ &\leq -4\sqrt{2d} \int_0^{\tilde{w}_i(0)} \frac{y^3}{\sqrt{2\zeta - 6(w_i^\infty)^2}} dy \\ &= -\frac{\sqrt{d}}{\sqrt{\zeta - 3(w_i^\infty)^2}} \tilde{w}_i(0)^4 < 0. \end{aligned}$$

As $\inf \sigma_{ess}(L_2) = \zeta - 3(w_i^\infty)^2 > 0$, there is at least one negative eigenvalue of L_2 with

$$\lambda_1(L_2) \leq -\frac{\sqrt{d}}{\sqrt{\zeta - (w_i^\infty)^2}} \tilde{w}_i(0)^4 \|\tilde{w}_i\|_{L^2}^{-2}$$

where $\|\tilde{w}_i\|_{L^2}$ as in the proof of Lemma 13.1 (cf. Proposition 12.1 in [20]).

Now assume that there is a second negative eigenvalue $\lambda_2(L_2)$. In Section 4.1, we have seen that $\ker_{H^2}(L_2) = \text{span}\{\tilde{w}_i'\}$ and \tilde{w}_i' has exactly one zero. Hence, the eigenfunction

corresponding to $\lambda_2(L_2)$ is of fixed sign. However, this is only possible if $\lambda_2(L_2)$ is the smallest eigenvalue of L_2 . Consequently L_2 admits exactly one negative eigenvalue with

$$\lambda_1(L_2) \leq -\frac{\sqrt{d}}{\sqrt{\zeta - 3(w_i^\infty)^2}} \tilde{w}_i(0)^4 \|\tilde{w}_i\|_{L^2}^{-2}$$

where $\|\tilde{w}_i\|_{L^2}$ as in the proof of Lemma 13.1. □

The previous lemmas together with $0 \notin \sigma(L)$ (Section 4.1) now yield the main theorem of this section.

Theorem 14.4. *Let $d, \zeta > 0$, $0 < |f| < \frac{2\sqrt{3}}{9}\zeta^{3/2}$. Then,*

$$\sigma(L_1) \subset \left[\frac{f}{w_1^\infty + \tilde{w}_1(0)}, \infty \right) \quad \text{for } f < 0$$

and

$$\sigma(L_1) \subset \left[-\frac{f}{w_2^\infty + \tilde{w}_2(0)}, \infty \right) \quad \text{for } f > 0.$$

Furthermore,

$$\sigma(L_2) \subset \left(-\infty, -\frac{\sqrt{d}}{\sqrt{\zeta - (w_i^\infty)^2}} \tilde{w}_i(0)^4 \|\tilde{w}_i\|_{L^2}^{-2} \right] \cup (0, \infty)$$

and hence

$$\sigma(L) = \sigma(L_1) \cup \sigma(L_2) \subset \left(-\infty, -\frac{\sqrt{d}}{\sqrt{\zeta - (w_i^\infty)^2}} \tilde{w}_i(0)^4 \|\tilde{w}_i\|_{L^2}^{-2} \right] \cup (0, \infty).$$

15. Third Order Dispersion

Throughout this thesis, we have neglected higher order dispersion as, in general, they are several magnitudes smaller than the second order effect. Nevertheless, there are some cases, where one should take it into account. Especially for dark solitons ($d < 0$) and corresponding frequency combs with high comb bandwidth, third order dispersion (TOD) cannot be neglected, cf. [27],[43]. The modified equation then reads

$$-da'' - iea''' + (\zeta - i)a - |a|^2 a + if = 0, \quad a(\cdot) = a(\cdot + 2\pi). \quad (15.1)$$

In this case, we lack reversibility $x \rightarrow -x$, which means that if u is a solution, then $v(x) = u(-x)$ is not a solution. This causes numerical and analytical difficulties, as it is no longer possible to consider the equation on $[0, \pi]$ together with homogeneous Neumann boundary conditions. Therefore, it remains unclear how to deal with the shift invariance of the problem. However, we prove some a priori bounds for nontrivial periodic solutions.

In this section, we work in fractional Sobolev spaces. Following [9], for $s \in \mathbb{R}$ we denote the standard fractional Sobolev norm on \mathbb{T} by

$$\|a\|_s := \sum_{k \in \mathbb{Z}} (1 + |k|^{2s}) |\hat{a}_k|^2,$$

where

$$\hat{a}_k := \frac{1}{2\pi} \int_0^{2\pi} a(x) e^{-ikx} dx.$$

The fractional Sobolev space is then defined as

$$H^s(\mathbb{T}) := \{a = \sum_{k \in \mathbb{Z}} \hat{a}_k e^{ikx} \in L^2(\mathbb{T}) : \|a\|_s < \infty\}.$$

Theorem 15.1. *Let $d, e \neq 0$, $\zeta, f \in \mathbb{R}$. Then there is a constant $C = C(|d|, \frac{1}{|e|}, |\zeta|, |f|)$ such that every solution $a \in C^3(\mathbb{T})$ of (15.1) satisfies*

$$\|a\|_{3/2} \leq C.$$

Proof. Taking $a = v + iw$, we can rewrite (15.1) as a system

$$\begin{aligned} ew''' - dv'' &= -w - \zeta v + (v^2 + w^2)v, \\ -ev''' - dw'' &= v - \zeta w + (v^2 + w^2)w - f. \end{aligned}$$

First, we will give an L^2 -estimate. We define $G : [0, 2\pi] \rightarrow \mathbb{R}$ by

$$G := d(wv' - vv') + e\left(\frac{1}{2}v'^2 + \frac{1}{2}w'^2 - ww'' - vv''\right).$$

Using the differential equation we get for $g = G'$

$$\begin{aligned} g &= d(wv'' - w''v) - e(vv''' + ww''') \\ &= -w(-w - \zeta v + (v^2 + w^2)v) + v(v - \zeta w + (v^2 + w^2)w - f) \\ &= (v^2 + w^2) - fv. \end{aligned}$$

Since G is 2π -periodic, we get

$$0 = \int_0^{2\pi} g dx = \int_0^{2\pi} (v^2 + w^2 - fv) dx \geq \|a\|_2^2 - \sqrt{2\pi} |f| \|a\|_2,$$

which implies

$$\|a\|_2 \leq \sqrt{2\pi} |f|. \quad (15.2)$$

Now we can give a first $H^{3/2}$ -estimate. The Fourier coefficients of a satisfy

$$-ei(ik)^3 \widehat{a}_k - d(ik)^2 \widehat{a}_k = (i - \zeta) \widehat{a}_k + (\widehat{|a|^2 a})_k - if \delta_{0k}$$

for all $k \in \mathbb{Z}$. Thus, for $k \neq 0$

$$-ek^3 \widehat{a}_k = (-dk^2 + i - \zeta) \widehat{a}_k + (\widehat{|a|^2 a})_k.$$

Testing the equation with $\bar{a}_k \text{sign}(k)$ leads to

$$-e \sum_{|k| \geq 1} |\widehat{a}_k|^2 |k|^3 = \sum_{|k| \geq 1} (-dk^2 + i - \zeta) \text{sign}(k) |\widehat{a}_k|^2 + (\widehat{|a|^2 a})_k \bar{a}_k \text{sign}(k).$$

By definition and using the differential equation as well as Hölder's inequality, we get a first $H^{3/2}$ -estimate for $r \in (0, \frac{3}{2})$ and $s = \frac{r}{r-1}$

$$\begin{aligned} \|a\|_{3/2}^2 &= \sum_{k \in \mathbb{Z}} (1 + |k|^3) |\widehat{a}_k|^2 \\ &= \frac{1}{2\pi} \|a\|_2^2 + \sum_{|k| \geq 1} |k|^3 |\widehat{a}_k|^2 \\ &\leq f^2 + \sum_{|k| \geq 1} \frac{1}{|e|} (|d|k^2 + 1 + |\zeta|) |\widehat{a}_k|^2 + \sum_{|k| \geq 1} \frac{1}{|e|} |(\widehat{|a|^2 a})_k| |\widehat{a}_k| \\ &\leq f^2 + \frac{|d|}{|e|} \sum_{|k| \geq 1} (1 + k^2)^{\frac{3}{2r}} |\widehat{a}_k|^{\frac{2}{r}} |\widehat{a}_k|^{\frac{2}{s}} (1 + k^2)^{1 - \frac{3}{2r}} \\ &\quad + \frac{1 + |\zeta|}{|e|} \sum_{|k| \geq 1} |\widehat{a}_k|^2 + \sum_{|k| \geq 1} \frac{1}{|e|} |(\widehat{|a|^2 a})_k| |\widehat{a}_k| \\ &\leq f^2 + \frac{|d|}{|e|} \left(\sum_{|k| \geq 1} (1 + k^2)^{\frac{3}{2}} |\widehat{a}_k|^2 \right)^{1/r} \left(\sum_{|k| \geq 1} |\widehat{a}_k|^2 \right)^{1/s} + \frac{1 + |\zeta|}{|e|} \cdot f^2 + \frac{1}{|e|} \sum_{|k| \geq 1} |(\widehat{|a|^2 a})_k| |\widehat{a}_k|. \end{aligned}$$

Using the estimate $(1 + k^2)^{\frac{3}{2}} \leq 2^{\frac{3}{2}}(1 + |k|^3)$, we obtain

$$\begin{aligned} \|a\|_{3/2}^2 &\leq f^2 + 2^{\frac{3}{2r}}(2\pi)^{-\frac{1}{s}} \frac{|d|}{|e|} \|a\|_{3/2}^{\frac{2}{r}} \|a\|_{\frac{2}{s}}^{\frac{2}{s}} + \frac{1 + |\zeta|}{|e|} f^2 + \frac{1}{|e|} \sum_{|k| \geq 1} |(\widehat{|a|^2 a})_k| |\widehat{a}_k| \\ &\leq f^2 + 2^{\frac{3}{2r}} \frac{|d|}{|e|} |f|^{\frac{2}{s}} \|a\|_{3/2}^{\frac{2}{r}} + \frac{1 + |\zeta|}{|e|} f^2 + \frac{1}{|e|} \underbrace{\sum_{|k| \geq 1} |(\widehat{|a|^2 a})_k| |\widehat{a}_k|}_{=: S_1}. \end{aligned} \quad (15.3)$$

Then we get

$$\begin{aligned} S_1 &= \sum_{|k| \geq 1} |(\widehat{|a|^2 a})_k| |\widehat{a}_k| \\ &= \sum_{|k| \geq 1} |(\widehat{|a|^2 a})_k| |\widehat{a}_k \cdot k^{\frac{3}{2}}| |k|^{-\frac{3}{2}} \\ &\leq \left\| \widehat{|a|^2 a} \right\|_{\infty} \left\| \widehat{a}_k \cdot k^{\frac{3}{2}} \right\|_2 \cdot \underbrace{\left(\sum_{|k| \geq 1} |k|^{-3} \right)^{\frac{1}{2}}}_{=: \tilde{C}} \\ &\leq \tilde{C} \left\| \widehat{|a|^2 a} \right\|_{\infty} \|a\|_{3/2}. \end{aligned}$$

Using $(a \star b)_l := \sum_{m \in \mathbb{Z}} a_{l-m} b_m$, we observe that

$$\begin{aligned} (\widehat{a\bar{a}a})_k &= \frac{1}{2\pi} \int_0^{2\pi} a(t) \bar{a}(t) a(t) e^{-ikt} dt \\ &= \frac{1}{2\pi} \int_0^{2\pi} \left(\sum_l \hat{a}_l e^{ilt} \right) \left(\sum_m \bar{\hat{a}}_m e^{-imt} \right) \left(\sum_n \hat{a}_n e^{int} \right) e^{-ikt} dt \\ &= \frac{1}{2\pi} \sum_l \sum_m \left(\sum_n \hat{a}_l \bar{\hat{a}}_m \hat{a}_n \int_0^{2\pi} e^{i(-m+l+n-k)t} dt \right) \\ &= \sum_l \hat{a}_l \sum_m \bar{\hat{a}}_m \hat{a}_{k-l-m} = (\widehat{\hat{a} \star \bar{\hat{a}} \star \hat{a}})_k. \end{aligned}$$

Now, by Young's inequality, we calculate

$$\left\| \widehat{|a|^2 a} \right\|_{\infty} = \left\| \widehat{a\bar{a}a} \right\|_{\infty} = \left\| \widehat{\hat{a} \star \bar{\hat{a}} \star \hat{a}} \right\|_{\infty} \leq \frac{1}{2\pi} \left\| \hat{a} \star \bar{\hat{a}} \star \hat{a} \right\|_{\infty} \leq \|\widehat{a}\|_{3/2}^3.$$

Then we get by a triple Hölder's inequality for $\alpha \in (0, \frac{4}{3})$

$$\begin{aligned} \|\widehat{a}\|_{3/2}^{\frac{3}{2}} &= \sum_{|k| \geq 1} |\widehat{a}_k|^{\frac{3}{2}} \\ &= \sum_{|k| \geq 1} |\widehat{a}_k|^{\alpha} |\widehat{a}_k|^{\frac{3}{2}-\alpha} |k|^{\frac{3}{2}(\frac{3}{2}-\alpha)} |k|^{\frac{3}{2}(\alpha-\frac{3}{2})} \\ &\leq \frac{1}{(2\pi)^{\alpha/2}} \|a\|_2^{\alpha} \|a\|_{3/2}^{\frac{3}{2}-\alpha} \cdot \underbrace{\left(\sum_{|k| \geq 1} |k|^{\frac{3}{2}(\alpha-\frac{3}{2}) \cdot 4} \right)^{1/4}}_{=: \sqrt{\tilde{C}_{\alpha}}}, \end{aligned}$$

where $\alpha < \frac{4}{3}$ is necessary for the convergence of \tilde{C}_α . Therefore,

$$\|\widehat{a}\|_{3/2}^3 \leq \frac{\tilde{C}_\alpha}{(2\pi)^\alpha} \|a\|_2^{2\alpha} \|a\|_{3/2}^{3-2\alpha}.$$

Finally this leads to

$$\begin{aligned} S_1 &= \sum_{|k| \geq 1} (\widehat{|a|^2 a})_k |\widehat{a}_k| \\ &\leq \tilde{C} \tilde{C}_\alpha (2\pi)^{-1-\alpha} \|a\|_2^{2\alpha} \|a\|_{3/2}^{4-2\alpha} \\ &\leq \tilde{C} \tilde{C}_\alpha (2\pi)^{-1} |f|^{2\alpha} \|a\|_{3/2}^{4-2\alpha}. \end{aligned}$$

By (15.3), we get for $\alpha \in (0, \frac{4}{3})$, $r \in (0, \frac{3}{2})$ and $s = \frac{r}{r-1}$

$$\|a\|_{3/2}^2 \leq f^2 + 2^{\frac{3}{2r}} \frac{|d|}{|e|} |f|^{\frac{2}{s}} \|a\|_{3/2}^{\frac{2}{s}} + \frac{1+|\zeta|}{|e|} f^2 + \frac{1}{|e|} \tilde{C} \tilde{C}_\alpha (2\pi)^{-1} |f|^{2\alpha} \|a\|_{3/2}^{4-2\alpha}.$$

As $r \in (0, \frac{3}{2})$ we have $\frac{2}{r} > \frac{4}{3}$ and $4 - 2\alpha \in (\frac{4}{3}, 4)$. For r close to $\frac{3}{2}$ and α close to $\frac{4}{3}$ we write $\frac{2}{r} = \frac{4}{3} + \delta = 4 - 2\alpha$ for $\delta > 0$ close to 0. This leads to

$$\|a\|_{3/2}^2 - \underbrace{\frac{|f|^{\frac{2}{3}-\delta}}{|e|} \left(2^{1+\frac{3}{4}\delta} |d| + \tilde{C} \tilde{C}_\alpha (2\pi)^{-1} f^2 \right)}_{=: C_1(f, e, d)} \|a\|_{3/2}^{\frac{4}{3}+\delta} \leq \underbrace{\left(1 + \frac{1+|\zeta|}{|e|} \right) f^2}_{=: C_2(f, \zeta, e)}.$$

With these definitions of $C_1(f, e, d)$ and $C_2(f, \zeta, e)$

$$\|a\|_{3/2}^2 \left(1 - C_1(f, e, d) \|a\|_{3/2}^{-\frac{2}{3}+\delta} \right) \leq C_2(f, \zeta, e).$$

Defining $g : (0, \infty) \rightarrow \mathbb{R}$, $g(x) := 1 - C_1(f, e, d)x^{-\frac{2}{3}+\delta}$, we have

$$g(x) = \frac{1}{2} \quad \Leftrightarrow \quad x = \left(\frac{1}{2C_1(f, e, d)} \right)^{\frac{3}{-2+3\delta}}$$

and consequently $\|a\|_{3/2} \leq (2C_2(f, \zeta, e))^{1/2}$ for $\|a\|_{3/2} \geq \left(\frac{1}{2C_1(f, e, d)} \right)^{3/(-2+3\delta)}$. Finally,

$$\|a\|_{3/2} \leq \max \left\{ (2C_2(f, \zeta, e))^{1/2}, \left(\frac{1}{2C_1(f, e, d)} \right)^{3/(-2+3\delta)} \right\}.$$

□

Remark 15.2. In Theorem 11.1, we calculated L^∞ -bounds for higher order damping. They were used to determine a maximal value κ^* such that all solutions are constant provided $\kappa > \kappa^*$. Although it would be possible to obtain them, we omit L^∞ -bounds within this section, as they cannot be used further.

16. Summary and Outlook

In this thesis, we have presented several approaches in order to investigate the stationary Lugiato-Lefever equation

$$-da'' + (\zeta - i)a - |a|^2 a + if = 0.$$

We have described analytical and numerical approaches to find periodic patterns as well as nontrivial solutions on \mathbb{R} , based on

- continuation of bright solitons of the NLS in the regime of damping and forcing,
- bifurcation with respect to ζ from the constant solution curve.

The first approach was covered in Part II, where we analytically continued the soliton solutions of the undamped and undriven cubic NLS on \mathbb{R} into the situation with forcing and damping present. This was done in three steps. First, we rigorously recalled the soliton solutions $a(x) = e^{i\alpha}\varphi(x)$ of the NLS, lying on the sphere. In a second step, we could prove that bifurcation from this sphere is only possible for $\alpha \in \left\{\frac{\pi}{2}, \frac{3\pi}{2}\right\}$ and that therefore only purely imaginary solutions bifurcate. Finally, using a rescaled version of the Lugiato-Lefever equation together with the Implicit Function Theorem, we could prove the existence of soliton solutions for large values of f and ζ . This analytical approach was supported by a large amount of numerical experiments based on numerical path continuation in the case of $d = 0.01$. Using the solutions on \mathbb{R} as an approximation to periodic solutions, we numerically continued them into a region with forcing and damping present and we covered a large region of the (ζ, f) -plane, where solitons exist. Numerically, we also investigated the stability of these solutions. Furthermore, we compared the lower and upper envelope to bounds given in the literature.

The second approach in Part III was based on a rigorous bifurcation analysis. We developed heuristics, which allowed to determine the most localized solitons on branches bifurcating from the curve of trivial solutions. In applications, soliton solutions with high comb bandwidth together with high power conversion efficiency are favorable. We approached this, by finding heuristics for the location of the most pronounced solitons and performing a large parameter study in bifurcation diagrams. We found solitons both for anomalous dispersion and for normal dispersion and found out that for $d > 0$ our results are in good agreements with the approximations found in the literature. However, our approach is also valid for $d < 0$ and can therefore be used independently of the dispersion of the material.

Part IV discussed the effect of two photon absorption, where two photons are absorbed and electrons from the valence band are excited into the conducting band. This leads to an additional nonlinear loss term in the Lugiato Lefever equation

$$-da'' + (\zeta - i)a - (1 + i\kappa)|a|^2 a - if = 0.$$

We proved the persistence of bifurcation points for small $\kappa > 0$, their disappearance for $\kappa > \kappa_*$ and the absence of any nontrivial solutions for $\kappa > \kappa^*$ with $0 < \kappa < \kappa^*$. Furthermore, we supported our analysis by some numerical experiments, showing that the number of bifurcation points reduces with increasing values of κ until a value κ_*^{num} is reached, where bifurcation points cease to exist. Comparing the numerically obtained value κ_*^{num} with the theoretical value κ_* show a good agreement.

However, closely related to TPA, there is another effect called free carrier absorption, where free carriers are excited from one state into another within the same band. Introducing the free carrier density n , the model including free carrier absorption is given by

$$\begin{aligned} -da'' + (\zeta - i)a - (1 + i\kappa)|a|^2a + if - s(i - \mu)na &= 0 \\ n' = \kappa|a|^4 - \frac{n}{\tau} \end{aligned}$$

with $\kappa, s, \mu, \tau \geq 0$, cf. [18]. However, due to lack of reversibility of the extended model, the approach of Neumann boundary conditions together with reflecting the resulting solutions is not applicable. At the moment, analytical results are out of reach for us.

An additional effect, that can be considered is higher order dispersion. Although this effect is several magnitudes smaller than the second order effect, it should not be neglected in the case of normal dispersion ($d < 0$). In Section 15, we proved a priori bounds for the Lugiato-Lefever equation third order dispersion

$$-da'' - iea''' + (\zeta - i)a - |a|^2a + if = 0.$$

Due to the lack of reversibility, there are new analytical and numerical difficulties that need to be overcome, e.g. bifurcation from the trivial solutions may be lost for $e \neq 0$ and the character of solitons changes drastically cf. [11],[45].

List of Figures

1.	System for generation of frequency combs	9
2.	Energy level diagram for non-degenerate four-wave mixing.	10
3.	Solitons and corresponding frequency combs	11
4.	Homoclinic orbits	23
5.	Sketch of (3.5).	25
6.	Bifurcation from the sphere	26
7.	Property of w_i^∞ for $f > 0$	34
8.	Illustration of lower envelope.	39
9.	Solutions of (LLE).	42
10.	Continuation of the approximate solution	45
11.	(ζ, f) -map	46
12.	Soliton solutions found by continuation	47
13.	Predictor corrector method	56
14.	Bifurcation diagram	59
15.	1-soliton, 2-soliton and 3-soliton	59
16.	Bifurcation diagrams, solutions and frequency combs	63
17.	Illustration of $\text{FWHM}_{a/i}$	65
18.	$\text{FWHM}_{a/i}$ along bifurcating branches	66
19.	Bandwidth and power conversion efficiency	69
20.	Bifurcation diagrams for increasing values of κ for $d > 0$	77
21.	Solitons for increasing values of κ	77
22.	Bifurcation diagrams for increasing values of κ for $d < 0$	78
23.	Illustration of κ_*	79
24.	Solutions of (9.1)	95
25.	w_1 for $f > 0$ and w_2 for $f < 0$	103

References

- [1] Changjing Bao, Lin Zhang, Andrey Matsko, Yan Yan, Zhe Zhao, Guodong Xie, Anuradha Agarwal, Lionel Kimerling, Jurgen Michel, Lute Maleki, and Alan Willner. Nonlinear conversion efficiency in Kerr frequency comb generation. *Optics letters*, 39(21):6126–6129, 2014.
- [2] Feliks A. Berezin and Michail A. Shubin. *The Schrödinger equation*. Mathematics and its applications: Soviet series; 66. Kluwer, Dordrecht [u.a.], 1991.
- [3] F. Brezzi, J. Rappaz, and P. A. Raviart. Finite dimensional approximation of nonlinear problems. *Numerische Mathematik*, 36(1):1–25, 1980.
- [4] Thierry Cazenave. *Semilinear Schrödinger equations*. Courant lecture notes in mathematics; 10. Courant Institute of Mathematical Sciences, New York, 2003.
- [5] Stéphane Coen and Miro Erkintalo. Universal scaling laws of Kerr frequency combs. *Optics letters*, 38(11):1790–2, 2013.
- [6] Michael G. Crandall and Paul H. Rabinowitz. Bifurcation from simple eigenvalues. *J. Functional Analysis*, 8:321–340, 1971.
- [7] Michael G. Crandall and Paul H. Rabinowitz. Bifurcation, Perturbation of Simple Eigenvalues and Linearized Stability. *Arch. Rational Mech. Anal.*, 52(2):161–180, 1973.
- [8] Edward B. Davies. *Heat kernels and spectral theory*. Cambridge tracts in mathematics; 92. Cambridge Univ. Pr., Cambridge [u.a.], 1990.
- [9] Eleonora Di Nezza, Giampiero Palatucci, and Enrico Valdinoci. Hitchhiker’s guide to the fractional Sobolev spaces. *Bull. Sci. Math.*, 136(5):521–573, 2012.
- [10] Tomas Dohnal, Jens Rademacher, Hannes Uecker, and Daniel Wetzel. pde2path 2.0: multi-parameter continuation and periodic domains. 2014.
- [11] J.N. Elgin, T. Brabec, and S.M.J. Kelly. A perturbative theory of soliton propagation in the presence of third order dispersion. *Optics Communications*, 114(3):321 – 328, 1995.
- [12] Lawrence C. Evans. *Partial differential equations*. American Mathematical Society, Providence, R.I., 2010.
- [13] Janina Gärtner, Tobias Jahnke, Christian Koos, Rainer Mandel, and Wolfgang Reichel. Bandwidth and Conversion Efficiency Analysis of Dissipative Kerr Soliton Frequency Combs Based on Bifurcation Theory. *CRC1173 Preprint 2018-56*, 2018.
- [14] Janina Gärtner, Rainer Mandel, and Wolfgang Reichel. The Lugiato-Lefever equation with nonlinear damping. *arxiv.org/pdf/1811.12200.pdf*, 2018.

- [15] David Gilbarg and Neil S. Trudinger. *Elliptic Partial Differential Equations of Second Order*. Classics in mathematics. Springer, Berlin, 2001.
- [16] Cyril Godey. A bifurcation analysis for the Lugiato-Lefever equation. *The European Physical Journal D*, 71(5):131, 2017.
- [17] Hairun Guo, M. Karpov, E. Lucas, Arne Kordts, M.H.P. Pfeiffer, V. Brasch, G. Lihachev, V. E. Lobanov, M. L. Gorodetsky, and T. J. Kippenberg. Universal dynamics and deterministic switching of dissipative Kerr solitons in optical microresonators. *Nature Physics*, 2016.
- [18] Tobias Hansson and Stefan Wabnitz. Dynamics of microresonator frequency comb generation: Models and stability. *Nanophotonics*, 5(2):231–243, 2016.
- [19] T. Herr, V. Brasch, J. Jost, C.Y. Wang, N.M. Kondratiev, M.L. Gorodetsky, and T.J. Kippenberg. Temporal solitons in optical microresonators. *Nature Photonics*, 8:145–152, 2014.
- [20] Peter D. Hislop and Israel Michael Sigal. *Introduction to spectral theory: with applications to Schrödinger operators*. Applied mathematical sciences; 113. Springer, New York, 1996.
- [21] Tobias Jahnke, Marcel Mikl, and Roland Schnaubelt. Strang splitting for a semi-linear Schrödinger equation with damping and forcing. *J. Math. Anal. Appl.*, 455(2):1051–1071, 2017.
- [22] Svante Janson. Roots of polynomials of degrees 3 and 4. www2.math.uu.se/~svante/papers/sjN7.pdf, 2010.
- [23] Herbert B. Keller. Lectures on numerical methods in bifurcation problems. www.math.tifr.res.in/~publ/ln/tifr79.pdf, 1987.
- [24] Hansjörg Kielhöfer. *Bifurcation Theory: An Introduction with Applications to Partial Differential Equations*. Applied Mathematical Sciences; 156SpringerLink: Bücher. Springer New York, New York, NY, 2012.
- [25] T. J. Kippenberg, R. Holzwarth, and S. A. Diddams. Microresonator-Based Optical Frequency Combs. *Science*, 332(6029):555–559, 2011.
- [26] Ryan K. W. Lau, Michael R. E. Lamont, Yoshitomo Okawachi, and Alexander L. Gaeta. Effects of multiphoton absorption on parametric comb generation in silicon microresonators. *Opt. Lett.*, 40(12):2778–2781, 2015.
- [27] Valery E. Lobanov, Artem V. Cherenkov, Artem E. Shitikov, Igor A. Bilenko, and Michael L. Gorodetsky. Dynamics of platons due to third-order dispersion. *The European Physical Journal D*, 71(7):185, 2017.

- [28] L. A. Lugiato and R. Lefever. Spatial dissipative structures in passive optical systems. *Phys. Rev. Lett.*, 58:2209–2211, 1987.
- [29] Rainer Mandel and Wolfgang Reichel. A priori bounds and global bifurcation results for frequency combs modeled by the Lugiato-Lefever equation. *SIAM J. Appl. Math.*, 77(1):315–345, 2017.
- [30] Bernd Marx and Werner Vogt. *Dynamische Systeme: Theorie und Numerik*. Spektrum Akad. Verl., Heidelberg, 2011.
- [31] T. Miyaji, I. Ohnishi, and Y. Tsutsumi. Bifurcation analysis to the Lugiato-Lefever equation in one space dimension. *Phys. D*, 239(23-24):2066–2083, 2010.
- [32] T. Miyaji, I. Ohnishi, and Y. Tsutsumi. Stability of a stationary solution for the Lugiato-Lefever equation. *Tohoku Math. J. (2)*, 63(4):651–663, 2011.
- [33] K. Nozaki and N. Bekki. Low-dimensional chaos in a driven damped nonlinear Schrödinger equation. *Physica D: Nonlinear Phenomena*, 21(2):381 – 393, 1986.
- [34] Kazuhiro Nozaki and Naoaki Bekki. Chaotic solitons in a plasma driven by an rf field. *Journal of the Physical Society of Japan*, 54(7):2363–2366, 1985.
- [35] P. Parra-Rivas, D. Gomila, L. Gelens, and E. Knobloch. Bifurcation structure of localized states in the Lugiato-Lefever equation with anomalous dispersion. *Phys. Rev. E*, 97:042204, 2018.
- [36] P. Parra-Rivas, D. Gomila, M. A. Matías, S. Coen, and L. Gelens. Dynamics of localized and patterned structures in the Lugiato-Lefever equation determine the stability and shape of optical frequency combs. *Phys. Rev. A*, 89:043813, 2014.
- [37] P. Parra-Rivas, E. Knobloch, D. Gomila, and L. Gelens. Dark solitons in the Lugiato-Lefever equation with normal dispersion. *Phys. Rev. A*, 93:063839, 2016.
- [38] Uwe Prüfert. OOPDE. www.mathe.tu-freiberg.de/nmo/mitarbeiter/uwe-pruefert/software, 2016.
- [39] Paul H. Rabinowitz. Some global results for nonlinear eigenvalue problems. *J. Functional Analysis*, 7:487–513, 1971.
- [40] Michael Reed and Barry Simon. *Methods of modern mathematical physics*, volume 4: Analysis of operators. Acad. Pr., New York, 2005.
- [41] Harvey A. Rose and Michael I. Weinstein. On the bound states of the nonlinear Schrödinger equation with a linear potential. *Phys. D*, 30(1-2):207–218, 1988.
- [42] Milena Stanislavova and Atanas G. Stefanov. Asymptotic stability for spectrally stable Lugiato-Lefever solitons in periodic waveguides. *J. Math. Phys.*, 59(10):101502, 12, 2018.

- [43] Jimmi H. Talla Mbé, Carles Milián, and Yanne K. Chembo. Existence and switching behavior of bright and dark Kerr solitons in whispering-gallery mode resonators with zero group-velocity dispersion. *The European Physical Journal D*, 71(7):196, 2017.
- [44] Hannes Uecker, Daniel Wetzels, and Jens D. M. Rademacher. pde2path—a Matlab package for continuation and bifurcation in 2D elliptic systems. *Numer. Math. Theory Methods Appl.*, 7(1):58–106, 2014.
- [45] Shaofei Wang, Hairun Guo, Xuekun Bai, and Xianglong Zeng. Broadband Kerr frequency combs and intracavity soliton dynamics influenced by high-order cavity dispersion. *Opt. Lett.*, 39(10):2880–2883, 2014.
- [46] Xiaoxiao Xue, Yi Xuan, Yang Liu, Pei-Hsun Wang, Steven Chen, Jian Wang, Dan E. Leaird, Minghao Qi, and Andrew M. Weiner. Mode-locked dark pulse Kerr combs in normal-dispersion microresonators. *Nature Photonics*, 9(9):594–600, 2015.
- [47] Xu Yi, Qi-Fan Yang, Ki Youl Yang, Myoung-Gyun Suh, and Kerry Vahala. Soliton frequency comb at microwave rates in a high-Q silica microresonator. *Optica*, 2(12):1078–1085, 2015.

Eidesstattliche Erklärung:

Hiermit erkläre ich an Eides statt, dass ich die vorliegende Arbeit selbstständig und nur unter Zuhilfenahme der ausgewiesenen Hilfsmittel angefertigt habe. Sämtliche Stellen der Arbeit, die im Wortlaut oder dem Sinn nach anderen gedruckten oder im Internet veröffentlichten Werken entnommen sind, habe ich durch genaue Quellenangaben kenntlich gemacht.

Karlsruhe, den 22.01.2019

